FUNCTIONAL ANALYSIS OF *TBX2A* DURING DEVELOPMENT OF THE PHARYNGEAL ARCHES

NGUYEN THI THU HANG
(B.Sc Hons, Hanoi University of Science)

A THESIS SUBMITTED
FOR THE DEGREE OF DOCTOR OF PHILOSOPHY
DEPARTMENT OF BIOLOGICAL SCIENCES
NATIONAL UNIVERSITY OF SINGAPORE

2009

Acknowledgements

First of all, I would like to express my great gratitude to my supervisor, A/Prof Vladimir Korzh who accepted me from the National University of Singapore (NUS) into his lab (VK) in the Institute of Molecular and Cell Biology (IMCB). I am indebted to him for his invaluable expert guidance in science, consistent support in logistic issues, and sincere care in life. Without all these favors, I could not have achieved my PhD dream.

My deep thanks will next go to Dr Steven Fong, who is such a talented mentor, for his patient instruction and support throughout the course of my PhD. Research ideas and excellent technical strategies have formed through many fruitful discussion sessions with him. My project has benefited from his directional suggestions and smart advice.

I would like to take this opportunity to thank the NUS for offering me the graduate research scholarship and the IMCB for providing me such a favorable working condition. I also thank staff from the general office of the Department of Biological Sciences (DBS) and the fish facilities in Temasek Life Science Laboratories (TLL) and IMCB for their great assistance. In addition, I would like to express my appreciation to my current boss, A/Prof Dr Jimmy So (Surgery, NUHS) for allowing me to take leave for thesis writing.

My sincere thanks are to all members and ex-members of VK's lab for their help and encouragement. Especially, I would like to express my heartfelt thanks to my seniors who are also my closest friends, Lana, Marta, Cathleen, Kar Lai, Li Zhen, Lee Thean, William and Igor for their warm affection and care.

Finally, I dedicate this thesis to my beloved parents and sister, my husband Pham Thai Ha, my in-laws and my newborn daughter Pham Hoang Anh, who have been by my side in all ups and downs; their love and unconditional support have empowered me to pursue and develop an interest in research.

Table of Contents

Summary

Tbx2 is a member of the T-box family of transcription factors that function during embryonic development and organogenesis in all metazoans. In addition to the growing body of recent findings about roles of *Tbx2* during cancer progression, study of the gene function during embryonic development is also essential. In this study, we characterize functions of the paralog *tbx2a* during embryonic development using zebrafish as a model.

tbx2a was cloned and mapped to Chromosome 5. Analysis of tissue distribution of *tbx2a* transcripts revealed a number of conserved domains and species specific domains. *tbx2a* was consistently expressed in the pharyngeal endoderm and gene knock-down led to a total loss of pharyngeal arches, which suggests its indispensable role in this region. The pharyngeal apparatus is a conserved structure across species. It develops into the jaw and gills in fish, and numerous structures in the human neck and face. While there are many human disorders of the face and neck, the genes and molecular mechanisms responsible are largely unknown. This work used zebrafish as a model to explore the function of *tbx2a* during pharyngeal arch development. This well-structured organ is constituted by derivatives from all three embryonic germ layers – endoderm pouches, mesodermal cores and neural crest cells. We showed that although *tbx2a* expression was mostly restricted to the endodermal pouches, gene knock-down led to a total loss of pharyngeal arches in a p53-independent manner. We provided evidence for a cell-autonomous role of *tbx2a* during specification of the endodermal pouches, which affects the whole pharyngeal apparatus. Furthermore, we identified a secondary effect of *tbx2a* on other components such as mesodermal cores, neural crest cells (NCCs) and epibrachial

ganglia. We did not observe any changes in patterning of migratory NCCs in the absence of *tbx2a*; instead, their cartilage differentiation was strongly affected. Finally, we demonstrated that knock-down *tbx2a* resulted in cell apoptosis within pharyngeal arches. Taken together, we hope the understanding provided about the role of *tbx2a* during pharyngeal arch development in zebrafish could be extended for studying human disorders in the face and neck.

Our data strongly support the hypothesis that the endodermal pouches play a leading role during the development of pharyngeal arches. Analysis of expression pattern showed that *tbx2a* is also expressed in other endodermal derivatives such as swim bladder, anterior gut and liver. Thus, there could be a common mechanism where *tbx2a* acts to regulate the development of all endoderm-budding organs.

Finally, in the appendix, we briefly demonstrate the function of *tbx2a* in hypothalamus patterning and neurogenesis. We provide preliminary data to show that Tbx2a might inhibit *shh* expression to promote the fate of posterior hypothalamus as well as neurogenesis in this region.

List of Tables

List of Figures

List of Schemes and Charts

List of Common Abbreviations

AP	antero-posterior
App.	Appendical
BCIP	5-bromo-3-chloro-3-indolyl phosphate
BMP	bone morphogenetic protein
bp	base pair
cDNA	DNA complementary to RNA
CIP	calf intestinal alkaline phosphatase
cyc	*cyclops*
DEPC	diethyl pyrocarbonate
DIG	digoxygenin
DMSO	dimethylsulphoxide
DNA	deoxyribonucleic acid
dNTP	deoxyribonucleotide triphosphate
dpf	days post fertilization
DTT	dithiothreitol
DV	dorso-ventral
EDTA	ethylene diaminetetraacetic acid
FBS	fetal bovine serum
FITC	Fluorescein isothiocyanate
GFP	green fluorescent protein
hpf	hours post fertilization
IPTG	isopropyl beta-D-thiogalactopyranoside
kb	kilo base pair
LB	Luria-Bertani medium
min	minute / minutes

MO	morpholino oligonucleotide
mRNA	messenger ribonucleic acid
NTP	ribonucleotide triphosphate
ON	over night
oep	one-eyed-pinhead
PBS	phosphate-buffered saline
PBST	PBS with 0.1% Tween 20
PCR	polymerase chain reaction
PFA	paraformaldehyde
PTU	1-phenyl-2-thiourea
RFP	red fluorescent protein
RNA	ribonucleic acid
rpm	revolution per minute
RT	room temperature
RT-PCR	reverse transcriptase-polymerase chain reaction
Shh	Sonic Hedgehog
SSC	sodium chloride-trisodium citrate solution
UTR	untranslated region
UV	ultraviolet
WISH	whole-mount in situ hybridization
WT	wild type
X	streght of solution or times of repeatition
Xgal	5-bromo-4-chloro-3-indolyl-beta-D-galactopyranoside
ZFIN	zebrafish information network

List of Publications

List of Publications

Journal Papers

1. Chong SW, **Nguyen TT**, Chu LT, Jiang YJ, Korzh V. "Zebrafish id2 developmental expression pattern contains evolutionary conserved and species-specific characteristics", (2005), Dev. Dyn., 234(4):1055-63.

2. **Hang Nguyen**, Steven Fong, Vladimir Korzh, "*Tbx2a* regulates endodermal pouch morphogenesis to affect zebrafish pharyngeal arch development". (In preparation)

Symposia Presentation

1. **Hang Nguyen**, Steven Fong, Vladimir Korzh, "Developmental analysis of *tbx2a* in zebrafish", 5th European Zebrafish Genetics and Development Meeting, (2007) No. 223, p. 254.

Chapter 1

Introduction

1.1 Overview of *T-box* genes

T-box is a family of genes encoding transcription factors with a unique and evolutionarily conserved DNA-binding domain, namely the T-box domain (Bollag et al., 1994). All of member of the *T-box* family typically recognize palindromic T boxes of the target genes, however these may differ depending on a particular T-box protein (Kispert and Herrmann, 1993). For example, Xbra can bind to two half sites arranged head-to-head (TCACACCTAGGTGTGA) while Eomesodermin cannot. Conversely, Eomesodermin can bind to two core motifs arranged head-to-tail (TCACACCTaaatTCACACCT) while Xbra cannot (Conlon et al., 2001). This family of genes has been found to play important roles during embryogenesis. In fact, a number of mutations in *T-box* genes have been characterized to be involved in human developmental syndromes such as Ulnar-mammary (Bamshad et al., 1997), Holt_Oram (Basson et al., 1997; Li et al., 1997) and DiGeorge (Jerome and Papaioannou, 2001; Yagi et al., 2003).

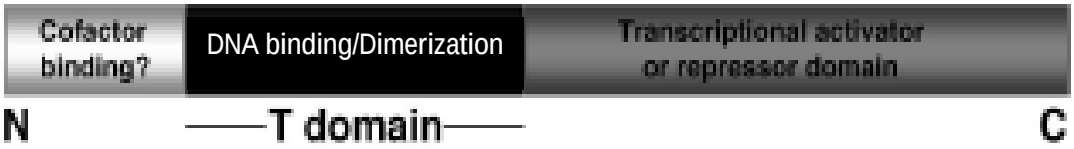

Scheme 1:. **General structure of T-box transcription factors.** Members of T-box family are typical with a conserved DNA binding domain_T-box, transactivation domain is at C-terminus, N-terminus may interact with cofactor. Adapted from Minguilon and Logan, (2003)

Tbx2 is one of the relatively recent additions to the *T-box* family, but it is actively studied since it is not only implicated in organogenesis but also in carcinogenesis (Rowley et al., 2004; Jerome_Majewska et al., 2005; Bilican and Goding., 2006). Tbx2 is deregulated in pancreatic, breast and melanoma cancers

(Mahlamaki et al., 2002; Sinclair et al., 2002; Packham and Brook, 2003; Vance et al., 2005). Its function in carcinogenesis has been supported by the findings suggesting that Tbx2 regulates cellular proliferation and/or survival by inhibiting downstream targets such as $p19^{ARF}$, $p16^{INK4a}$ and p21, which in turn negatively affect expression of one of the most important anti-apoptotic genes encoding Tp53 (Jacobs et al., 2000; Lingbeek et al., 2002; Prince et al., 2004). Also, *tbx2* has been implicated in cell adhesion by regulating the gap junction *connexin43_cx43* (Borke, 2003; Chen, 2004), and *collagen, type I, alpha 2_col1a2* (Teng et al., 2007). Microarray analysis of Tbx2-overexpressing fibroblasts suggests that Tbx2 is upstream of factors responsible for osteogenesis (Chen et al., 2001). Whereas many studies suggest that Tbx2 negatively represses transcription of target genes (Carreira et al., 1998; Smith et al., 1999), Chan et al. (2001) observed that overexpression of Tbx2 caused Col1a2 up-regulation in mouse NIH3T3 fibroblasts and down-regulation in rat OS17/2.8 osteoblastic cell line. This suggests that Tbx2 regulatory outcomes could vary upon cell type or tissue contexts. Although these cellular findings have contributed to the body of basic knowledge about *tbx2* functions, animal models are required as a comprehensive study system for further investigation of roles of this gene during embryonic development.

Thus far, there is still no report on the link between *TBX2* mutations with any human disorders. This could be due to the prenatal lethality of the mutants which suffer from cardiac insufficiency, as demonstrated in the *tbx2* null mouse (Harrelson et al., 2004; Plagemen and Yutzey, 2005). Therefore, it is necessary to utilize animal models to study functions of this gene during normal embryonic development. By using mouse, it has been found that *Tbx2* is involved in development of limb (King et

al., 2006), heart (Plageman and Yutzey, 2005) and mammary gland (Rowley et al., 2004).

Over the last two decades, the zebrafish has been accepted as a useful model, which complements other model vertebrate animals such as mice, chick and frogs (Lieschke and Currie, 2007; and elsewhere). From the moment this gene has been discovered in the zebrafish (Dheen et al., 1999) until now zebrafish researchers have obtained evidence of its developmental role in the heart, eyes, and ears (Gross et al., 2005; Ribeiro et al., 2007; Chi et al., 2007; Snelson et al., 2008), which is compatible with studies in mammals mentioned above. Interestingly, due to partial genome duplication, *tbx2* in zebrafish is represented by two paralogs - *tbx2a* and *tbx2b* (Dheen et al., 1999; Fong et al., 2005). Genomic sequence comparison reveals that *tbx2a* and *tbx2b* contain 100% of the conserved sequence of the T-box domain (Dheen et al., 1999; this study). Comparison of *tbx2a* and *tbx2b* expression patterns demonstrated some similarity and some divergence of expression domains, suggesting the possibility that *tbx2a* and *tbx2b* may play partially redundant and partially distinct roles during development. Given the diversity of developmental roles of *tbx2* in vertebrates, the divergence of these two genes in zebrafish provides a convenient way of tackling them individually. That in turn would lead to a more complete understanding of *tbx2* function, supplementing that from other species. Recently, several studies have focused on one of the two genes without referring to the redundant roles. During specification of the eye, *tbx2a* knock-down has been found to affect only the dorsal eyes (Gross et al., 2005). In early neurogenesis, *tbx2b* has been shown to drive the process of cell migration into the neural plate (Fong et al., 2005). In the heart, *tbx2a* has been reported to be indispensable for cardiac chamber formation (Ribeiro et al., 2007). Moreover, Chi et al. (2007) identified *foxn4* as a

direct regulator of *tbx2b* expression and atrioventricular canal formation in zebrafish heart. Most recently, Snelson et al. (2008) have characterized a nonsense mutation in the *tbx2b* gene and found that Tbx2b regulates parapineal asymmetry by specifying the correct number of parapineal cells.

However, not all developmental roles of *tbx2* have been studied. Harrelson et al. (2004) while characterizing the gene function in the heart using the *Tbx2* null mouse, also reported a defect in the pharyngeal arches. So far, there has been no study exploring the role of *tbx2* in this region. In this study, we present for the first time a systematic investigation of the role of *tbx2a* during organogenesis of the pharyngeal apparatus. We observed a consistent expression of *tbx2a* in the pharyngeal arches from around 22 hpf (hour post fertilization) onwards. Importantly, morpholino-mediated *tbx2a* gene knockdown led to abnormal development of the pharyngeal apparatus, which suggests a crucial role of *tbx2a* in this set of organs. Moreover, *tbx2* expression in the pharyngeal arches is conserved in all vertebrate models: mouse (Harrelson et al., 2004), chick (Gibson-Brown et al., 1998), *Amphibia* (Hayata et al., 1999). Kimmel et al. (2001) compared patterning of the early branchiomeres in the zebrafish, which represents actinopterygians, and recognized a similarity with that of distantly related sacropterygians such as the *Amphibia*, birds, and mammals. Thus, zebrafish as a representative of the larger group of gnathostomes (*Pisces*, *Amphibia*, *Avia* and *Mammalia*) is a good model for studying pharyngeal arch development. Despite the consistent and prominent expression of *tbx2* during development of the pharyngeal arches, the developmental roles of this gene in this part of the body remain unknown.

Although mature mammals including humans do not possess functional pharyngeal arches for respiration as fish do, they do develop this apparatus during

early stages of development that later gives rise to the lower jaw and many structures of the face and neck (reviewed by Schoenwolf et al., 2009). Despite a high rate of birth defects of the face and neck in human, only a few have been shown to be caused by faulty genes and signaling pathways – *TBX1* (DiGeorge syndrome), retinoic acid metabolism, FGF (fibroblast growth factor) and SHH (Sonic Hedgehog) signaling pathways, etc (reviewed by Schoenwolf et al., 2009). Using animal models to study gene function during development will hopefully uncover conserved developmental mechanisms and help us understand the underlying cause of such birth defects in humans. Due to the evolutionarily conserved nature of gene function, our findings on *tbx2a* during embryogenesis are important for understanding human anomalies of the face and neck. However, a full understanding of these matters will require additional studies in other animal models.

1.2 Overview of development of the pharyngeal arches

Segmented pharyngeal apparatus is a common feature of all chordates (Schaeffer, 1987). For feeding and respiration, the vertebrate pharyngeal apparatus has evolved with complicated modifications recruiting the contribution of all three embryonic germ layers. Each of the pharyngeal arches has its own function (reviewed by Graham, 2001). The most anterior first arch (mandibular) forms the lower jaw. The second arch (hyoid) plays a role as the jaw support (hyoid), and the more posterior arches become gill bearing in teleosts or associated with the throat in amniotes. However, maybe due to the shift in usage of respiratory organs from pharyngeal gills to lungs in tetrapods, the number of caudal segments was reduced from 5 in teleosts to 3 in amniotes (reviewed by Graham, 2001; Schoenwolf et al., 2009).

The pharyngeal apparatus can be described as a series of bulges located on the lateral surface of the head that develop into pharyngeal arches with a repeated structure for each mature arch. The central most is the mesodermal core which is encapsulated by neural crest cells. Endoderm marks the inner covering, whereas the ectoderm marks the outer covering for the arch. The three germ layer derived components also give rise to their own derivatives to facilitate the full function of the apparatus as a whole. The innermost endoderm establishes the pouches separating the arches; and forms the thyroid, parathyroid and thymus (Cordier and Haumont, 1980). The ectoderm forms the epidermis and the sensory neurons of the epibranchial ganglia (Couly and Le Douarin, 1990). The neural crest cells develop into skeletal elements and connective tissue of the arches while the mesodermal cores form musculature cells (Noden, 1983; Coulyet al., 1993; Trainor et al., 1994).

The three embryonic germ layers contribute to the structure of the arches by working out their own movement and specification which in turn bring them into

more intimate contact to provide the anatomical basis for signalling interactions (Kimmel et al., 2001). The pharyngeal endoderm branches into slits or out-pockets which extend dorsoventrally to reach the ectoderm. Around the same time, neural crest cells migrate from the dorsal neural tube toward out-pocketing endodermal pouches and wrap round the mesodermal cores (Kimmel et al., 2001; Cerny et al., 2004). Vertebral pharyngeal apparatus is highly evolved with innervating nerves connected to the central nervous system for conveying sensation and receiving controlling signals. Epibranchial placode induction is a crucial step during pharyngeal neurogenesis since it requires active interaction with the surrounding tissues including the pharyngeal endoderm (Webb and Noden, 1993).

Previous studies have proposed a central role for neural crest cells in the development of the pharyngeal arch (Noden, 1983; Köntges and Lumsden, 1996). However, as mentioned, pharyngeal arch development is an orchestra of several complicated processes contributed by all three germ layers.

1.2.1 The contribution of the neural crest cells to pharyngeal development

Neural crest cells (NCCs) are a population of migratory embryonic cells from the border between ectoderm and neural plate (Le Douarin and Kalcheim, 1999). They diversify into many cell types that include pharyngeal neural crest (Le Douarin and Kalcheim, 1999). To become pharyngeal cartilage, these NCCs have to go through the journey from the dorso-lateral edge of the closing neural folds to the future pharyngeal arches by migration under intrinsic and extrinsic signals (reviewed by Noden, 1983; Graham, 2001).

The NCCs were long held to play a master role during pharyngeal arch development until mounting evidence of the leading role of the endodermal pouches forced a revision (Graham et al., 2005). Nevertheless, the NCCs are still an important

and indispensable component of the complete pharyngeal arches (Kimmel et al., 2001). The pharyngeal NCCs migrate in a conserved manner in all vertebrates, separately in three main streams: trigeminal, hyoid and postotic (Lumsden et al. 1991; Schilling & Kimmel, 1994; Horigome *et al.* 1999; Trainor, 2002). The trigeminal stream which arises from the posterior midbrain and the anterior hindbrain segments, rhombomeres 1 and 2 will populate the first arch (the lower jaw). The hyoid which emigrates from the central hindbrain region, primarily from rhombomere 4 contributes to the second arch. The rest - the caudal branchial arches are contributed by the postotic crest cells from the caudal hindbrain, rhombomere 6 and 7. This prior separation of the migratory crest cells into streams seems to be a prerequisite to the organisation of the future pharyngeal apparatus. Fate-mapping experiments in chick (Köntges & Lumsden, 1996) as well as in axolotl (Cerny et al, 2004) have shown that these NCC streams never inter-mix. Noden (1983) observed that if the avian midbrain or anterior hindbrain NCCs were heterotopically transplanted into the more caudal hindbrain region, it would produce a duplication of the first arch. This experiment suggested that the premigratory NCCs might carry intrinsic positional information, at least at this early stage, for their future skeletal development. However, Couly *et al*. (2002) based on transplantation experiment of the anterior endoderm argued that the fate of the pharyngeal NCCs is plastic to the skeletal element identity, meaning the positional signals are dependent on the external environment - the endoderm. Piotrowski and Nusslein-Volhard (2000) also highlighted the patterning role of the endoderm in zebrafish; so did Veitch et al. (1999) in chick. However, a study in mouse suggested that head mesoderm might play a role in segmentation of the neuroectoderm, including NCCs (Trainor & Krumlauf, 2000; Trainor et al., 2000). Cerny et al. (2004) with a study in axolotl argued that intrinsic signals might be

effective during the early migrating stage to maintain the three streams of NCCs; however, once intimate contacts with endoderm and mesoderm occur, extrinsic signals should take over the role of directing the NCC differentiation.

1.2.2 Chondrogenesis – cartilage formation

The mesenchymal core is formed internally by the mesodermal core and externally by NCCs (Kimmel, 2001). These mesenchymal cells are chondro-progenitors which will undergo steps of differentiation to build up cartilage. After committing to the chondrogenic fate, pre-chondrocytes differentiate into chondrocytes and then to early chondroblasts. From that, the cartilage anlagen are formed so as to pre-frame the future skeletal elements. Through each step, they may acquire a specific histological feature, cellular activity and especially, gene expression profile (reviewed in Lefebvre and Smits, 2005). In the first step, prechondrocytes turn off expression of mesenchymal markers and start to express *col2a1* and subsequently other cartilage markers *col9a1, col9a2, col9a3* and *col10a1*. The type II collagen is the most abundant in the framework of the cartilage matrix. *sox9* is expressed in chondrogenic mesenchymal cells even before condensation and maintained in prechondrocytes and chondroblasts. It is turned off when chondroblasts start prehypertrophy (Wright et al., 1995; Ng et al., 1997; Zhao et al., 1997). *pax1/9* is also expressed in the same chondrogenic stage with that of *sox9*. Inactivation of *sox9* in mouse or *sox9a* in zebrafish leads to the same result in which pre-chondrogenic cores are formed normally but they cannot proceed with chondroblast differentiation (Akiyama et al., 2002; Yan et al, 2002). Chondrogenesis consists of multiple steps, so there should be more transcription factors to be characterized in future.

To dissect the role of *tbx2a* during pharyngeal arch development, it is important to resolve the question of whether the gene is involved in pharyngeal neural

crest patterning and/or differentiation/cartilage formation as an intrinsic signal or upstream of extrinsic signals.

1.2.3 The role of the endoderm pouches during pharyngeal arch formation

Previously, pharyngeal arch malformation was conventionally attributed as a consequence of defects in neural crest specification. However, some mutants that exhibit malformed pharyngeal arch e.g. *vgo* (*tbx1*$^{-/-}$) possess normally patterned NCCs (Piotrowski et al., 2003), arguing for the possibility that the pharyngeal apparatus is patterned by components other than NCCs.

The pharyngeal endodermal pouches arise from the anterior endodermal bulges on the lateral surface of the pharynx. These bulges are pushed out to reach the ectoderm and extend along the proximo-distal axis as a pocket consisting of two halves. The anterior half faces one arch in front and the posterior half is in contact with the contiguous arch behind. The pouches are chronologically formed. In zebrafish, the first pouch is formed at around 17hpf, and then consecutively with 2 hour-intervals (Kimmel et al., 2001). All the pouches are fully formed at around 30hpf. To date, there are accumulating lines of evidence for the leading role of endodermal pouches, but not the NCCs, during pharyngeal development. Strikingly, Veitch et al. (1999) demonstrated in chick that endoderm pouch identity is unchanged in the absence of NCCs so that the pharyngeal arches are still formed. In the study, the neural tube was removed before production of NCCs, but the expression patterns of endodermal pouch markers were normally maintained. Zebrafish *cas* (defective in Sox-related factor Casanova) and *bon* mutants (defective in homeobox transcription factors Mixer/Bonnie and clyde), which affect Nodal signalling, do not develop endoderm and possess a weak trace of mesoderm (Dickmeis et al., 2001; Kikuchi et al., 2001; Kikuchi et al., 2000). As a result, the pharyngeal arch cartilages disappear in

these mutants although neural crest migration is not affected (David et al., 2002). Rescue experiment with endoderm-derived cells confirmed the solitary role of the endoderm. In the same study, it was found that Fgf3 is important for the endoderm to control the chondrogenic fate of the NCCs. Other evidence is provided by the studies in zebrafish *vgo* mutant, which carries a mutation in the locus of *tbx1* (Piotrowski et al., 2003), an orthologue of human *TBX1* – a key factor in DiGeorge deletion syndrome (DGS) (Jerome and Papaioannou, 2001; Lindsay et al., 2001; Merscher et al., 2001). *vgo* exhibits undeveloped pharyngeal arches (Piotrowski & Nusslein-Volhard, 2000). Despite the fact that the NCCs are formed normally and migrate to the prospective pharyngeal area, the pharyngeal cartilages fail to form in the caudal arches and become fused together in the first two arches. That was attributed to defect in the endodermal pouches (Piotrowski & Nusslein-Volhard, 2000). The anterior endoderm is not segmented and the pouches are not formed. Study in *Tbx1*$^{-/-}$ mice also recognized the same defects as in *vgo* fish. The mice also have defective endodermal pouches which lead to malformation in their derivatives such as the parathyroid, thymus and aortic arches_the major blood vessels of the pharyngeal arches (Garg et al, 2001; Zhang et al., 2005). In chick, it was found that specific ablation of particular domains of the pharyngeal endoderm accordingly leads to the failure of future neural crest-derived skeletal elements (Couly et al., 2002). Conversely, the orientation of the additional skeletal element will follow the orientation of the ectopically transplanted endodermal pouch. Altogether, there are lines of convincing evidence that development of the pharyngeal arch relies on instructional cues from endoderm pouches.

The leading role of the endodermal pouches may reflect the evolutionary origin of the segmented pharyngeal patterned from endoderm prior to the contribution

of the NCCs. Recently, Rychel and Swalla (2007) recognized a highly conserved expression pattern of genes, such as *soxE*, *type II collagen* and *pax1/9,* regulating pharyngeal cartilage development in lancelets, tunicates, hemichordates and vertebrates. Importantly, in hemichordates pharyngeal endodermal cells are able to secrete cartilage, whereas in lancelets, all three germ layer derived cells contribute to cartilage formation. It suggests that the endodermal pouch structure is the most evolutionarily primary structure in pharyngeal arch development (Graham et al., 2005). Moreover, it is noticed that alterations of the pharyngeal apparatus during the evolution of vertebrates highly correlate with modifications to the pharyngeal endoderm. Indeed, the number of arches is determined by the number of endodermal pouches. There is a general trend in the reduction of arch number; whereas lampreys possess nine arches developing from nine endodermal pouches, most teleosts have seven and this number is decreased to five in amniotes (reviewed by Graham et al., 2005). Altogether, evolutionary evidence strongly supports the hypothesis about the leading role of the endodermal pouch during pharyngeal arch development.

1.2.4 Role of endodermal pouches during neurogenesis in epibranchial placodes

The endodermal pouches do not only regulate cartilage formation but also induce neurogenesis of the pharyngeal arches. Pharyngeal arches are innervated by cranial nerves associated with sensory ganglia. The sensory ganglia are of dual embryonic origin; they derive from NCCs and neurogenic placodes (Ayer Le Lievre and Le Douarin, 1982; D'Amico-Martel and Noden, 1983). Originally, placodes are generated by focal thickening of ectoderm (Webb and Noden, 1993). They include dorsolateral placodes, which are close to the neural tube and epibranchial placodes, which are dorsally and caudally adjacent to the endoderm pouches (Webb and Noden, 1993; Begbie et al., 1999). In zebrafish, each placode is associated with a respective

pharyngeal arch: the facial placode with the second arch, the glossopharyngeal placode with the third arch, and four vagal placodes with the four posteriormost arches. It has been hypothesized that the induction of these two types of placodes (dorsolateral and epibranchial) is dependent on their proximity to the external signals from surrounding tissues. Begbie et al. (1999) has shown in chick that epibranchial placodes can be induced by endodermal pouches. The induction signal is shown to be Bmp7 secreted by endodermal pouches. This study also shows that epibranchial placode induction is strongly independent of NCCs. These authors show that upon the removal of NCCs before migration, the epibranchial placodes are still normally patterned. Recently, Holzschuh *et al.* (2005) have provided evidence in which the pharyngeal endoderm defective mutants *casanova* (*cas*, *sox23*$^{-/-}$) and *van gogh* (*vgo*, *tbx1*$^{-/-}$) exhibit failure in inducing epibranchial placodes but not dorsolateral placodes. They further show that BMP signaling (Bmp2b and Bmp5) from the endodermal pouches is required for epibranchial neurogenesis. Mosaic analyses on *cas* and *acerebellar* (*ace*, *fgf8*$^{-/-}$) mutants also suggest a role for pharyngeal endoderm during pharyngeal neurogenesis (Nechiporuk et al., 2005). Fgf3 and Fgf8 have been identified as important signalling molecules secreted by endoderm to regulate the process of epibranchial neurogenesis (Crump et al., 2004). Taken together, endodermal pouches may serve as a signalling centre providing cues for epibranchial placode induction, an important process during the pharyngeal arch development.

1.2.5 Endodermal pouch patterning and morphogenesis

Studies in mice suggest that retinoic acid synthetic enzyme *Retinaldehydespecific dehydrogenase type2* (*raldh2*) plays a role during patterning of the pharyngeal endoderm (Niederreither *et al.*, 1999; Wendling *et al.*, 2000). This mechanism may be conserved in zebrafish since *neckless* mutant (*raldh2*$^{-/-}$) is also

defective in the endoderm with a corresponding failure to form the caudal arches (Begemann et al., 2001). Moreover, a deficiency in vitamin A which results in the inactivation of retinoic acid signalling can cause malformed pharyngeal pouches in chick (Quinlan et al., 2002). Independent from retinoic acid signalling, the role of *tbx1* is also evident in pharyngeal endoderm patterning. Indeed, *vgo* (*tbx1*$^{-/-}$) mutant lacks all caudal endodermal pouches, and in turn all caudal pharyngeal arches are not formed.

Even when pharyngeal endoderm is patterned successfully into discrete initial out-pockets, if the pouches fail to enter the next step of morphogenesis then development of the pharyngeal arches will still be affected (Graham, 2001). The morphogenesis of the pharyngeal endodermal pouch is the process in which the pouch extends along the dorsoventral axis into a narrow slit-like shape. Throughout the extension process, it has been noticed that f-actin is highly accumulated and form actin cables covering the apical region of the inner surface of the pouch pockets, but not the outer surface or the interpouch endoderm (Quinlan et al., 2004). These actin cables are connected via N-cadherin-based adherens junctions. The importance of these actin cables has been established by blocking their formation with cytochalasin D, leading to disruption of the narrow slit-like morphology of the pouches. The cables may function in a mechanical manner by providing a constraining force to direct the movement of the double sided sheet of endodermal cells (Quinlan et al., 2004). Double reduction of Fgf8 and Fgf3 has been shown to regulate pharyngeal endoderm morphogenesis and affect formation of the pharyngeal cartilages (Crump et al., 2004).

1.3 Aims of study

Although *tbx2* has not yet been linked to any human disorders, developmental roles of this gene are being gradually discovered in animal models. This study was initiated with a desire to understand the role of *tbx2a* in the development of pharyngeal arches in zebrafish. Despite the high number of human birth defects affecting the face and neck, the genetic and molecular mechanisms responsible are largely unknown (Schoenwolf et al., 2009). We noticed that the pharyngeal expression of *tbx2* is conserved across species including mouse, chick, frog and fish (Chapman *et al.*, 1996; Gibson-Brown *et al.*, 1998; Hayata et al, 1999; Ruvinsky *et al.*, 2000; this study). Moreover, dysmorphic pharyngeal arches have been documented in *Tbx2* null mice (Harrelson et al., 2004) without detailed analysis. In view of the expression of *tbx2a* in the developing pharyngeal apparatus, we aimed for a functional analysis based on morpholino-based gene knockdown to answer the following questions:

(1) Does Tbx2a play a developmental role in the specification of pharyngeal arches?

(2) If it does, what is a specific role of *tbx2a* in endodermal pouches?

(3) Is *tbx2a* involved in specification of the NCC and mesodermal cores and further differentiation into cartilage?

(4) Does *tbx2a* play a role during differentiation of epibranchial placodes?

(5) Is *tbx2a* acting as an anti-apoptotic factor in the pharyngeal arches?

Chapter 2

Materials and Methods

2.1 Molecular applications

2.1.1. Isolation of total RNA from zebrafish tissue and RNA agarose gel electrophoresis

Fish embryos subjected to RNA isolation using RNeasy® mini kit (Qiagen, Germany) ranged from blastula stage to 5 dpf. 30 embryos without chorions were collected into 1.5 ml Eppendorf tubes without any trace of excess liquid. They were immediately disrupted in 50 µl of denaturing guanidine isothiocyanate (GITC, which inactivates RNases) containing buffer namely RLT with a disposable polypropylene pestle (Sigma). Another 300µl of RLT buffer was added into the tube and the total lysate was homogenized by passing through a syringe fitted with a 30-gauge needle (BD Biosciences). The procedure was continued according to the manufacturer's instructions with on-column DNase digestion using the RNase-Free DNase Set (QIAGEN, Germany). First, the lysate was spun down and the supernatant was transferred to 350 µl of 70% ethanol for binding onto the RNeasy mini spin column. The column was washed with 350 µl of RW1 buffer before addition of 80 µl of RNase-free DNAse (QIAGEN, Germany) incubation mix and allowed to stand at RT for 15min. The DNase digestion was followed by washing with 350 µl RW1 buffer and 500µl of RPE buffer. Total RNA was eluted in 40µl of RNase-free water and then aliquoted to be stored at –20ºC for further use.

Total RNA integrity could be checked by 1.8% native agarose gel electrophoresis in 1X TBE buffer (0.089 M Tris Base, 0,089 M Borate and 0,002 M EDTA, pH 8.0). RNA sample was denatured in Gel Loading Buffer II (Ambion, USA) containing 95% formamide, 18 mM EDTA, 0.025% xylene cyanol, 0.025%

bromophenol blue, 0.025% SDS at $+80^0$C for 5 minutes, followed by quenching on ice for 2 minutes before being loaded to the wells.

2.1.2 Determination of DNA and RNA concentration

1.7µl of purified RNA or DNA was taken for quantification by optical density reading of the absorbance at 260 nm (A_{260}) in a spectrophotometer ND-1000 UV/Vis (NanoDrop Technologies). The ratio between the absorbance values at 260 and 280 nm gives an estimate of DNA and RNA purity. Pure DNA usually has an A_{260}/A_{280} ratio of 1.8-1.9 in 10 mM Tris-HCl, pH 8.5, while pure RNA has an A_{260}/A_{280} ratio of 1.9-2.1 in 10 mM Tris-HCl, pH 7.5.

2.1.3 One step RT-PCR

Qiagen® OneStep RT-PCR kit (QIAGEN, Germany) contains a formulated combination of recombinant heterodimeric enzymes of Omniscript and Sensiscript reverse transcriptases, and is chemically modified HotStar Taq DNA polymerase. This kit was used to perform cDNA synthesis and subsequent PCR together in one PCR tube using the following program:

Step 1: cDNA synthesis at 50°C for 30 min

Step 2: Initial PCR activation at 94°C for 15 min

Step 3: Amplification for 25-35 cycles of

- Denaturation: 94°C for 45 sec
- Annealing: 55 to 63°C for 45 sec (vary according to particular primers)
- Extension: 72°C for 30 sec to 2 min (1 min for each 1 kb)

Step 4: Final extension at 72°C for 10 min

The reaction mix was composed of 100 µg of total RNA, 5 units RNAse inhibitor, 2 mM dNTP mix (400 µM of each dNTP), 0.6µM of each primer, 5X

QIAGEN OneStep RT-PCR Buffer containing 12.5 mM $MgCl_2$, and water was added to make up 50µl of total reaction mix.

2.1.4 Preparation of genomic DNA

In this study, genomic DNA was isolated from zebrafish embryos for the purpose of checking nucleotide sequence of intron-exon junctions in order to design morpholino oligos. 20 embryos at 1 dpf were collected and lysed in 500 µl of lysis solution [7 M Urea, 0.3 M NaCl, 0.02 M EDTA, 0.05 M Tris-HCl, pH 8.0, 1% N-lauroylsarcosine]. The lysate was then incubated at $+37^0$C for 30 minutes. An equal volume of phenol/chloroform/isoamyl alcohol (25:24:1) (Fluka) was added and followed by additional extraction with an equal volume of chloroform (BDH). Genomic DNA was precipitated with an equal volume of 2-propanol (Merck), washed with 70% ethanol (Merck). The precipitate was allowed to dry and resuspended in an appropriate volume of 10 mM Tris-HCl, pH 8.5. 1 µl of genomic DNA was taken for quantification by optical density reading using Nanodrop/spectrophotometer (UV-1601, Shimadzu, Japan). It was then aliquoted and stored at –20ºC for further use.

2.1.5 Standard PCR

Template DNA used for PCR can be genomic DNA, plasmid constructs or from single bacterial colonies. Reactions were performed in Programmable Thermal Controller PTC-100 (MJ Research Inc. USA) according to established protocol using the HotStarTaq® DNA Polymerase Kit (QIAGEN, Germany). For PCR products of high fidelity and high specificity from genomic and plasmid DNA, Expand High Fidelity PCR System (Roche Applied Science, Germany) was used. The reactions were carried out for 35 cycles.

Step 1: Denaturing at 94°C for 2 min

Step 2: Amplification for 30-35 cycles of

- Denaturation: 94°C for 45 sec
- Annealing: 55 to 63°C for 45 sec (vary according to particular primers)
- Extension: 72°C for 30 sec to 2 min (approximately 1 min for each 1 kb)

Step 3: Final extension at 72°C for 5 min

The reaction samples were stored at 4°C until further analysis or directly subjected to purification using QIAquick PCR Purification Kit (QIAGEN, Germany). 5 volumes of Buffer PB were added to 1 volume of PCR mix, and applied onto a spin column. After washing with 0.75 ml of Buffer PE, the purified PCR product was eluted with 20-30 μl of sterile water or TE buffer and stored at –20ºC for further use.

2.1.6 Restriction endonuclease digestion of DNA

Restriction enzyme digestion was employed for digesting PCR products and plasmids for cloning, screening recombinant clones, and linearizing plasmid constructs of cDNA fragments for probe synthesis. All the restriction enzymes used in the study were purchased from New England Biolabs or Promega (USA). Most of the digestions were performed at 37°C or 25°C for 2 hours, with proper restriction buffers, with or without BSA according to manufacturer's instructions. One unit of enzyme was used to digest 1 μg of plasmid DNA. For thorough digestion of DNA fragments e.g. for cloning, a further dilution of enzyme was made (20 times instead of the standard of 10 times) and incubation time was extended to 6 hours. After digestion, CIP (calf intestinal alkaline phosphatase) was added to the reaction mix to prevent recircularization or religation of linearized plasmid by dephosphorylation of the 5-phosphorylated ends of DNA.

2.1.7 Agarose Gel Electrophoresis of DNA

A mixture of different DNA fragments can be separated and checked and on 1% agarose gel. The agarose powder was dissolved in 1X TAE (0.04M Trisacetate; 0.001M EDTA) by heating. After the solution was cooled to 60°C, ethidium bromide was added to a final concentration of 0.5 μg/ml before the agarose gel was casted. DNA samples were mixed with loading dye [(0.25% (w/v) Bromophenol blue, 0.25% (w/v) Xylene cyanol FF, 15% (v/v) Ficoll Type 4000, 120 mM EDTA in H_2O] and loaded to the wells of the gel submerged in 1X TAE. Voltage of 1-5 V/cm was applied during the electrophoresis. 1 or 10 kb DNA ladder molecular weight marker (New England BioLabs, Inc.) was loaded in parallel with the DNA samples to determine approximate size of DNA fragments.

2.1.8 Recovery of DNA fragments from Agarose gel

DNA fragments of interest were excised and purified using the QIAquick Gel Extraction Kit (QIAGEN, USA) according to the manufacturer's instructions. The DNA fragments could be PCR products, linearized plasmids, or digestion products. Briefly, 3 volumes of buffer QG was added to each volume of agarose and incubated at 50 °C until the gel slice had completely dissolved and then loaded into a QIAquick spin column. The column was washed with 0.75 ml of Buffer PE before being eluted with 30 μl of H_2O to obtain purified DNA fragment and the DNA stored at -20°C.

2.1.9 DNA ligation

The PCR products generated with Taq polymerases which have an extra Adnosine nucleotide added to both ends were ligated into the pGEM®-T Easy vector (Promega, USA) which contains Thymidine nucleotides at both ends. Reaction was mixed according to manufacturer's instructions and carried out overnight at $+4^0$C. For

the ligation of both blunt and cohesive ended DNA fragments into other vectors, we used T4 DNA ligase (New England BioLabs, Inc.) with supplied buffer. The reactions were carried out overnight at $+16^0$C. For blunt end ligation, ligase enzyme was increased to 10 times in comparison with that in cohesive-end ligation. The insert:vector molar ratio was set at at least 3:1.

2.1.10 Transformation

To prepare competent cells (*E.coli* strain XL1-Blue or DH5α), a single host bacterial colony was picked and cultured in 3 ml LB, overnight at 240 rpm, 37°C. 0.2 ml of the saturated culture was next inoculated into 50 ml LB in a 500 ml flask at 37°C, 240 rpm until it reached exponential phase when A_{600} is approximately 0.5 (approximately 3 hrs). The bacterial culture was harvested by centrifugation at 5000 rpm for 10 min at 4°C. The cell pellet was re-suspended in 5 ml of ice-cold TSB solution [85% (v/v) LB broth, 5% (v/v) DMSO, 10% (w/v) PEG (Av molecular weight 3,350), 10 mM $MgCl_2$, 10 mM $MgSO_4$] and incubated on ice for 10 minutes before use. 200 µl of the freshly made competent cells was used in each transformation reaction. The rest was transferred into 1.5 ml tubes in aliquots (100 µl each) and snap-frozen in liquid nitrogen. These aliquots can be stored at -80°C up to several months.

Transformation was carried out with ice-chilled 2 µl out of 10 µl of ligation reaction added into an aliquot of competent cells and mixed by gentle pipetting. After placing on ice for 30 min, cells were heat shocked by placing tubes into a $+42^0$C water bath for 90 secs and immediately back on ice for 2 min. To allow the bacterial cells to recover, 900 µl pre-warmed LB medium containing 20 mM glucose was added to the cells and placed on a shaker at 250 rpm, 37^0C for 1 hour. For

transformation of plasmid constructs, that recovery step was omitted. Next, the bacterial culture mix was then spun down and the pellet was re-suspended in 300 µl. It was then split into 1/10 and 9/10 portions and plated onto two separate LB plates supplemented with appropriate antibiotics in order to obtain proper density of transformant colonies. For blue/white screening of recombinants, 40 µl of 20 mg/ml Xgal and 10 µl of 0.1 M IPTG were added to the bacterial suspension before being plated onto LB agar plates. The following day, colonies were picked for screening of the insertion by PCR. One primer from the plasmid vector, and the other from the insert were used to amplify the inserted fragment. PCR products were checked with agarose gel electrophoresis to visualize the insert with the desired orientation. To avoid false positives, the number of PCR cycles was limited to 30.

2.1.11 DNA sequencing reaction

DNA sequencing was performed using BigDye™ Terminator chemistry. The reaction mix included 4 µl of Terminator Ready Reaction Mix, 200-500 ng of double strand DNA, and 1 µl of either forward or reverse primer (0.2 µg/µl), with water in a total volume of 10 µl. PCR was performed on PTC-200 Peltier Thermal Cycler (MJ Research) with the following cycle sequencing conditions: (1) 96^0C, 1 min; (2) 96^0C, 10 secs; (3) 50^0C, 10 sesc; (4) 60^0C, 4 min. Steps 2 to 4 were repeated 25 times. Ramp between steps 2, 3 and 4 was 1^0C/sec. Post cycle sequencing purification was performed using DyeEx™ 96 Kit (QIAGEN, Germany). Sequenced products were separated and analyzed using ABI 3700 Automated DNA Sequencer (PE Applied Biosystems, USA).

2.1.12 *In vitro* synthesis of 5' capped mRNA

Tbx2a full-length cDNA was cloned into the pGEM-T Easy vector and sub-cloned into expression vector **pFLAG-*CMV*™-*5a***. Template plasmid DNA was thoroughly linearized with the appropriate restriction enzyme downstream of the insert and subsequently checked with agarose gel electrophorensis before being purified with the QIAquick PCR Purification Kit (QIAGEN, Germany).

The mMESSAGE mMACHINE® Kits (Ambion, USA) was use to synthesize capped mRNA *in vitro* in 20 µl total volume [1 µg linearized plasmid, 2X NTP/CAP, 10X buffer, and the appropriate enzyme, i.e., either SP6, T7 or T3 RNA polymerase]. The synthesized mRNA was purified with the RNeasy® Mini Kit (QIAGEN, Germany) according to RNA Cleanup protocol. The size and integrity of synthesized mRNA was examined by agarose gel electrophoresis.

2.1.13 *In vitro* synthesis of labeled antisense RNA

Antisense RNA labelled with fluorescein-12-UTP (FITC) or digoxigenin-11-UTP (DIG) was synthesized *in vitro* using the MEGAscript® Kits (Ambion, USA). A mixture of 1 µg linearized DNA template, 4 µl 10X DIG or FITC RNA Labeling Mix (Roche Applied Science, Germany), 2 µl appropriate enzyme mix (either T3, T7 or SP6) and 2 µl 10X reaction buffer, 0.25 µl of RNase inhibitor (40 U/µl) (Promega, USA) in a total volume of 20 µl was incubated at $+37^0$C for 4 hours. The size and quality of synthesized RNA was checked by agarose gel electrophoresis. After confirmation of RNA fragment on agarose gel, 1 µl RNase-free DNase was directly added to stop reaction by digesting the template DNA at $+37^0$C. After 15 minutes of DNA template digestion, synthesized antisense RNA was purified using the RNeasy® Mini Kit (QIAGEN, Germany). In brief, the sample volume was topped up to 100 µl

with RNase-free water. RLT buffer with β-mercaptoethanol was added and mixed gently. It was subsequently mixed with 250 µl of 96-100% ethanol. The mixture was then applied onto RNeasy mini spin column. After a spin down, the column was washed with 500 µl of RPE buffer. The RNA was eluted with 30-50 µl of Rnase-free water and stored at -80°C.

2.1.14 Design of Antisense Oligonucleotides (morpholinos)

Morpholino oligos (MOs) obtained from Gene Tools, LLC are short chains of Morpholino subunits. Each subunit is comprised of a nucleic acid base, a morpholine ring and a non-ionic phosphorodiamidate intersubunit linkage. Morpholinos act via a steric block mechanism (RNAse H-independent) and with their high mRNA binding affinity and exquisite specificity they yield reliable and predictable outcomes. Designing of morpholinos in this study were optimized according to manufacturer guidelines: (1) Standard length of Morpholinos is 25 nucleotides with minimal self-complementarity (less than 4); (2) There are no more than 7 total guanines or more than 3 contiguous guanines in a 25-mer oligo for water solubility; (3) Negative control MOs with 4 or 5 base~~s~~ changes in the experimental design is sufficient to eliminate specific binding activity; (4) To minimize the possibility of non-specific effects, 3 MOs complementary to non-overlapping sequences of the studied gene were designed. MO sequences are listed in Table 1.

MOs were resuspended from lyophilized powder, and then diluted to a 1 mM stock in 1X Danieau's solution and stored at -80°C. The MOs were diluted to the appropriate concentration and these were injected according to the injection protocol described in section 2.2.2.

Prior to synthesis, all the sequences of MOs designed were double checked carefully by sequencing the genomic fragments containing those MO binding sites.

2.2 Embryological applications

2.2.1 Fish maintenance

Zebrafish (*Danio rerio*) were raised and maintained in the fish facility of the Institute of Molecular and Cell Biology (Singapore) according to instructions by Westerfield (1995). Fish were fed three times per day with brine shrimps and the photoperiod cycle was kept for 14 hrs of daylight and 10 hrs of darkness. Crosses were set after the third meal of the day in the evening with dividers which were removed the following morning to stimulate spawning behaviour. Embryos were then collected with a sieve, rinsed gently and then kept in 1X egg water (10% NaCl, 0.3% KCl, 0.4% $CaCl_2$, 1.63% $MgSO_4$) at 28.5^0C. Live embryos were staged by examination under a dissecting stereomicroscope (Leica, Germany) according to Kimmel et al. (1995). To inhibit pigment formation 0.2 mM 1-phenyl-2-thiourea (PTU) was added to the egg water at 16 hours post fertilization but not later than 22 hpf. For anesthetizing, 0.2% solution of 3-aminobenzoic acid ethyl ester, containing Tris buffer, pH 7.0, was used. This study used the wild type AB strain (Oregon), the mutant line *oep*^{z1} (Zhang et al., 1998), and the transgenic line ET ET33-1B produced from enhancer trap screening (Parinov et al., 2004).

2.2.2 Microinjection into 1-cell stage embryos

Injection needles were pulled from borosilicate glass capillaries with 0.50 mm internal diameter and filament (Sutter Instruments, BF100-50-10) using a Flaming/Brown micropipette puller (Sutter Instruments Co, P-97). The needles were clipped with a blade to an appropriate opening for desired injection volumes. The

needle was plugged into a needle holder connected to a nitrogen-fed picolitre gas injector (PLI-100, Havard Apparatus, Medical Systems Corp., USA). All the injections were performed manually for quick and flexible manipulation.

For 1-cell stage embryos, the injection volume was always set to a maximum dose of 2 nl/embryo. Morpholinos and mRNA samples were diluted at desired concentrations in 1X Danieu solution (58 mM NaCl; 0.7 mM KCl; 0.4 mM $MgSO_4$; 0.6 mM $Ca(NO_3)_2$; 0.5 mM HEPES, pH 7.6). Fertilized eggs with chorions were placed on a glass slide and stabilized by withdrawing excess water with laboratory lint-free tissue paper (KimWipes). Solutions were injected into the cytoplasmic stream of 1-2 cell stage zebrafish embryos using a MPPI-2 pressure injection system (Applied Scientific Instrumentation, USA), under dissecting microscope. Injected zebrafish embryos were raised in 1X egg water.

2.2.3 Single cell microinjection at 16-cell stage

An agar moulded chamber with multiple wells (1.5 mm per well) for single cell injection was made with 2% agarose in 1X egg water. It can be kept at 4°C for re-use. Fertilized eggs were allowed to develop to 4-cell stage and then gently dechorionated with a pair of 25-gauge needles. A glass pipette was used to transfer dechorionated embryos (20 embryos) into the wells, which were filled with egg water earlier. All the embryos were oriented such that the blastomeres faced the right side (for right handed persons). Injections were performed free-hand, i.e. without the aid of a micromanipulator. Injection solutions included 70 kD fluorescein dextran dye as a tracer with or without mRNA. For single blastomere, injection volumes do not exceed 200 pl. The embryos were then transferred into agarose-coated plates with 1X egg water and observed under a UV dissecting microscope to remove improperly injected embryos. Thereafter, embryos were allowed to develop at 28°C to the desired stages.

2.2.4 Use of Anesthetic to Immobilize Embryos

Live embryos older than 19 hpf are able to twitch and move so that affects the process of imaging. To facilitate mounting and imaging, Tricaine (3-amino benzoic acidethylester) was used to anesthetize the embryos. Tricaine solution was made by dissolving 400 mg of Tricaine (Sigma, USA) powder in 97.9 ml of sterile water and the pH was adjusted to 7 using Tris pH 8.0. For final solution, 5 µl of Tricaine solution was added into a 6 cm Petri dish with selected embryos in egg water. The embryos were immobilized shortly and ready for manipulation.

2.2.5 Embryo collection and fixation

Zebrafish embryo develops in a chorion which was removed manually with a pair of 26-gauge hypodermic needles. Embryos were then collected into 1.5 ml tube and placed on ice for 10 min before being fixed with 4% PFA (paraformaldehyde) /PBS (0.8% NaCl; 0.02% KCl; 0.0144% Na_2HPO4; 0.024% KH_2PO4, pH 7.4) for 6 hours at room temperature or overnight at 4°C. Embryos younger than 15 hpf were dechorionated after fixation. The embryos were then washed with PBST (0.1% Tween-20 in PBS) twice for 1 min each followed by four thorough washes, 20 min each on Nutator (CLAY ADAMS® Brand, Becton Dockinson, USA) at room temperature. After this step, embryos are ready for cryostat sectioning. For whole-mount immunostaining, embryos were treated for 10 to 20 minutes in -20°C pre-chilled acetone prior to incubation with antibodies.

2.2.6 Proteinase K treatment

For embryos older than 14 somites (16 hpf), proteinase K treatment is required to enhance permeability of the tissue by partially digesting cellular proteins. Efficiency of proteinase treatment depends on the size of embryos, treatment duration

(since surface tissues are digested better than the deeper tissues), as well as batches of enzyme. For each new batch, the enzyme efficiency was determined by testing on embryos of different stages for different durations. The standard protocol suggested 10 μg/ml proteinase K. However, we found the treatment with 7.5 μg/ml proteinase K for extended durations gave a better result. Basically, embryos at 24, 30, 48 and 72 hpf were exposed to 7.5 μg/ml proteinase K solution for 10, 20, 30 and 40 min respectively. To stop the proteinase K reaction, the proteinase K solution was completely removed, and the embryos were fixed again in 4% PFA/PBS for 1 hour at room temperature. Embryos were then washed carefully in PBST twice for 1 min each and four times for 20 min each. After this step, embryos can be used for *in situ* hybridization (ISH) and Alcian Blue staining.

2.2.7 Prehybridization

500 μl of prehybridization buffer [50% formamide; 5X SSC; 50 μg/ml heparin; 500 μg/ml tRNA; 0.1% Tween-20; pH 6.0 (adjusted by citric acid)] was used for 30 embryos in each 1.5 ml tube. Tubes were placed into a circulating water bath (Julabo, Germany) set at 68°C. Incubation time was at least 4 hrs but not longer than overnight, otherwise embryos turned brownish. The prehybridized embryos can be kept in -20°C up to 3 months.

2.2.8 Hybridization

Probe sensitivity may vary from gene to gene. However, for most probes used in this study, probe concentrations were standardized by one formula which is according to our own observation. For each hundred μl of hybridization solution, amount (ng) of DIG-labelled probe was calculated by multiplying the probe length (Kilo base pairs) and 100. For example, if a probe is 3 Kilo base pairs, then 300 ng of

that probe was used for each hundred μl of hybridization solution. For fluorescein-labelled probe, the amount was slightly increased.

Probe in hybridization solution was denatured by incubation at 80°C for 5 min, followed by 5 min on ice. 15 selected embryos were placed in a 1.5 ml Eppendorf tube with the original prehybridization solution removed and replaced with hybridization solution. The reaction was incubated overnight at 68°C in a circulating water bath. The following morning, the embryos were incubated in four changes of washing solution containing a decreasing percentage of formamide in 2X SSCT (each wash solution contains 25% less formamide than the previous one). All washes were performed in the 68°C water bath for a period of 15 min per wash. This was followed by the fifth wash with 2X SSCT without formamide for 30 min. The two final washes were with 0.2X SSCT at 68°C for 15 min each.

Subsequently, the embryos were washed twice with PBST (PBS with 0.1% Tween20) at room temperature for 5 minutes each.

2.2.9 Preparation of Preabsorbed Anti-DIG and Anti-Fluorescein Antibody

To decrease the staining background and to increase signal-to-noise ratio, sheep anti-DIG-AP and anti-Fluorescein-AP antibodies (Boehringer Mannheim, Germany) were diluted to 1:200 and 1:50 respectively in MAB [Maleic Acid Buffer; 0.1 NaCl, 0.15 M maleic acid, pH 7.5, 0.1% Tween-20] containing 5% blocking reagent (Roche, Germany) and incubated with disrupted pieces of 4% PFA fixed zebrafish embryos on a nutator at 4°C overnight. The mixture was then spun down, and the antibody contained supernatant was transferred to a new tube and stored as stock solution in 4°C up to 3 months. Working solution was made by further dilution to 1:3000 for anti-DIG-AP antibody and 1:500 for anti-Fluorescein-AP antibody with

PBS in 5% blocking reagent (Roche Applied Science, Germany), 10 µl of 0.5 M EDTA (pH 8.0) and 5 µl of 10% sodium azide in a final volume of 10 ml to prevent bacterial growth. Used antibody solution was stored at 4°C and can be reused several times.

2.2.10 Incubation with pre-absorbed antibodies

Embryos from previous washing step were transferred from 68°C water bath onto the nutator and subjected to two washes with MAB prior to incubation with blocking solution [5% blocking reagent in MAB] for 2h at RT or overnight at 4°C. After removing the blocking solution, the embryos were incubated with preabsorbed antibody at 4°C overnight.

2.2.11 DIG or Fluorescein Staining

The following day after antibody incubation, the antibody solution was transferred into another tube and stored in 4°C for reuse. Embryos were then washed 4 times, 20 min each in MAB on the nutator at RT. This was followed by 3 washes of 5 min each in detection buffer (100 mM Tris pH9.5, 50 mM $MgCl_2$, 100 mM NaCl, 0.1% Tween-20). *In situ* signal for alkaline phosphatase can be detected with NBT-BCIP (Sigma-Aldrich, USA) or fast red tablet (Roche Biochemicals, Switzerland). NBT-BCIP color substrate development was performed in the presence of 0.3375 µg/ml of nitroblue tetrazolium (NBT) and 0.175 µg/ml of 5-bromo, 4-chloro, 3-indolil phosphate (BCIP) dissolved in detection buffer. Fast red staining solution was prepared by dissolving 1/2 of the fast red tablet (Roche Biochemicals, Switzerland) in 1 ml detection buffer (100 mM Tris pH8.2, 50 mM $MgCl_2$, 100 mM NaCl) and clarified by centrifugation before mixing with an equal volume of Naphthol AS-MX phosphate (Sigma, MO, USA) solution (500 µg/ml in fast red detection buffer).

Colour development was kept in the dark at RT and monitored occasionally under light microscopy until the desired intensities were achieved. The staining reaction was stopped by a 2X 5 min PBS wash followed by 4% PFA fixation for a minimum period of 30 min before storing the appropriately stained embryos in PBS containing 50% glycerol overnight for further processing such as whole-mount imaging or cryostat sectioning.

2.2.12 Two-colour whole mount *in situ* hybridization

For two-colour whole mount Akaline Phosphatase based *in situ* hybridization, two distinct RNA probes labelled with DIG or Fluorescein with the a ratio of 1.5:1 Fluorescein to DIG (since Fluorescein detection is less sensitive than DIG) were applied on the same embryos. The hybridization step was performed prior to the DIG detection as described in section 2.2.8. Thereafter, NBT-BCIP staining buffer was removed and the embryos were washed with MAB twice for 10 min. To inhibit the phosphatase activity of anti-DIG antibody, the embryos were incubated with glycine buffer (0.1 M, pH 2.2) for 1 hour at RT.

To develop the second colour, the embryos were first washed with MAB four times for 10 min each and then incubated in blocking buffer (5% Blocking reagent in MAB at room temperature for 1 hr. Embryos were subsequently incubated with anti-Fluorescein-AP antibody overnight at 4°C. The following day, embryos were washed with MAB prior to detection step with Fast Red in pH 8.2 buffer as described in section 2.2.11. The stained embryos were also stored in PBS containing 50% glycerol at 4°C.

2.2.13 Whole-mount Immunohistochemical staining

After fixation with 4% PFA/PBST, additional treatment with -20ºC cold acetone (to remove lipids from cell membrane) for 5 minutes was done to improve the penetration of antibodies into the tissue. The embryos were then washed rapidly with deionised water once and PBST three times, 10 minutes each. This was followed by two washes in MAB, 20 min each and blocked with 5% blocking reagent for 1 hr on a nutator at RT. Primary antibodies were not pre-absorbed. They were diluted 1:200 (or as recommended by the manufacturer) in MAB containing blocking solution. For double colour staining, the two primary antibodies added at the same time must be raised in different species (e.g one from mouse and the other from rabbit). The incubation with selected embryos was on the Nutator at 4°C overnight. The following day, the embryos were washed 4 times, 20 min each in MAB, pH7.4 prior to incubation with the appropriate secondary antibodies (1: 200 dilution) which were pre-adsorbed in MA blocking solution. Secondary antibodies used were Alexa Fluor 488 F(ab')2 fragment of goat anti-mouse/rabbit IgG and/or Alexa Fluor 594 F(ab')2 fragment of goat anti-mouse/rabbit IgG (Invitrogen) (1:500). Incubation was done overnight at 4ºC or 2-3 hours at RT, in the dark. The staining of secondary antibody labeled with fluorescent Alexa Fluor dye was monitored under a fluorescence dissection microscope. Alexa Fluor 488 was observed under a blue filter (450-490 nm), and Alexa Fluor 594 was observed under a yellow filter (546 nm). When it reached the desired intensity, the embryos were washed two times with MA buffer, pH7.4 on a nutator at RT and fixed in 4% PFA/PBST for 1 hour. Thereafter, embryos were stored in 50% glycerol in PBS and ready for con-focal imaging.

2.2.14 Alcian Blue Cartilage Staining

Adopted from Neuhauss (Neuhauss et al., 1996), the Alcian Blue staining protocol was modified accordingly. Embryos at 3, 4 or 5 dpf (without pigments by PTU treatment) were collected into 1.5 ml tube and kept on ice for 10 min. After removing excess water, embryos were fixed in 4% PFA/PBST on nutator overnight at 4°C or 6 hours at RT. After washing in PBST 4 times, 20 min each, embryos were digested with proteinase K (as described in section 2.2.6) for better exposure of the cartilage elements to the dye. Next, embryos were briefly fixed with 4% PFA and extensively washed with PBST. The treated embryos were then stained for 4 hours in 0.1% Alcian Blue dissolved in acidic ethanol (70% ethanol, 5% concentrated hydrochloric acid). Stained embryos were then washed extensively in acidic ethanol, re-hydrated and stored in PBS containing 50% glycerol before photography.

2.2.15 Cryostat section

Caps of 1.5 ml Eppendorf tubes were cut out and used as containers for mounting the stained or fixed embryos (without trace of excess liquid) in 50°C pre-warmed 1.5% bactoagar containing 5% sucrose in PBS. A common syringe needle was used to position the embryo while the agar solidified. The agar block was then picked out and cut into a pyramid shape with a razor blade. The block was then transferred into 30% sucrose solution and allowed to stand at 4°C overnight or until the agar block sank to the bottom of the tube. Next, the block was taken out and excess liquid was absorbed with tissue paper before being placed on the surface of a layer of frozen tissue freezing medium (Reichert-Jung, Germany) on a pre-chilled tissue holder. It was then coated with one drop of freezing medium (without bubbles) and frozen in liquid nitrogen until the block had solidified completely. The frozen block was placed into a cryostat chamber (Leica, Germany) for 30 min to be

equilibrated with the temperature of the chamber which is at –25ºC. 10 to 15 μm thick sections were cut with Leica CM1900 Cryostat machine (Leica, Germany). The sections were collected onto pre-warmed Polysine™ slides (Menzel-Glaser, Germany) which were then dried on a 42°C hotplate for 30 min. The sections were briefly rinsed with PBST and ready for further processing (e.g Tunel staining), otherwise a cover slip was placed on the slide with several drops of 50% glycerol/PBS and sealed with nail polish.

2.2.16 Cell death assay by Tunel staining

TUNEL in situ cell death detection kit, florescein (Roche) involves labeling of the 3'-hydroxyl DNA ends generated during DNA fragmentation by means of terminal deoxynucleotidyl transferase (TdT) and labeled dUTP (fluorescein). It was used on cryostat sections of 3 dpf embryos or 2 dpf wholemount embryos.

The embryos were collected and fixed in 2% PFA ON at 4°C. After washing off PFA with PBST (PBS with 0.1% Tween 20), embryos were subjected to sectioning as described in section 2.2.15. Section specimens collected on Polysine™ slides (Menzel-Glaser, Germany) were fixed again in 2% PFA at RT for 1 hour before Tunel assay. Specimens were prepared for one set of negative control and one set for experiment. It was followed by a dehydration step by dripping onto the slides with 50%, 70%, 95% and 100% Methanol (in PBS); each solution was kept on the slides for 5 min. It was followed by 3 washes with PBST, 5 min each. Specimens were then permeabilized in freshly made 0.1% Sodium Citrate in PBST for 15 min, at RT. After washing with PBST 3 times, the specimens were ready for detection step. For wholemount embryos, incubation in 100% acetone at -20°C for 10 min and proteinase K treatment are required prior to permeabilization.

Specimens especially cryo-sections were first coated with BigDye™ mix (used for gene sequencing) to block unspecific binding of the enzyme. Thereafter, the TUNEL mix [450 µl labelling solution, 50 µl enzyme] was applied onto the specimens and the reaction was kept in the dark. After 30 min, they were checked under a dissecting microscope with UV. Wholemount embryos are required longer time of staining. Until the desired signal was obtained, the specimens were fixed with 2% PFA prior to imaging.

2.2.17 Photography Using Upright Light Microscope

To facilitate whole mount photography, a chamber was made by placing 2 stacks of 1-5 small cover glasses, which are held together with a tiny trace of Permount in between, on both sides of a 25.4 x 76.2 mm microscope glass slide. A selected embryo was transferred to the chamber in a small drop of 50% glycerol/PBS. All the manipulations on the embryo were done with a needle fit into a syringe. A 22 x 44 mm cover slip with a small drop of the same buffer was placed over the embryo. The orientation of the embryo was adjusted by gently moving the cover slip.

Embryos which were previously treated with proteinase K and stored in 50% glycerol/PBS were easily detached from the yolks by needles therefore could be mounted as flat specimens. For Alcian blue stained embryos which were injected with 70kD fluorescein dextran dye, the pharyngeal apparatus was isolated and also mounted as a flat specimen. A glass pipette with a blunt opening, achieved by brief exposure to a Bunsen flame, was used to transfer the specimens onto a slide. A small fragment of cover slip (approximately 3 x 3 mm) was cut and carefully put over the specimen without introducing bubbles. Excess water was withdrawn with tissue paper. Photos were taken using a camera mounted on an AX-70 microscope (Olympus, Japan) or an Axiophot2 photomicroscope (Zeiss, Germany) with software

supplied by the manufacturers or Kodak Gold 400ASA film. For imaging of the 70 kD fluorescein dextran dye labelled pharyngeal apparatus, the specimens were visualized with a Leica MZ FLIII stereomicroscope (Leica, Germany) equipped for UV epifluorescence viewing. Overlapping of images and measuring of relative areas were performed using Adobe® Photoshop CS2.

2.2.18 Photography using Confocal Microscopy

For live confocal imaging, embryos were anesthetized as described in section 2.2.4. One or several of them were transferred to a 35 mm external diameter dish with 12 mm internal, optical clearance (1 mm deep well). They were then mounted by pipetting 0.5% low-temperature melting agarose with 0.016% tricaine and PTU. Embryos mounted in the imaging chamber still maintained heartbeat and circulation throughout the imaging period.

Confocal images were acquired using a Zeiss LSM510 scanning laser (Carl Zeiss Inc., Germany) using 488 nm excitation and 510-550 nm band-pass filters. Serial optical sections were taken at desired intervals using a 10X Plan-Neofluar 0.3 objective. Raw image collection and processing were performed using the LSM510 Software (Carl Zeiss Inc., Germany). Combined images were made on Adobe® Photoshop CS2.

2.3 Cloning of *tbx2a* gene

The full-length *tbx2a* was cloned with a pair of primers (table 2) which were based on the sequence published by ENSEMBLE project (**http://www.ensembl.org**), transcript ID **ENSDART00000024207**, at **Chromosome 5: 50,031,583-50,038,526** reverse strand,t

http://www.ensembl.org/Danio_rerio/Transcript/Exons?db=core;g=ENSDARG00000018025;r=5:50031583-50038526;t=ENSDART00000024207. The fragment amplified by Taq polymerase was cloned into pGEM® T Easy (Promega, USA) by A-T ligation. The construct was then used for probe synthesis. To make a construct for mRNA synthesis, *tbx2a* full-length fragment without the stop codon was subcloned into expression vector **pFLAG-*CMV*™-*5a***.

We used the BLAST program (Altschul et al., 1990) on the NCBI web server (**http://www.ncbi.nlm.nih.gov**) for checking cloned sequences. Sequences were managed and manipulated with DNASTAR Lasergene v6.0 software (DNASTAR Inc.). ImageJ software was used to estimate dot intensity for DNA bands on agarose gel picture. Motif search was done with MyHits© 2003-2009 (**http://myhits.isb-sib.ch/cgi-bin/clustalw**).

Table 1: Sequences of Morpholino oligos designed and used for *tbx2a* gene

	MOs	**Sequences**	**Purposes**
1	I1e2	GGAAACATTCTCCTATGGACGAAAG	Target acceptor site at intron 1
2	I1e2 mismatch	cGAAACAcTCgCCTAcGGACcAAAG (lower cases denote replaced bases)	Mismatch control for i1e2
3	E1i1	AGACCTTACCTTCCTGATTTAGTGA	Target donor site at intron 1
4	I5e6	TTGTCTTCTGGAAAAACAAATGTTA	Target acceptor site of intron 5
5	p53 MO	GCGCCATTGCTTTGCAAGAATTG (Langheinrich et al., 2002)	Target ATG

Table 2: Sequences of primers for cloning *tbx2a* gene and for verifying MOs

	Primers	**Sequences**	**Purposes**
1	4Tbx2a(-3)Fw61	GCTATGGCTTATCACCCTTTTC	Forward primer to amplify full length tbx2a
2	4Tbx2aRv60	GAAGTTTTGCGCTTTATGTCACA	Reverse primer to amplify full length tbx2a

Chapter 3

Results

"*Tbx2a* is required for development of pharyngeal arches"

3.1 Cloning *tbx2a* cDNA

A fragment containing the full-length *tbx2a* (approximately 2.1 kb) was cloned based on sequence information obtained from the Ensembl database http://www.ensembl.org/Danio_rerio/Gene/Summary?g=ENSDARG000000018025). This sequence was subsequently compared with that stored in the NCBI database (http://www.ncbi.nlm.nih.gov). Blast result shows the fragment is mapped to Locus NW_001879028 with 7 hits (7 exons), *Danio rerio* chromosome 5 genomic contig, reference assembly based on Zv7_scaffold474 (Griffiths-Jones, 2006; Griffiths-Jones, 2004; Lowe and Eddy, 1997),

http://www.ncbi.nlm.nih.gov/entrez/viewer.fcgi?list_uids=189519532. The identity rates are 99% for the first two hits (first two exons) and 100% for the last five hits (last five exons). The sequences of the first two hits were confirmed by sequencing the fragment containing the first two exons. Tbx2a shares 80% full-length and 100% T-box sequence identity with Tbx2b. The sequence obtained was listed in Scheme 2a, 2b, 2c on the following pages (red line marks the 1st exon sequence, green line marks T-box domain).

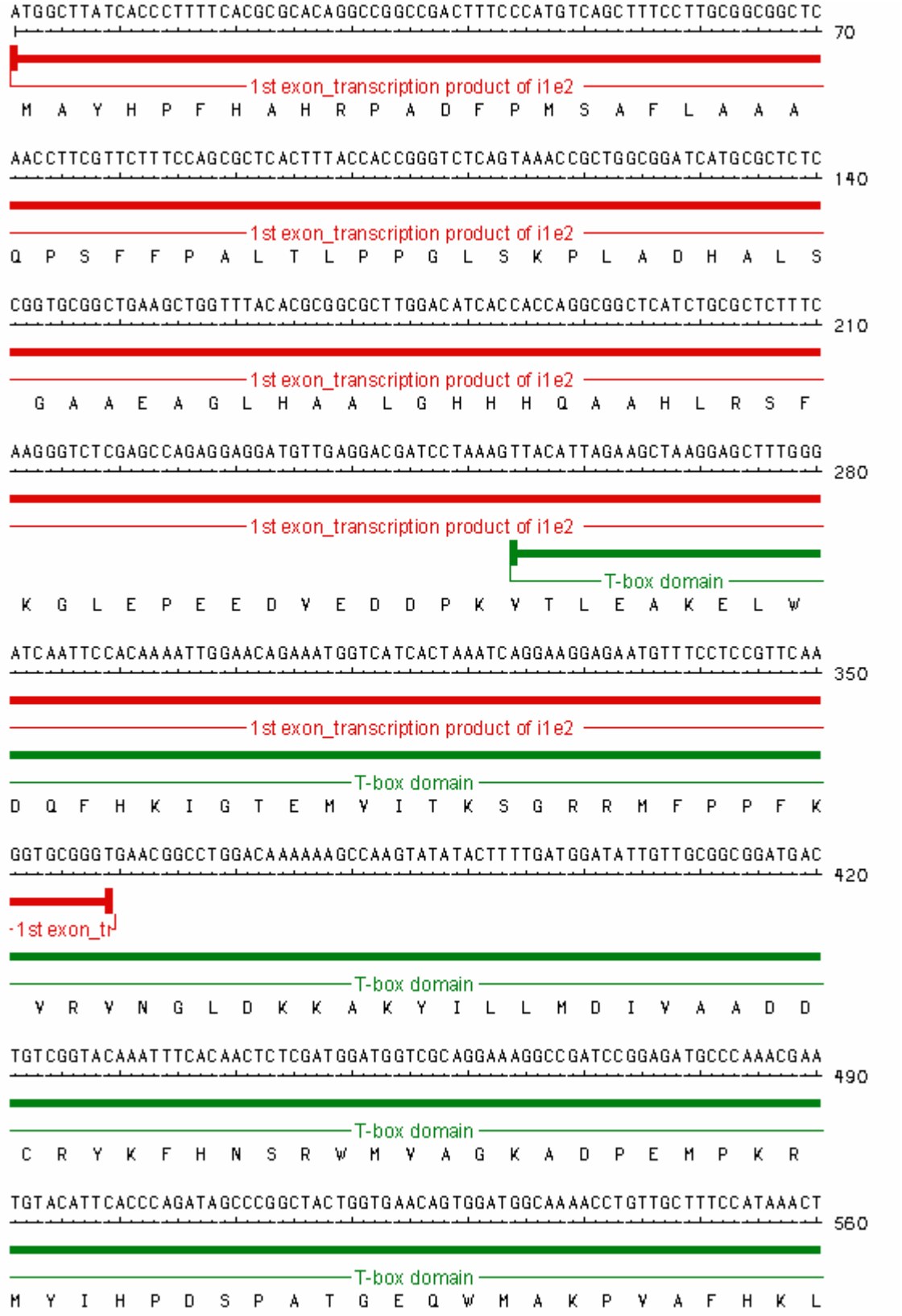

Scheme 2a: Sequence of *tbx2a* gene from nucleotide (nu) 1 to 560 (red line marks premature transcript resulted from i1e2 MO binding. Green line marks T-box encoded sequence expanded from partial exon 1, entire exon 2, 3 and partial exon 4)

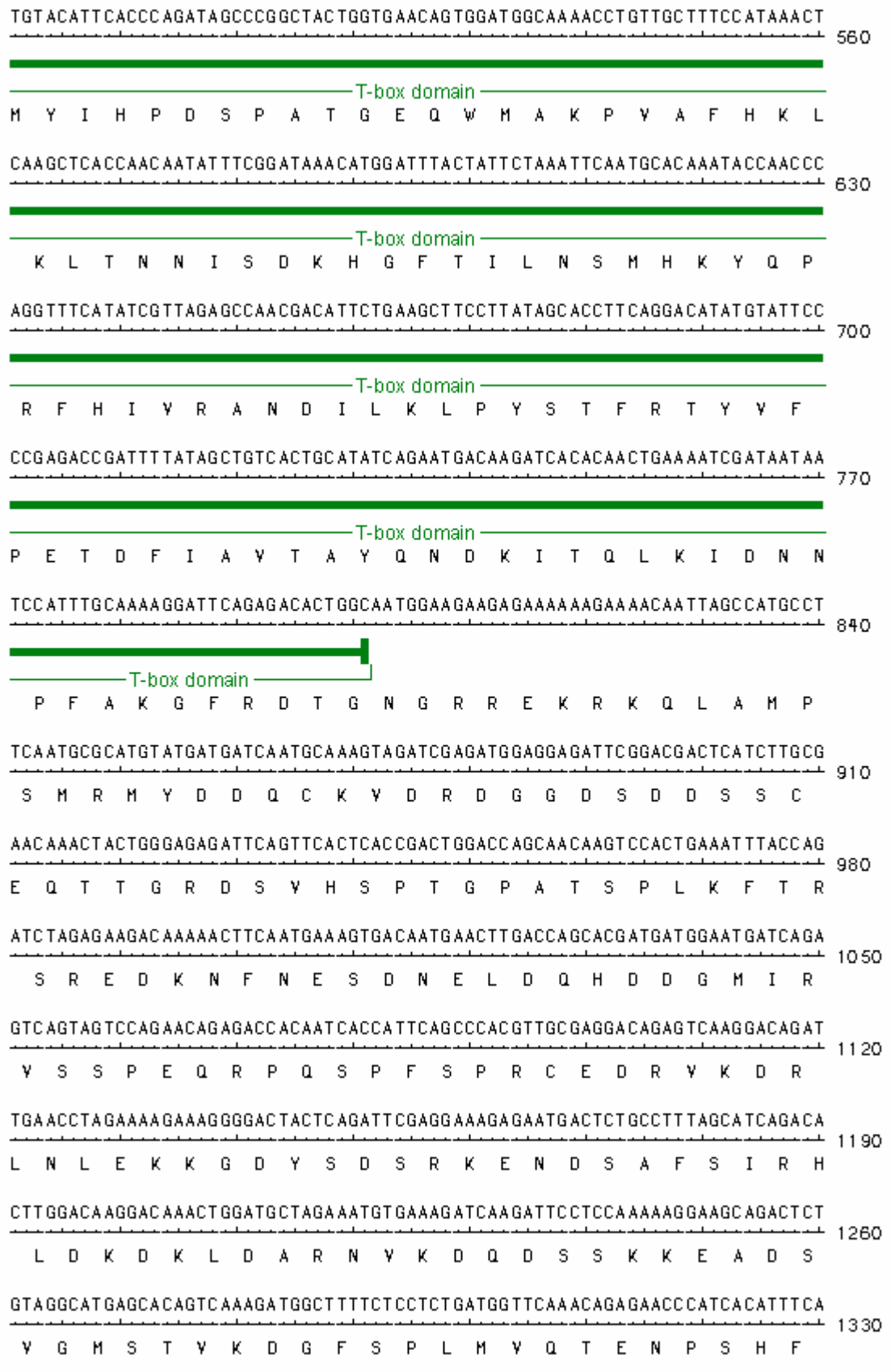

Scheme 2b: Sequence of *tbx2a* gene from nu 561 to 1330

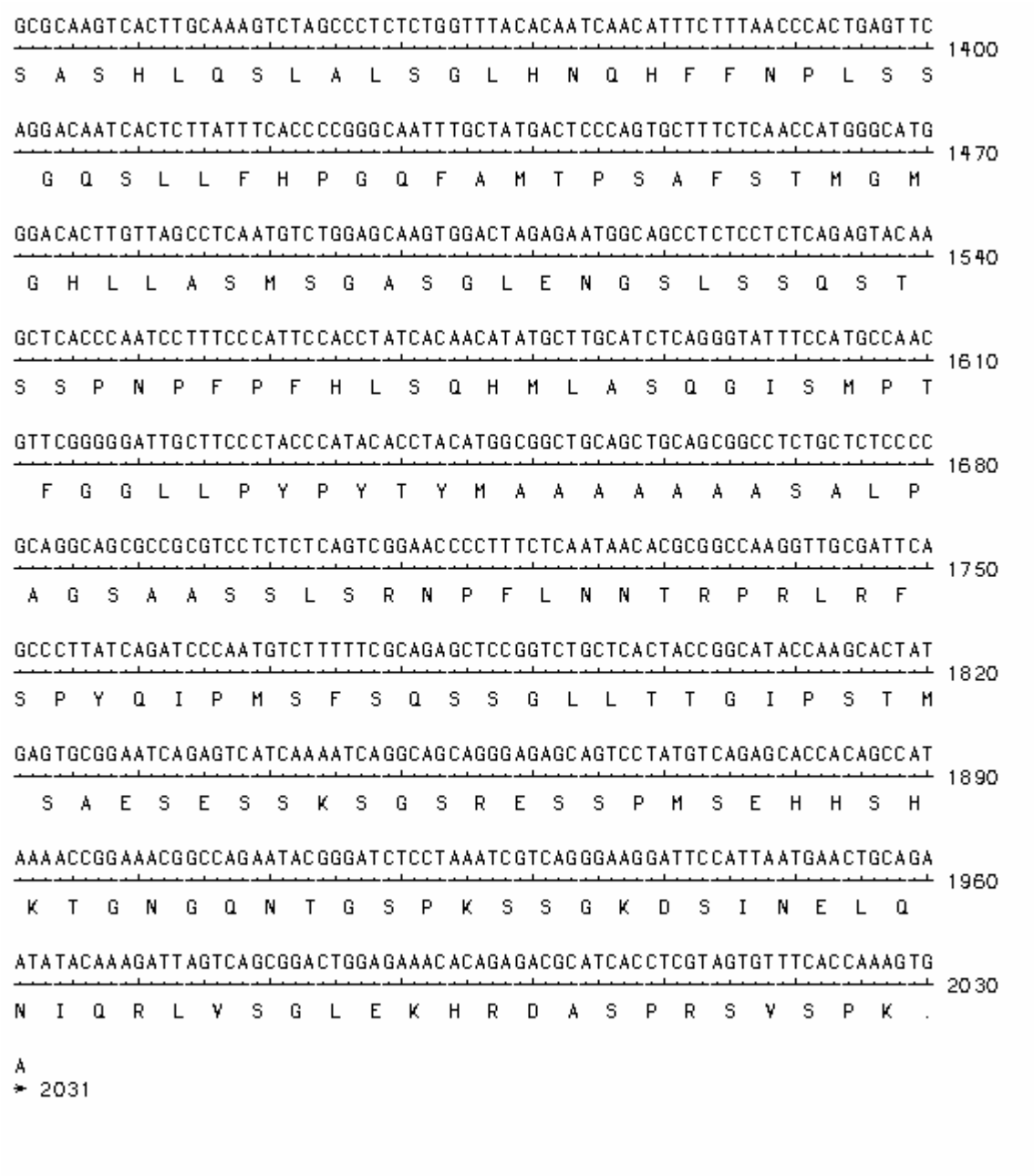

<u>Scheme 2c:</u> Sequence of *tbx2a* gene from nu 1331 to 2031

3.2 Overall analysis of *tbx2a* expression pattern

To investigate the spatio-temporal tissue distribution of *tbx2a* during the early development of zebrafish embryos, we conducted whole-mount *in situ* hybridization (WISH) using a full-length antisense digoxigenin (DIG)-labeled riboprobe. *tbx2a* transcript was not maternally detected either by Reverse Transcription Polymerase Chain Reaction (RT-PCR) or WISH (data not shown). Only after 11 hpf was *tbx2a* mRNA present in the dorsal eye primodia and otic placodes. *tbx2a* has a similar expression pattern with that of *pax2.1* featuring the two lateral stripes of the intermediate mesoderm. These will develop into the pronephric epithelia later (Drummond et al., 1998). However, the expression of *tbx2a* is more posteriorly restricted. In the forebrain, *tbx2a* expression was detected in the ventral diencephalon. Also at this stage, there was a weak expression in the mesoderm lateral to the otic placode domain. These domains were maintained until 14 hpf (Fig. 1A).

From 20 hpf, low level of *tbx2a* transcript started to appear in the ventral posterior rhombomere 2 (Fig. 1B, C), where it increased at later stages (Fig. 1E). We carried out triple staining to demonstrate that *tbx2a*-positive domain was flanked by *fgfr3*-positive rhombomere 1 (Friedrich et al, 2001) and *krox20*-positive rhombomere 3 (Oxtoby and Jowett, 1993) (Fig. 1F). Later, the expression in pronephric ducts was present posteriorly at the anus (Fig. 1D) while extending towards the anterior compartment of the ducts (Fig. 1E). Around 1 dpf, *tbx2a* expression newly marked 2 stripes of cells proximal to the eyes (Fig. 1E). These cells later became mandibular and hyoid arch mesenchyme. *tbx2a* was also detected in the olfactory bulbs, pectoral fin buds and anterior gut. The expression in the dorsal eyes, ears, rhombomere 2 and ventral diencephalon was maintained during the course of larval development. By 28 hpf, *tbx2a* transcript was found in pharyngeal arches. In addition, the transcript

marked a thin layer of cells lining on the yolk that would form the common cardinal vein (Fig. 1G).

At 48 hpf, the expression was markedly detected in the liver at the level of second somite (Fig. 2C). It was also found in the swim bladder primordium, which is homologous to lungs of terrestrial animals (Fig. 2D). This is consistent with *tbx2* expression in the lungs of chick and mouse (Table 3). There was also a faint staining in the vagal motor nucleus (Fig. 1I). In the fins, *tbx2a* transcript was proximally restricted (Fig. 2A), whereas its paralog *tbx2b* appeared in both the distal and proximal part of the fins (Fig. 2B). Moreover, expression of *tbx2a* and *tbx2b* also differs in the hypothalamus (data not shown). That means although the two paralogs share 80% cDNA identity, the full-length probes are specific. In the heart, *tbx2a* was locally expressed in the valves (Fig. 2E). By this time, the expression in the eyes seemed to decrease while that in the pharyngeal arches became stronger (Fig. 1H, 1I and 2G, 2H). In the ears, *tbx2a* transcript marked the developing cristae (Fig. 2F).

In summary, *tbx2a* is expressed in many domains that are evolutionarily conserved in mouse, chick and frog (Table 3). These are: heart, nasal pits (olfactory region), neurohypophysis, hindbrain, eyes, otic vesicles, pharyngeal region, pronephros and gut, the pectoral fin buds (limbs) and swim bladder (lungs). The expression in fin and swim bladder provides the molecular evidence to support the notion that these teleost structures could be homologous to tetrapod limbs and lungs, respectively. It also suggests a common ancestral origin of these organs during evolution of teleost and tetrapod.

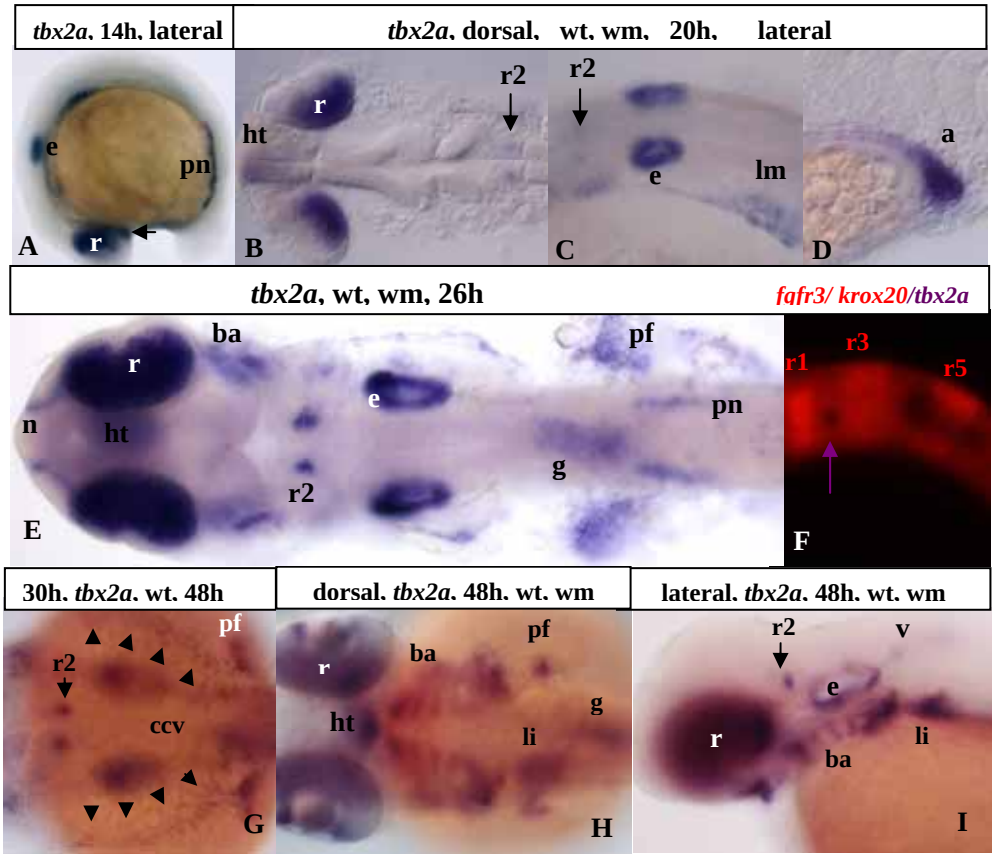

Figure 1: Expression pattern of *tbx2a* during larva development. (**A**) Lateral view at 14 hpf shows expression domains in the dorsal eye primodia, otic placodes, pronephric primodia, and ventral diencephalon which are maintained after initiation at 11 hpf. (**B, C**) Dorsal view of 20 hpf embryo shows staining in rhombomere 2 and lateral mesoderm where it was initiated at 14 hpf. (**D**) Expression in the anus (lateral view). (**E**) Dorsal view of 26 hpf embryo shows the additional expression domains in the nasal pits, primodia of mandibular arch, pectoral fins, pronephric ducts, swim bladder as well as the existing domains. (**F**) Co-staining with *fgfr3* (r1) and *krox20* (r 3, 5) confirms *tbx2a* staining in the ventral r2 (arrow). (**G**) Dorsal view at 30 hpf, arrow points r2, arrowheads mark common cardinal vein. (**H**) Dorsal view at 48 hpf reveals staining in pharyngeal arches, liver, gut and pectoral fin buds. (I) Anterior Lateral view at 48 hpf shows staining in eye, ear and vagal nuclei. Abbreviations: a: anus; ba: branchial arches; ccv: common cardinal vein; e: ear; g: gut; r: retina; r: rhombomere; ht: hypothalamus; li: liver; lm: lateral mesoderm; n: nose; pf: pectoral fin; pn: pronephric ducts; sb: swim bladder; v: vagal nucleus; wm: wholemount; wt: wild type.

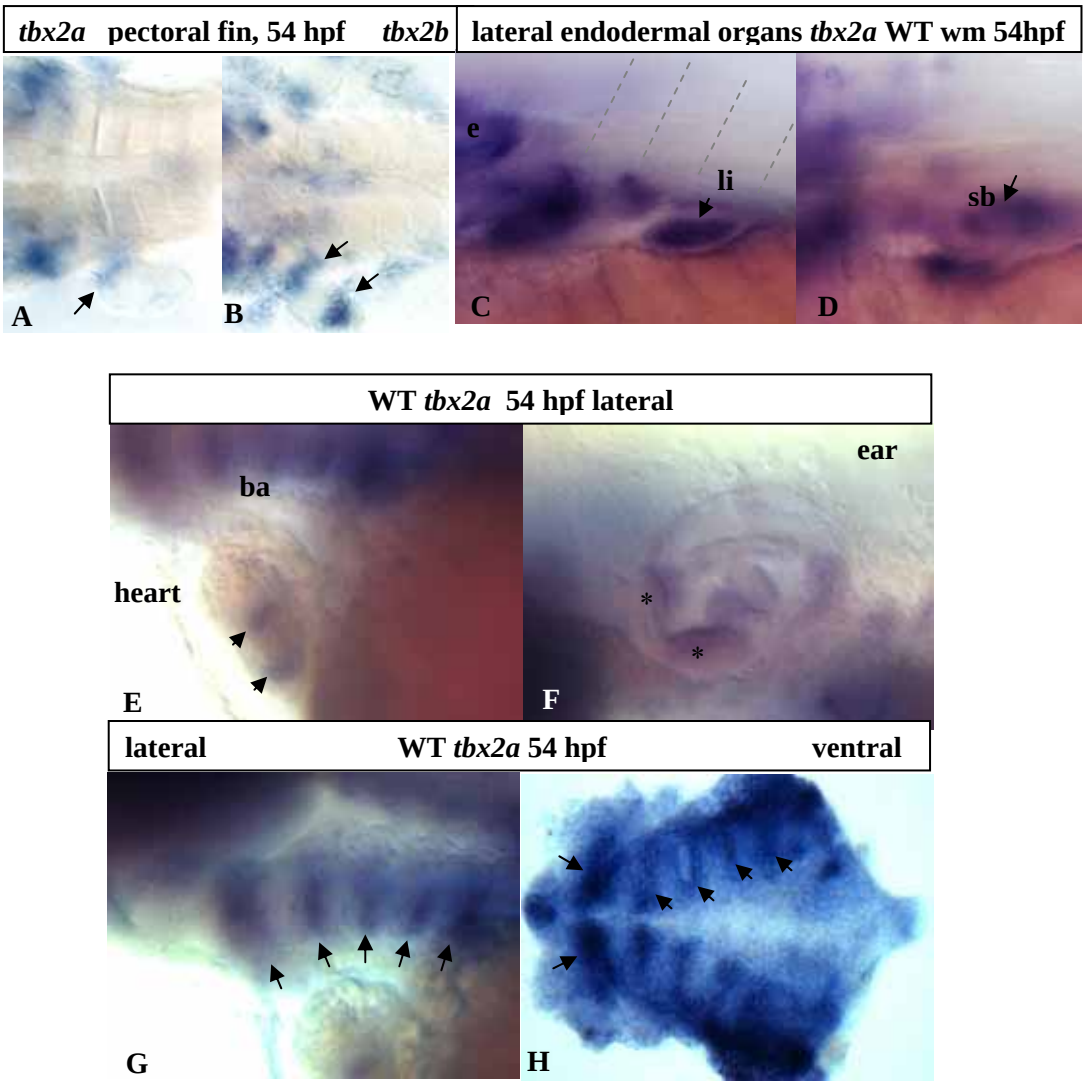

Figure 2: The detailed analysis of *tbx2a* expression at 54 hpf.
All the images are anterior to the left.
(A) *tbx2a* is restricted to the distal part (arrow), **(B)** whereas *tbx2b* in both distal and proximal parts of the pectoral fins (arrows), **(C)** liver (arrow) at the level of second somite dashed lines) of 54 hpf **(D)** swim bladder at 54 hpf **(E)** heart at 54 hpf **(F)** ear, stars indicate developing cristae, **(G)** pharyngeal arches on the lateral view and **(H)** dissected pharyngeal arches in the ventral view.

Organ/tissue	Mouse	Chick	Frog	Zebrafish	
				Tbx2b	*Tbx2a*
Gut-Muscle	+				+
Heart			+	+	+
Limbs/fins				+	+
Hindlimb	+	+			
Forelimb	+	+			
Lungs/Swim bladder					+
Mesenchyme	+	+			
Epithelium	-				
Mandible mesenchyme	+	+		+	-
Nervous system (CNS)					
Hindbrain	+	+			+
Neurohypophysis	+			+	+
Nervous system (PNS)					
Dorsal root ganglia	+	+	+		
Trigeminal ganglia	+		+	+	-
Notochord		-		+	-
Olfactory region (Nasal pit)	+	+	+		+
Optic vesicle		+	+	+	+
Neural retina	+				
Otic vesicle		+	+	+	+
Epithelium	+				
Mesenchyme	-				
Pharyngeal region			+		
Pouch epithelium	-	+		+/-	+
Arch mesenchyme	+	+		+	-
Pinnae of ear	+				
Rib Cartilage	+				
Pronephros			+	+	+

Table 3: Comparison of expression between zebrafish *tbx2a* and zebrafish *tbx2b* and *tbx2* of mouse, chick and frogs. Comparison based on Chapman et al., 1996; Gibson-Brown et al., 1998; Hayata et al, 1999; Ruvinsky et al., 2000; this study.

3.3 Investigation of Specificity of Morpholino-based knock-down

3.3.1 Design and testing MOs

Morpholino antisense oligonucleotides (MOs) were designed to target complementary sites which are either in the 5'UTR to block translation initiation in the cytosol or at splicing junctions to modify pre-mRNA splicing. Both targeting methods in theory can interfere with gene function. However, the efficiency of splice site-directed MOs can be evaluated by RT-PCR and sequencing for aberrant transcripts. In this study, two anti-sense morpholino oligos targeting two different splicing sites were designed:

- e1i1 MO targeting the donor site of intron 1; and
- i1e2 MO targeting the acceptor site of intron 1.

We carried out pan-embryonic injection for the two MOs. E1i1 MO prevented the splicing activity of intron 1 (Fig. 3A), resulted in an immature transcript that retained intron 1. RT-PCR analysis showed that the abnormal transcript is 0.7 kb bigger than it should, precisely the size of intron 1 (Fig. 3C). Sequence analysis of the abnormal fragment (red asterisk in Fig. 3C) confirmed the presence of intron 1 by blasting to Ensembl database. Moreover, the presence of an in-frame stop codon at the beginning of intron 1 (black box in Fig 3A) would produce a non-functional peptide lacking the T-box and 3'-activation domain (illustrated by Scheme 3).

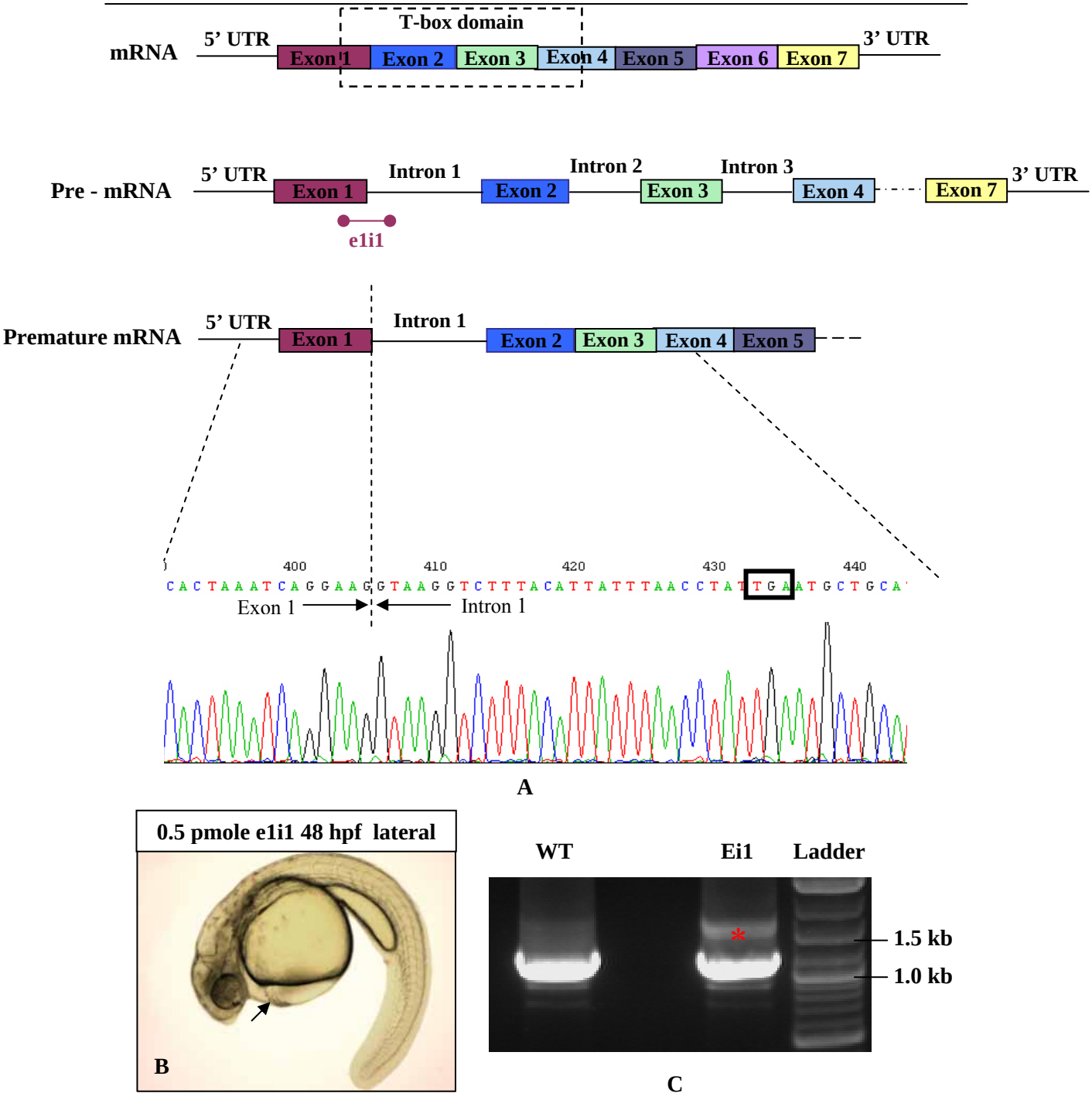

Figure 3: MO e1i1 prevents intron 1 splicing. (**A**) The diagram illustrates the genomic structure of *tbx2a* pre-mRNA included 759 bp 5' UTR plus exon1, 700 bp intron 1, 268 bp exon 2, 545 bp intron 2, 147 bp exon 3, 519 bp intron 3, 77 bp exon 4, 92 bp intron 4, 167 bp exon 5, 1459 bp intron 5, 605 bp exon 6, 324 bp intron 6 and 1491 bp exon 7 plus 3' UTR. The binding of e1i1 to the donor site of intron 1 blocks excision of intron 1. This results in the retention of intron 1 in the premature transcript. A stop codon within intron 1 (black box) terminates the translation of the mature transcript at the exon 1. (**B**) Lateral view of live e1i1-injected embryo at 48 hpf with heart edema, curved body, smaller ears and eyes, etc, albeit at a higher dose than that of i1e2. (**C**) Amplified mature transcripts of e1i1-injected embryos with primers extending from 5' UTR to exon 5 and flanking intron 1 ran on 0.8% agarose gel. Whereas only one mature transcript in the WT, an additional larger transcript is present in the e1i1-injected sample (asterisk). Sequencing reveals the intron 1 in the larger transcript containing the stop codon (black box – diagram **A**). Using 2-log DNA ladder (0.1-10.0Kb) from New England Biolabs. Abbreviation: bp: base pair, kb: kilo base pairs

I1e2 MO was designed to bind to the acceptor site of intron 1 to interfere with the normal splicing activity of intron 1. We predicted that the donor site of intron 1 would omit the acceptor site of intron 1, instead joined with alternative acceptor sites of downstream introns during splicing process. Although multiple reverse primers were used to amplify variable fragments extending from exon 1 toward exon 6 (data not shown), only one prominent abnormal transcript was amplified (Fig. 4C) with primers flanking exon 2. On agarose gel, the size of that transcript is 0.3 kb smaller than the normal transcript whereas the actual size of exon 2 is 268 bp. Sequencing revealed a continuous sequence reading from exon 1 to exon 3, omitting the entire exon 2 (Fig. 4A). Interestingly, the removal of exon 2 from the premature mRNA introduced a stop codon (black box in Fig. 4A) immediately at the beginning of exon 3. Therefore, both e1i1 MO and i1e2 MO should produce similar non-functional translated products encoded by only exon 1 (illustrated in Scheme 3).

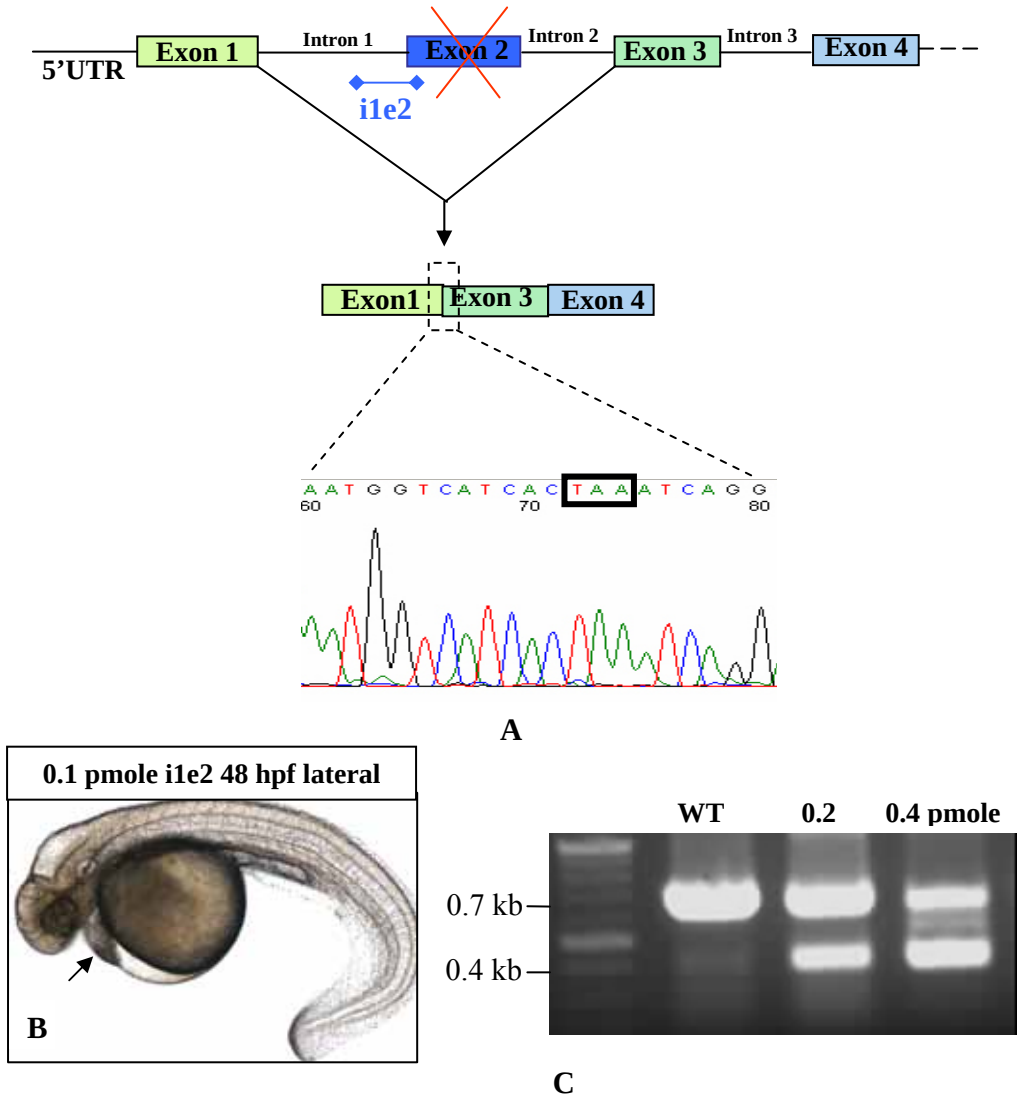

Figure 4: i1e2 MO causes excision of exon 2. (**A**) binding of i1e2 to acceptor site of intron 1 causes the excision of a fragment containing intron 1, exon 2 and intron 2, and results in the joining of exon 1 and exon 3 in the mature transcript. A stop codon (TAA-black box) is newly introduced at the beginning of exon 3 by the frame shifting. (**B**) Live i1e2-injected embryo at 48 hpf exhibits heart edema, curve body, smaller ears, smaller eyes, etc. (**C**) Amplified mature transcripts of i1e2-injected embryos with primers flanking the sequence from nucleotide 627 to 1300 ran on 0.8% agarose gel. Only one mature transcript in the WT, while an additional smaller transcript in i1e2-injected sample. Matching with sequencing result, the additional transcript is one exon-2-length (~0.3 kb) shorter than the normal one.

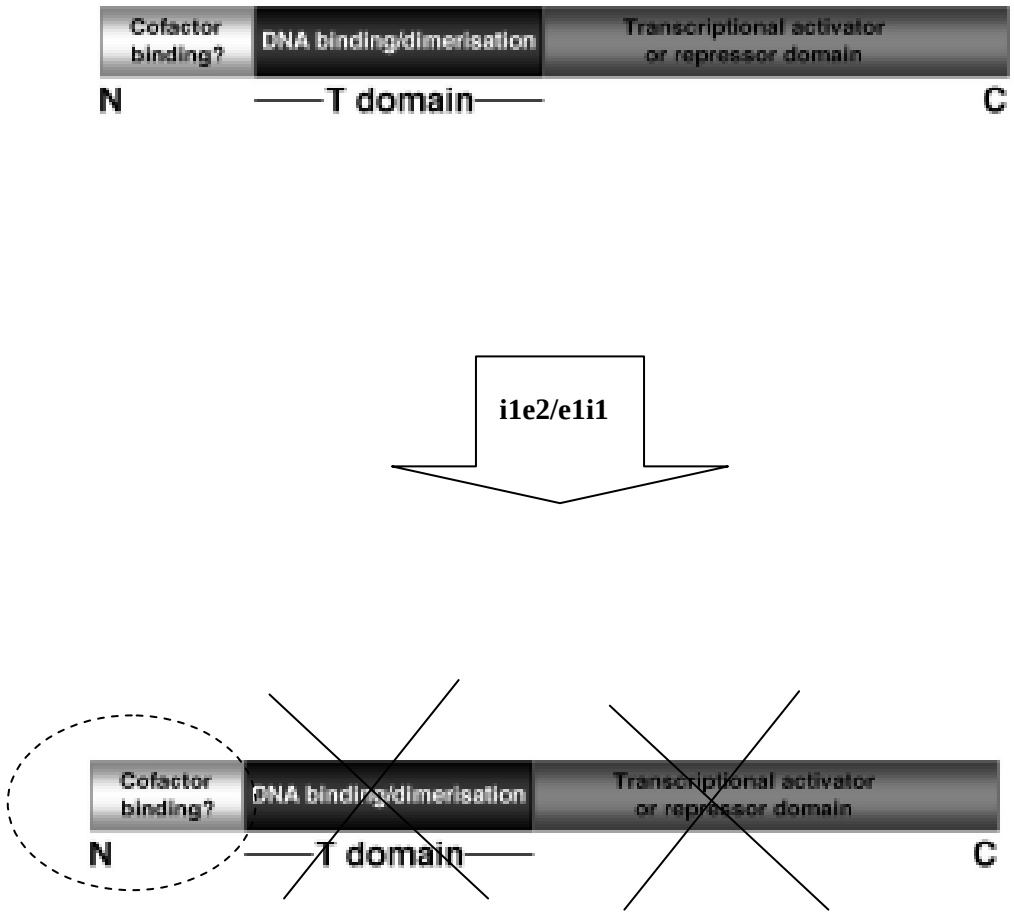

Scheme 3: Activity of e1i1 and i1e2 MOs. Both e1i1 and i1e2 MOs lead to the same non-functional translated products encoded by only exon 1, without T-box transcription domain and 3'-terminal transactivation domain. (Adapted and modified from Minguilon and Logan, (2003).

3.3.2 Selection of the most effective MO

It is noticeable that e1i1 MO and i1e2 MO have different optimal concentrations. So, we set out to compare the efficacy of the two MOs by semi-quantitative RT-PCR of the residual normal transcription product. After RT-PCR, amplification products from both the control and MO transcripts were analyzed on agarose gel. We injected 0.3 pmole/embryo for i1e2 MO and 0.5 pmole/embryo for e1i1 MO. RT-PCR result showed that the normal transcript decreased by about 76% in i1e2 MO morphants, and 47% in e1i1 MO morphants (Fig. 5; Chart 1). These estimations were obtained by using ImageJ software to read the intensity of the bands on the agarose gel image. It strongly suggests that i1e2 MO possesses a higher working efficacy than e1i1 MO.

To make sure alternative targeting site produced the same phenotype, we designed another morpholino to target acceptor site between intron 5 and exon 6 (namely i5e6 MO) in order to disrupt the trans-activation domain and create a dominant negative form of *tbx2a* (data not shown). Indeed, the i5e6 morphants (embryos injected with i5e6 MO) displayed defects in the pharyngeal arches, eyes, heart, and ears. The general phenotype of i5e6 morphants resembled that of i1e2 and e1i1 morphants. Previously, *tbx2a* expression in the heart was shown and this gene found indispensable for cardiac chamber formation (Ribeiro et al., 2007). During specification of the eye, *tbx2a* knock-down has been found to affect only the dorsal eyes (Gross et al., 2005). Therefore, the phenotype of the *tbx2a* morphants is highly relevant to its expression pattern and others' functional studies. In conclusion, with multiple MOs causing very similar phenotype, we are confident that we are not dealing with non-specific effects. Subsequent experiments were performed with i1e2 MO.

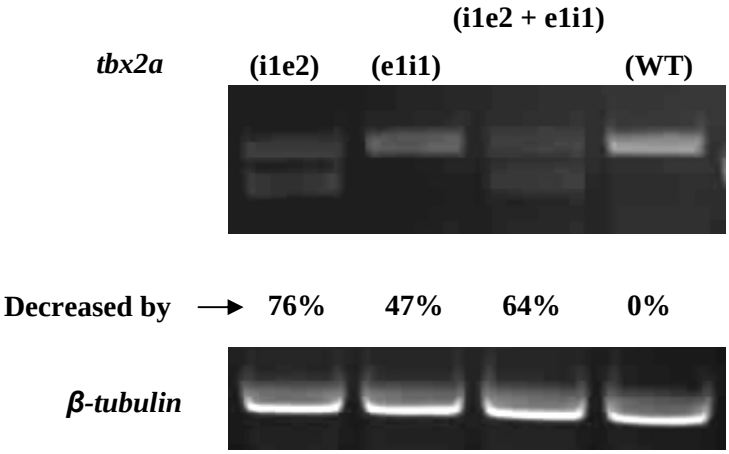

Figure 5: Comparison the efficacy of i1e2 and e1i1. (i1e2) shows normal transcript was decreased by 76% in i1e2-injected embryos at 0.3 pmole/embryo. **(e1i1)** removes 47% of the normal transcript even at higher dose (0.5 pmole/embryo)**. (i1e2 + e1i1)** Combination of i1e2 (0.25 pmole/embryo) and e1i1 (0.25 pmole/embryo) causes a deficiency of 64% of transcripts; **(WT)** normal transcript in WT embryos. *β-tubulin* as internal control.

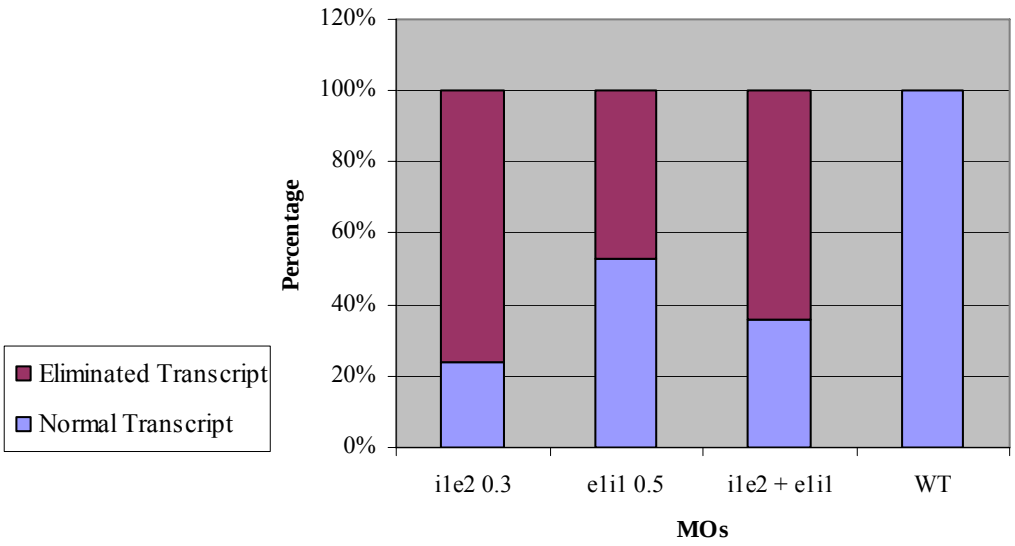

Chart 1: Comparison the efficacy between i1e2 and e1i1

3.3.3 Pan-embryonic Injection of MOs

In order to determine the best working concentration, we worked on a range of MO concentrations. The best concentration is the one that produced specific phenotype without any toxicity effect. Injection results are in agreement with those obtained from semi-quantitative RT-PCR. E1i1 MO has working concentration of 0.5 pmole/embryos, whereas i1e2 and i5e6 MO worked at 0.05-0.1 pmole/embryo. The more effective MO (i1e2 MO) as shown by RT-PCR required lower concentration to produce the same phenotype compared to the weaker MO (e1i1 MO). In the range of 0.1-0.8 pmole/embryo, 100% of i1e2 MO injected embryos produced consistent phenotype (more than 10 batches, 50 embryos/batch).

To avoid injection errors in subsequent experiments with i1e2 MO, we did not apply the lowest working dose but a slightly higher dose of 0.2-0.3 pmole/embryo. The MO-injected embryos displayed defects in accordance with the expression pattern, yet still survived up to 7 dpf. They have smaller overall size, smaller ears, malformed anus and heart edema. The yolk sacs of the morphants seem to be bigger in comparison with those of wild-type fish. Pigmentation was delayed in the early stage of 2 dpf, however it recovered from later stage onward. Swim bladders were not developed in the morphants. Interestingly, pharyngeal arches were dramatically dysmophic. The loss of pharyngeal arches was maintained throughout the course of embryonic development.

3.3.4 Analysis of the downstream target of Tbx2

To confirm MO based knock-down effect, a known downstream target gene of Tbx2 was examined. The *cx43* promoter has been shown to be repressed by Tbx2 (Borke et al., 2003; Chen et al., 2004). In zebrafish, we learned from the study of Chatterjee et al., (2005) that *cx43a* is also expressed in the branchial arches from 3 dpf onwards, which is later than *tbx2a*. The up-regulation of *cx43a* in the i1e2 MO morphants is clearly shown by in situ staining. Interestingly, an ectopic expression of *cx43a* was observed in the ventral diencephalon of the morphants (8 of 10 embryos tested, Fig. 6D) where *tbx2a* is expressed. Although this up-regulation of *cx43a* was obtained with a higher dose of MO (0.5 pmol/embryo), the data demonstrate the regulatory loop between *cx43a* and *tbx2a* and the MO used is effective in depleting Tbx2a function.

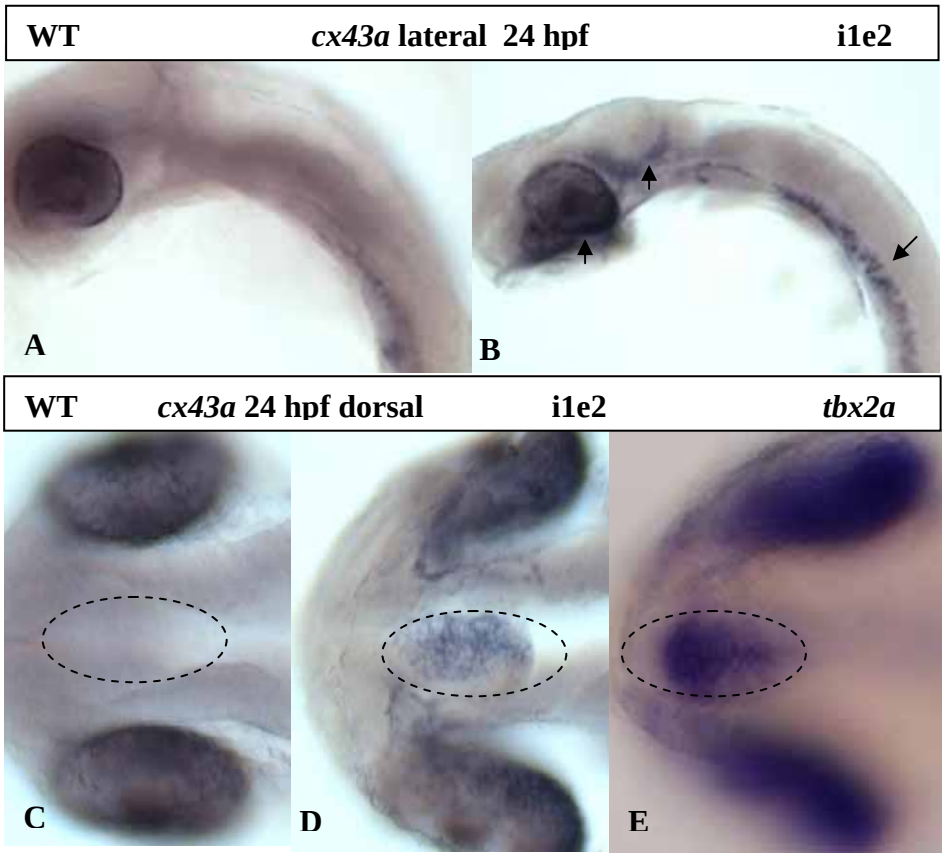

Figure 6: Downstream target *cx43a* employed to test MO specificity Compared to control **(A)**, *cx43a* expression increases in i1e2 morphants (arrows at eyes, notochord, midbrain) **(B).** Especially, ectopic expression of *cx43a* in the ventral diencephalon (broken circle) (**D**), where *tbx2a* is present **(E)**

3.4 *tbx2a* expressed in endodermal pouches of the branchial arches

Each pharyngeal arch is a complicated structure that is made up of all three germ layers' derivatives: mesodermal core, neural crest cells (NCCs) and endodermal pouch. By lateral view, if the seven arches could be anatomically imagined as a row of seven books, endodermal pouches would be constituted by the covers of the books; pages adjacent to the covers would be the NCCs derivatives, the most inner pages of a book would be the mesodermal core.

To get a closer look at the expression of *tbx2a* in the branchial arches, we carried out sagittal sectioning. *tbx2a* was found to mark the thin boundaries in between the rods of arches (Fig. 7A, B, C). Specifically, we found *tbx2a* expression in both the anterior and posterior halves of each pouch. However, this expression did not extend along the full length of the pouches, being restricted to the ventral part (Fig. 7C). The expression of *tbx2a* in the pharyngeal apparatus is maintained to 3 dpf (Fig. 7D, E, F). Thus, *tbx2a* is restricted to the pharyngeal endoderm.

To localize markers of mesodermal core or NCCs in respect of *tbx2a* expression domains, we performed two-color WISH. *sox9a* is a specific marker for mesodermal core within the arches (Yan et al., 2005). Our two-color WISH staining showed that *tbx2a* was excluded from the *sox9a* domain (Fig. 7G). Next, we co-stained *tbx2a* with the neural crest marker *dlx2a* (Akimenko, 1994) and found that *tbx2a* appeared at the borders of *dlx2*-positive domain; these fine borders are endodermal pouches (Fig. 7H). *tbx2a* was also confirmed to be expressed in the endodermal pouches by co-localization with endodermal pouch specific marker *nkx2.3* (Fig. 7I), whose expression in the arch started at 28 hpf and persisted until 3 dpf or later (Lee et al., 1996).

The *tbx2a* paralog, *tbx2b* (Dheen et al., 1998) is also expressed in the pharyngeal arches (Fig. 8A). However, expression patterns of these two genes differ. *tbx2b* staining labels the mesodermal cores at the proximal part of the pharyngeal arch (Fig. 8B). At the distal part, *tbx2b* is restricted to endodermal pouches (Fig. 8C). The difference in tissue distribution may lead to divergent functions of *tbx2a* and *tbx2b* within the pharyngeal arches. In this study, we focus on functional analysis of *tbx2a* which possesses discrete pattern within the endodermal pouches.

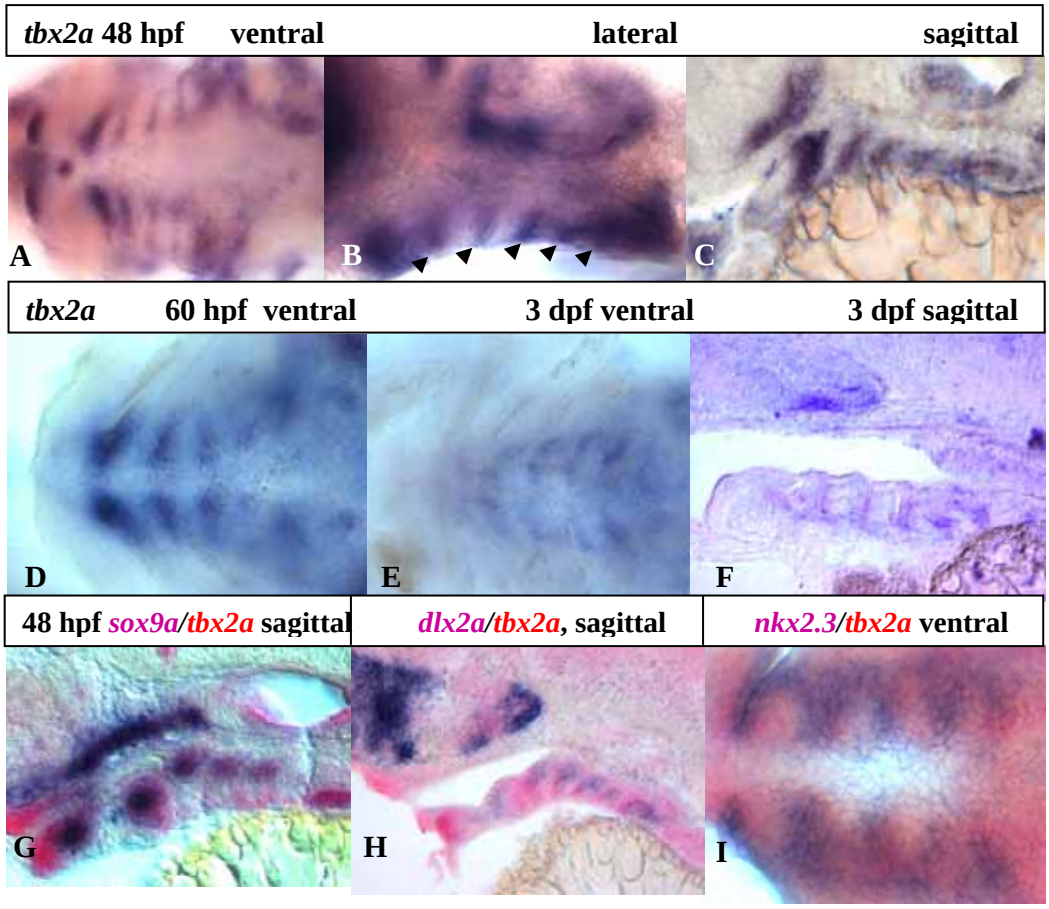

Figure 7: *Tbx2a* expression is restricted to the pharyngeal endodermal pouches.

(**A**) Ventral view of 2 dpf embryo shows expression of *tbx2a* in the pharyngeal arches. (**B**) Lateral view shows the expression was restricted to the two-cell layer thick endodermal pouches (arrowheads). (**C**) Sagittal section shows *tbx2a* staining is in more ventral part of endodermal pouches. (**D**) The expression is maintained up to 60 hpf and decreased by 3dpf (**E, F**).

(**G**) Sagittal section reveals expression of *sox9a* (purple) in mesodermal cores and *tbx2a* (red) in ventral pouches of 48hpf embryo. (**H**) Sagittal section shows mesenchyme (*dlx2*-purple) flanked by endodermal pouches (*tbx2a*-red) (**I**) *tbx2a* staining (red) overlaps with endodermal pouch specific marker (*nkx2.3*,purple).

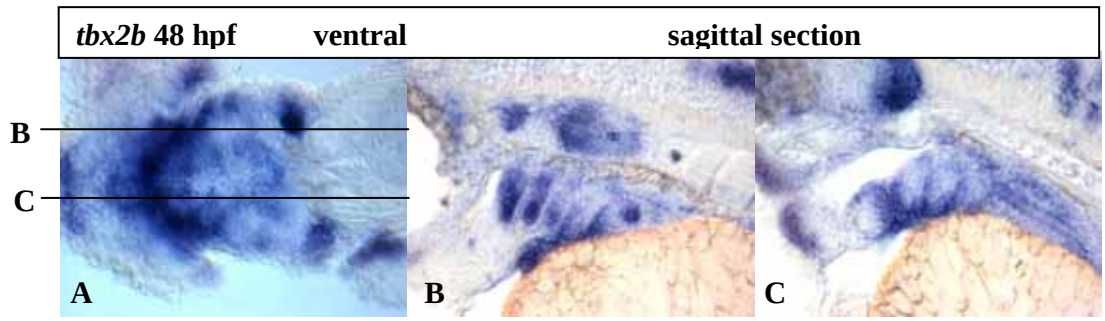

Figure 8: Expression of *tbx2b* in the pharyngeal arches. (**A**) *tbx2a* is expressed in the pharyngeal arches by ventral view. Sagittal sections show *tbx2b* is expressed in the mesodermal cores (**B**) and in the distal part of endodermal pouches (**C**).

3.5 *tbx2a* is indispensable for pharyngeal arch development

3.5.1 Alcian Blue staining reveals cartilage defect in *tbx2a* morphants

The *tbx2a* morphants exhibited a loss of cartilage in not only for the five posterior arches but also the mandibular and hyoid arches. Alcian blue is a copper phthalcyanin dye which can bind to the extra-cellular matrix of chondrocytes. Chondrogenic cartilage is first detected at 54 hpf (Schilling and Kimmel, 1997). To demonstrate the pharyngeal arch phenotype in morphants, we performed Alcian Blue staining on both the WT and morphant embryos (3 and 4 dpf). Co-injection of *p53* MO was to avoid off-target effect described as neural death caused by the activation of p53 signaling in the MO-injected embryos (Robu et al., 2007) There was no blue staining of chondrocytes in the morphants (with or without co-injection of *p53* MO, 0.4 pmole/embryo) on both stages 3 dpf and 4 dpf (Fig. 9), suggesting that the formation of neural crest-derived cartilages was disturbed upon the absence of *tbx2a* (on both the WT and *p53* morphant background), and this loss was maintained until later development.

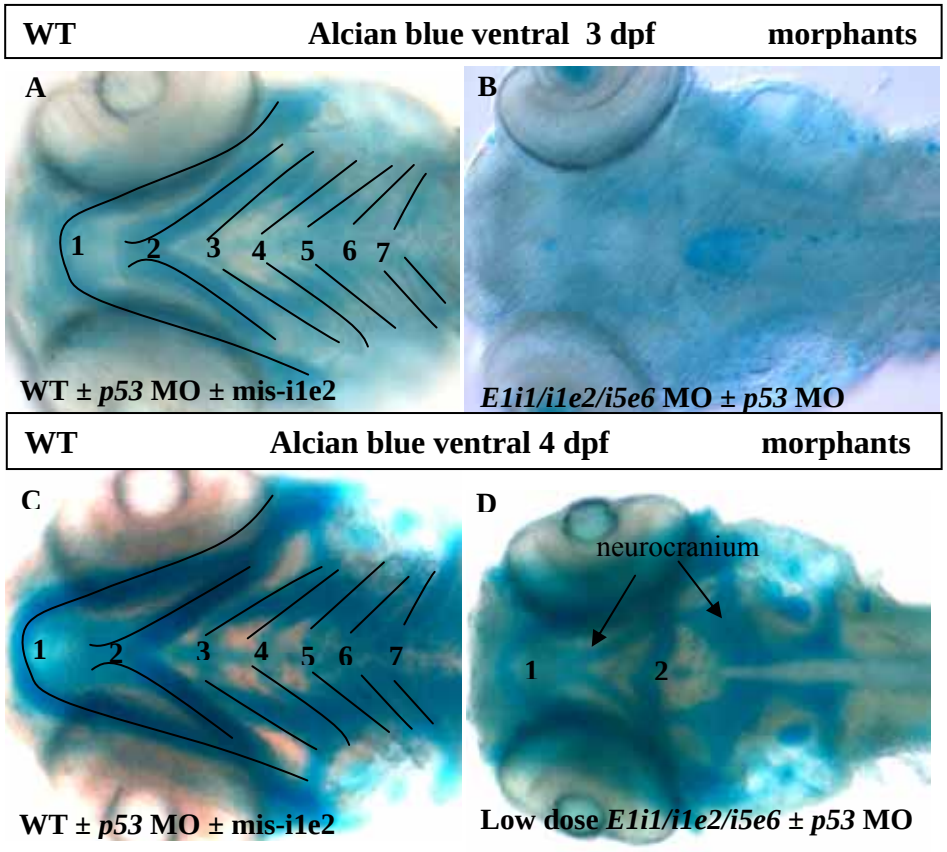

Figure 9: Cartilage staining by Alcian blue. Alcian blue stains pharyngeal cartilage of all seven arches in the wild type or *p53* morphant or mismatch MO of i1e2 **(A - 3 dpf, C - 4 dpf),** but not in /e1i1/i1e2/i5e6 morphants on the background of either WT or *p53* morphant **(B – 3 dpf, D – 4 dpf).**

3.5.2 *tbx2a* plays a role in development of endodermal pouches

Pharyngeal arch development requires the contribution of all three germ layers. However, there is increasing evidence of the leading role of pharyngeal endoderm during this process. It has been shown in chick that endodermal pouches and arches developed normally in the absence of neural crest (Veitch et al., 1999). However, when endodermal pouches are ablated, NCCs are unable to differentiate further into cartilages and bones. In amphibians, endoderm has been shown to influence the differentiation of chondrocytes (Seufert and Hall, 1990). In zebrafish, *cas* and *oep* mutants lacking endoderm (Alexander et al., 1999) display defect in cartilages of all pharyngeal arches (David et al., 2002). *tbx1* is present in the endodermal pouches; its mutant *van gogh* has been shown to be defective primarily in the endodermal pouches and secondarily in the morphology of arch cartilages, which are misshaped or fused together (Piotrowski and Nusslein-Volhard, 2000; Piotrowski et al., 2003). All these studies have demonstrated the role of endodermal pouches in cueing the paths for the NCCs to follow and assemble into discrete pharyngeal arches.

As seen in the sagittal section (Fig. 7C), *tbx2a* staining is restricted to the endodermal pouches and very minor diffusion in the neural crest domain, but not in the mesodermal cores. The question is whether *tbx2a* controls the normal induction and/or morphogenesis of the endodermal pouches. To answer, we checked several genetic markers specific for the pharyngeal endoderm. *nkx2.3* has been known to be specifically expressed in the five clefts between the six pharyngeal arches (Lee et al., 1996). It marks both rostral and caudal halves of the endodermal pouches. By the ventral view, *nkx2.3* clearly showed the five pouches in the morphant (Fig. 10B) as nicely as in the control (Fig. 10A), suggesting that endodermal pouch induction is unaffected by *tbx2a* knock-down. However, by the lateral view, the *nkx2.3* labeling

was restricted to the distal portion. That suggests a failure to elongate along the proximodistal axis that, in turn, may lead to the failure to inter-digitate with the neural crest-derived cartilage.

We utilized the transgenic line ET33-1B produced from transposon mediated enhancer trap screening (Parinov et al., 2004; illustrated in Suppl. Fig. 1). The enhancer trap is GFP-tagged, driven by a minimal promoter of *keratin4.* The line ET33-1B was generated from the line ET33 by remobilization of Tol2, and is GFP-positive in the endodermal pouches at 2 dpf (Fig. 10E). *Tbx2a* morphants of ET33-1B displayed disorganization of all the pouches compared to controls (Fig. 10F). *pea3* is an ETS family transcription factor (Roehl and Nüsslein-Volhard, 2001) and is expressed in endodermal pouches. Consistent with the above observation, *pea3* expression in the morphants indicated defects in the endodermal pouches: some of them disappeared (arrowheads in Fig. 11B) whereas others were disordered (asterisk in Fig. 11B).

Thymus primordium appears in zebrafish larva from 54 hpf as a derivative of the caudal half of endodermal pouch 3 (Gordon et al., 2001). *rag1* is expressed in maturing B and T lymphocytes of the thymus (Willett et al., 1997). WT embryos from 4 dpf express *rag1* (Fig. 12A). However, in the morphants *rag1*-positive thymus primordium was not present (Fig. 12B), suggesting that development of lymphocytes may be disturbed or the thymus structure itself is affected. Hence, our data showed that although the induction of pharyngeal endoderm is normal, its subsequent differentiation is strongly affected.

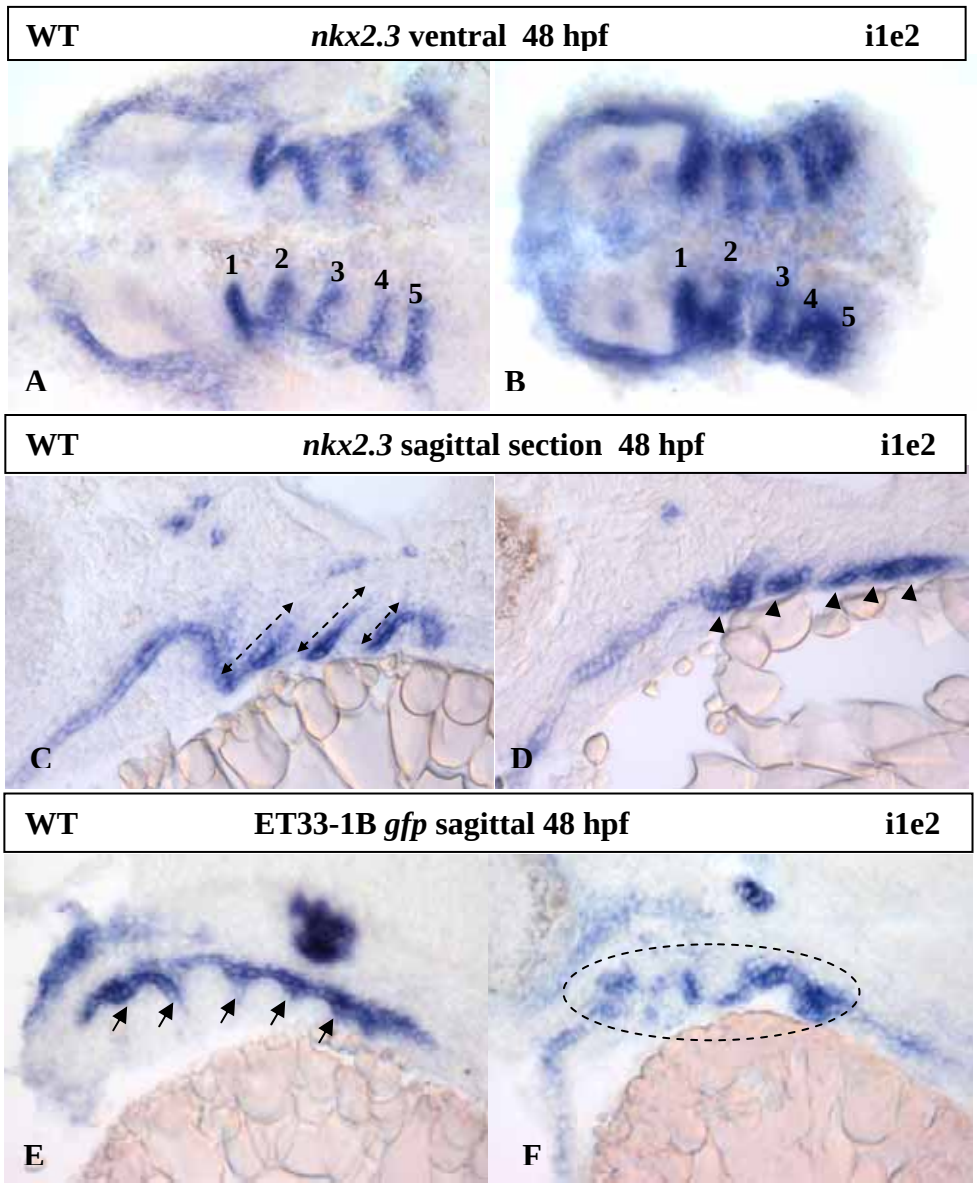

Figure 10: Endodermal pouch morphogenesis is affected by *tbx2a* knock-down. Ventral view of endodermal pouches labelled with *nkx2.3* riboprobe shows patterning in both WT **(A)** and morphant **(B)**. **(C)** endodermal pouches in the morphant (**D**) fail to extend along D-V axis. Moreover, the dorsal *gfp*-positive endoderm in ET33-1B **(E)** is malformed in the morphant **(F)**.

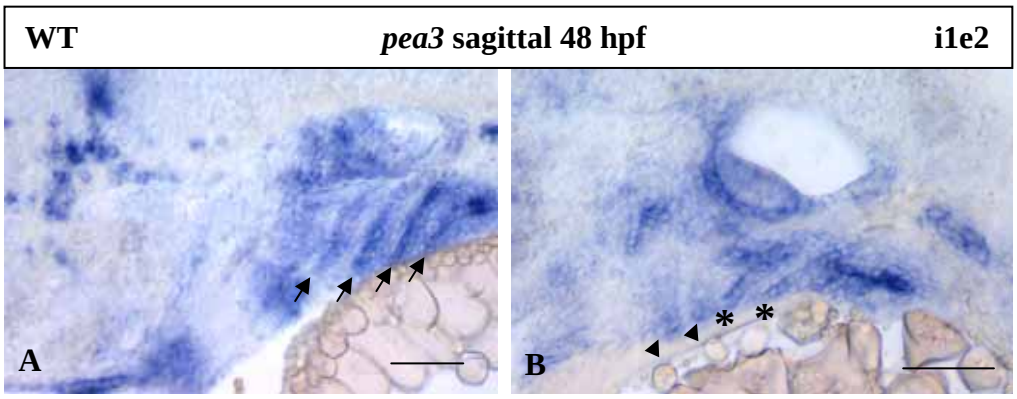

Figure 11: *pea3* is expressed in the posterior endodermal pouches **(A**-arrows**)** demonstrates in the morphant **(B)** the defect of the endodermal pouches which are undeveloped (arrowhead) or malformed (asterisc).

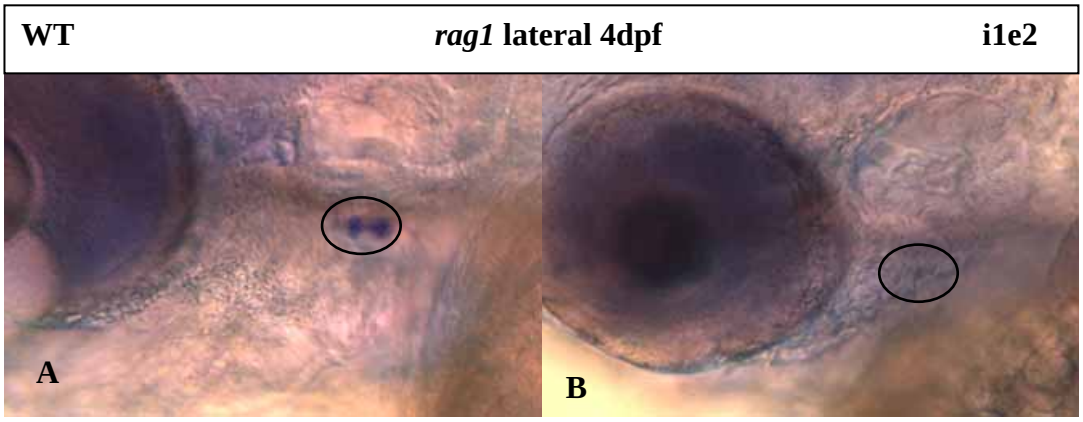

Figure 12: *rag1* is expressed in the thymus primordium (**A**-broken line oval), but it is absent in the morphant **(B)**.

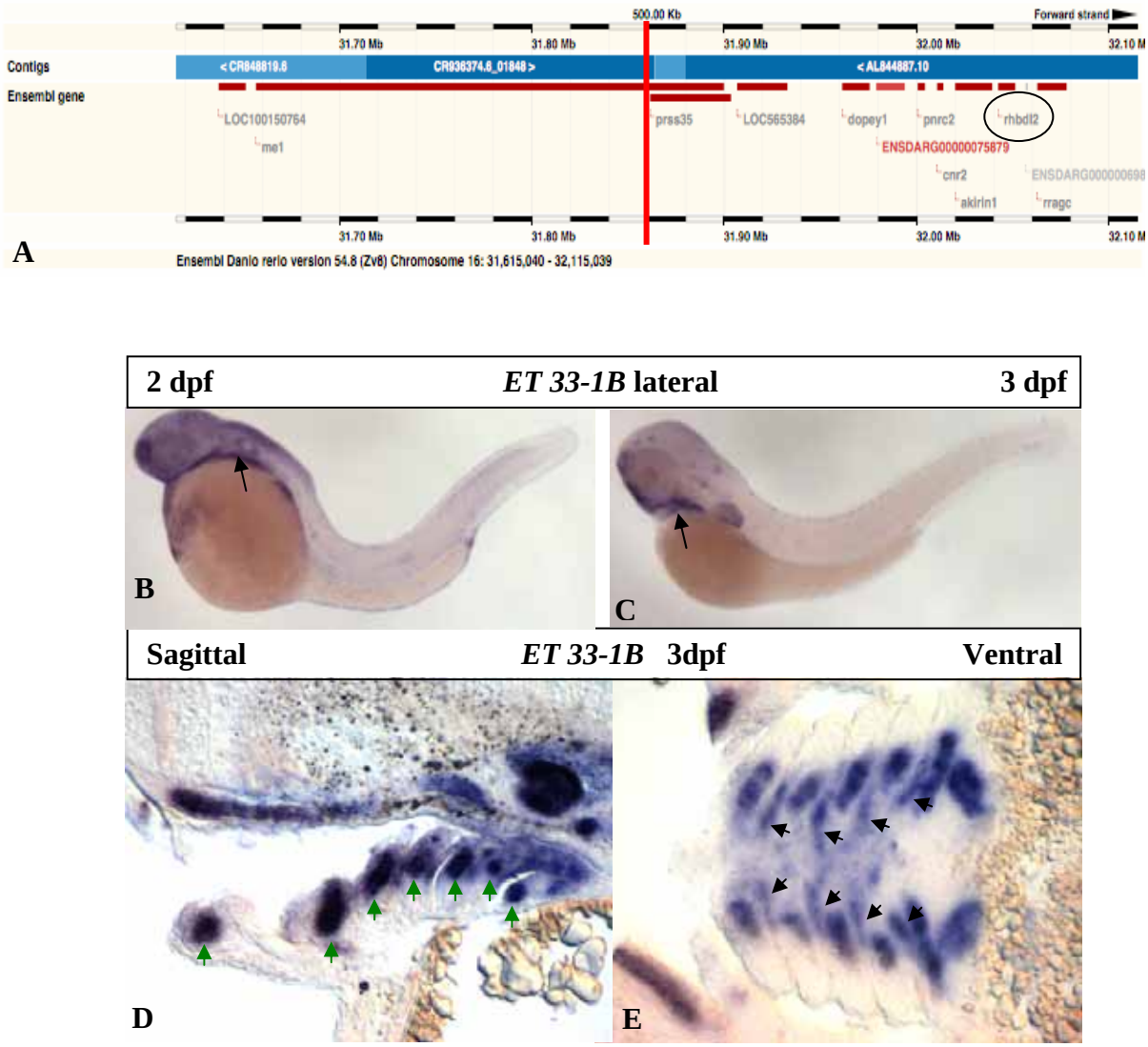

<u>Supplementary figure 1:</u> (A) ET33-1B has been mapped onto the chr.16: 31,804,358-31,808,630. The ET33-1B insertion is *5' tre* upstream of *rhbdl2* (ENSDARG00000069833), rhomboid, veinlet-like 2 (Drosophila), serine-type endopeptidase activity, the activator of EGF signaling. According to Thisse and Thisse (2004) *rhbdl2* is expressed in the epidermis, otic placode, otic vesicle, pectoral fin, peripheral olfactory organ, pharyngeal arches, which are capitulated by GFP expression of ET33-1B (from 2 dpf onwards, shown in **B, C**). **In the pharyngeal arches,** GFP is expressed in the mesodermal cores (**D**-green arrows) and distal part of endodermal pouches (**E**-black arrows).

3.5.3 *tbx2a*-depletion causes defect in mesodermal cores

ET33-1B embryos possess a strong GFP expression in the entire pharyngeal arches, cleithrum and swim bladder (Fig. 13A). To have a better view of GFP expression in the arches, we sectioned ET33-1B embryos and visualized with *gfp* riboprobe staining. The staining showed *gfp* transcript located in mesodermal cores within each pharyngeal arch (Suppl. Fig. 1D) and endodermal tissue in between the arches (arrows in Fig. 10E and Suppl. Fig. 1E). However, the GFP expression was restricted to the distal half of the arch from the mid-line (Suppl. Fig. 1E, arrows), but not the entire length of the arch. ET33-1B embryos injected with i1e2 MO demonstrated the ablation of the arches. At the lowest working dose of 0.1-0.2 pmole/embryo, injected embryos retained minor trace of GFP expression in the almost depleted madibular and hyoid arches (Fig. 13D). The ablation of GFP expression in the arches suggests that mesoderm core may be affected in the event of *tbx2a* knock down.

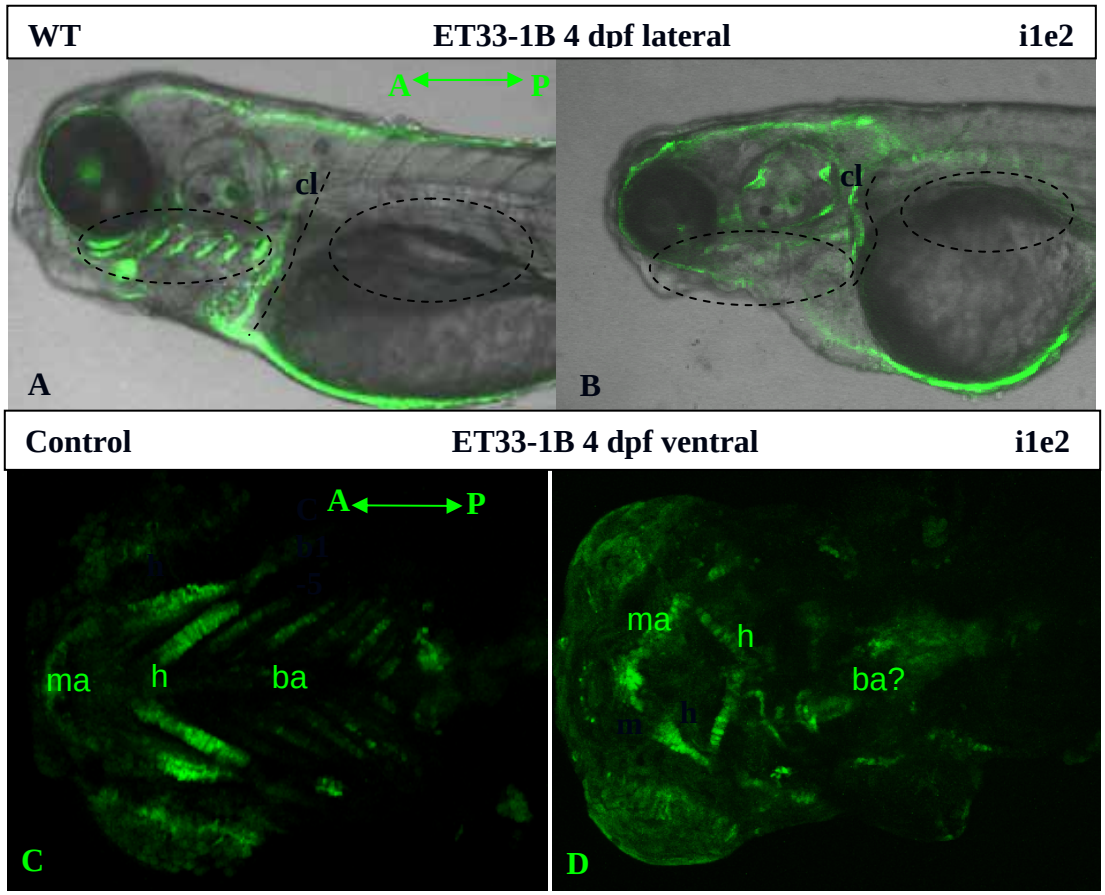

Figure 13: Illustration of *tbx2a* knock down effect on pharyngeal development in ET33-1B transgenic line. (**A**) Lateral view of live ET33-1B larva shows GFP-positive pharyngeal arches and cleithrum. (**B**) In i1e2 morphant GFP is absent in the pharyngeal arches, but maintained in the cleithrum. Ventral view of 4dpf ET33-1B larvae shows GFP-positive pharyngeal arches in the control (**C**) but only traces of mandharibular and hyoid arches in the morphant (**D**). Abbreviations: ba – branchial arches, cl - cleithrum, ma – mandibular, h – hyoid

To determine if the phenotype was a result of mesodermal defect, we checked some other specific markers for this component. *sox9a* is express in the central core of the arch (Fig. 14A, C). Thus, it can be used as a marker for mesoderm-derived component in the pharyngeal arch. This loss of *sox9a* expression within the branchial arches (Fig. 14B, D) supports the lack of cartilage elements observed in the morphant larvae. Similarly, expression of another mesodermal core specific marker, *runx2b* (Flores et al., 2004; Flores et al., 2006) in morphants was affected in a similar manner (Fig. 15A, B). In addition, both *tbx2b* and *pea3* staining were lost in the mesodermal cores of morphants (Fig. 15C, E, D, F).

Since all the mesodermal markers were still present at a certain level of expression (black asterisks, Fig. 14D, 15D), The finding led us to the conclusion that *tbx2a* knock-down was interfering with the mesodermal core, but not its induction. All together, data available suggest that *tbx2a* may play a non cell-autonomous role during specification of skeletal progenitors within the pharyngeal arches.

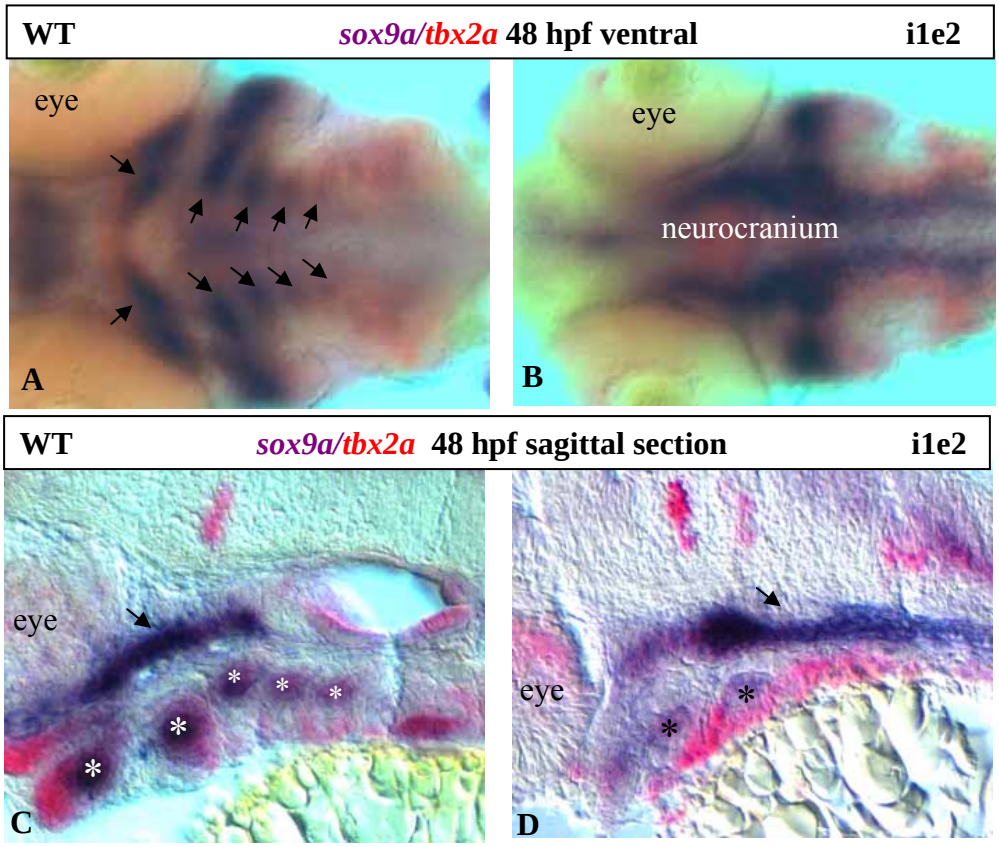

Figure 14: ***tbx2a*** **knock-down affected patterning of mesodermal cores.** In comparison with the control (**A**-ventral; **C**-sagittal section) s*ox9a* staining in the morphants (**B**-ventral, **D**: sagittal section) specifically disminished (D-black asterisks) in the pharyngeal arch domain whereas still remained in the neurocranium (arrow).

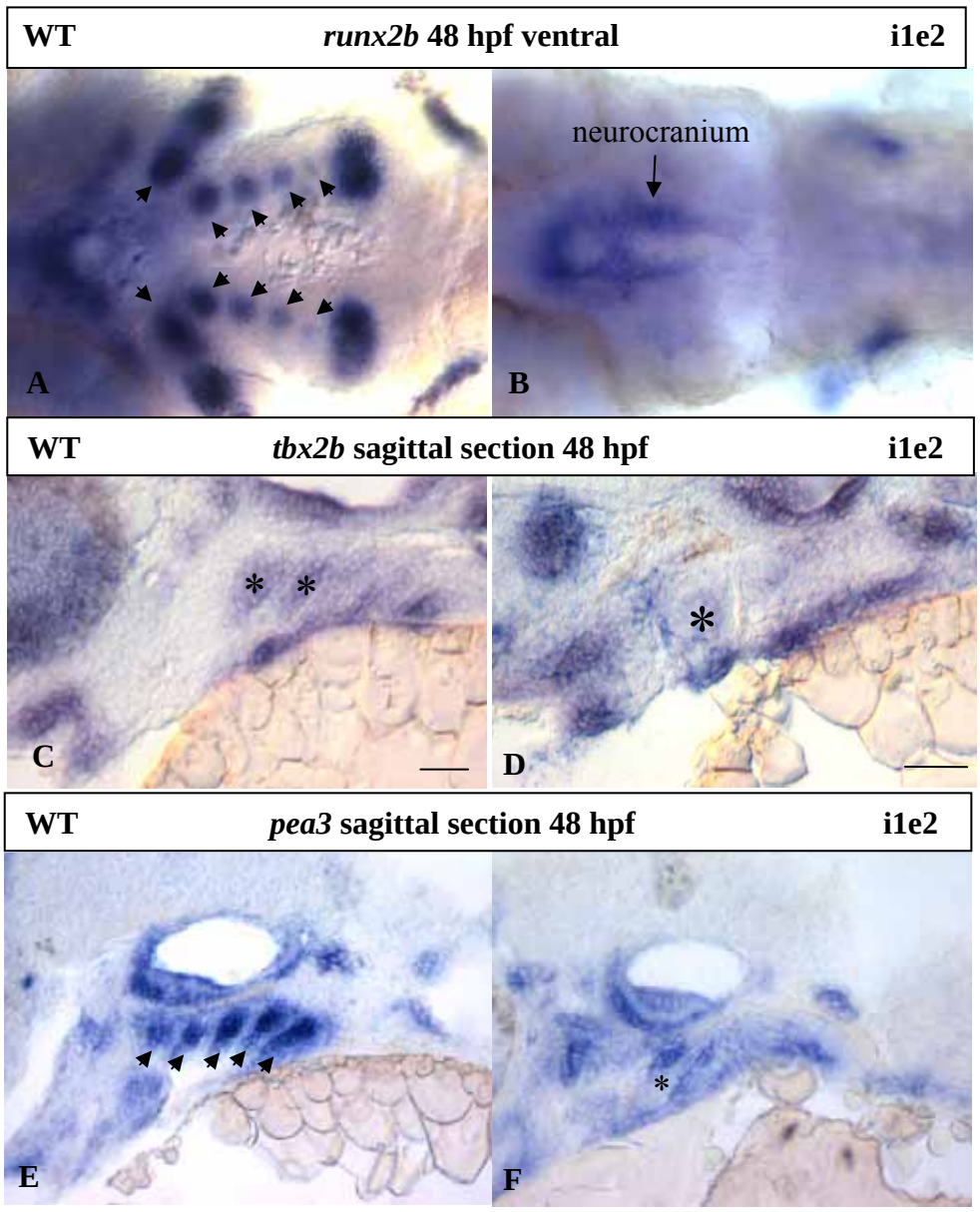

Figure 15: Molecular markers revealed deficiency of cell differentiation in the mesodermal cores in absence of Tbx2a. *runx2b* expressed in the mesodermal cores **(A)** is absent in the morphant **(B).** Similarly, *tbx2b* **(C)** as well as *pea3* **(E)** staining reveal changes in the mesodermal cores in the morphants **(D, F)**

3.5.4 *tbx2a* knock down does not affect hindbrain patterning and development of NCCs

As shown above, the pharyngeal arch phenotype observed in *tbx2a* morphants was not a direct result of Tbx2a on mesoderm specification. Since *tbx2a* is also expressed in some neural crests cells bordering the endodermal pouches especially in the region of the first pouch (Fig. 7C), there may be a possibility that neural crest specification or differentiation is contributing to the over all malformation of the arches. The patterning defect in neural crest-derived structures in pharyngeal arches may originate from changes in hindbrain organization. *hoxa2* is expressed in the hindbrain domain from rhombomeres 2 to 5. It is also expressed in the streams of NCCs originated from that rhombomere region in the second and more posterior pharyngeal arches (Prince et al., 1998). We checked the expression of *hoxa2* at early (Fig. 16A, B) and late developmental stages (Fig. 16C, D, E, F). The morphants displayed no significant changes in *hoxa2* expression in the hindbrain (Fig. 16B, D) and in the migratory and post-migratory NNC (Fig. 16D, F). Similarly, we obtained the same result for *krox20* staining whereby there is no change in the expression domain specific to rhombomeres 3 and 5 (data not shown). The results suggest that *tbx2a* does not play a role in hindbrain patterning and development of NCCs.

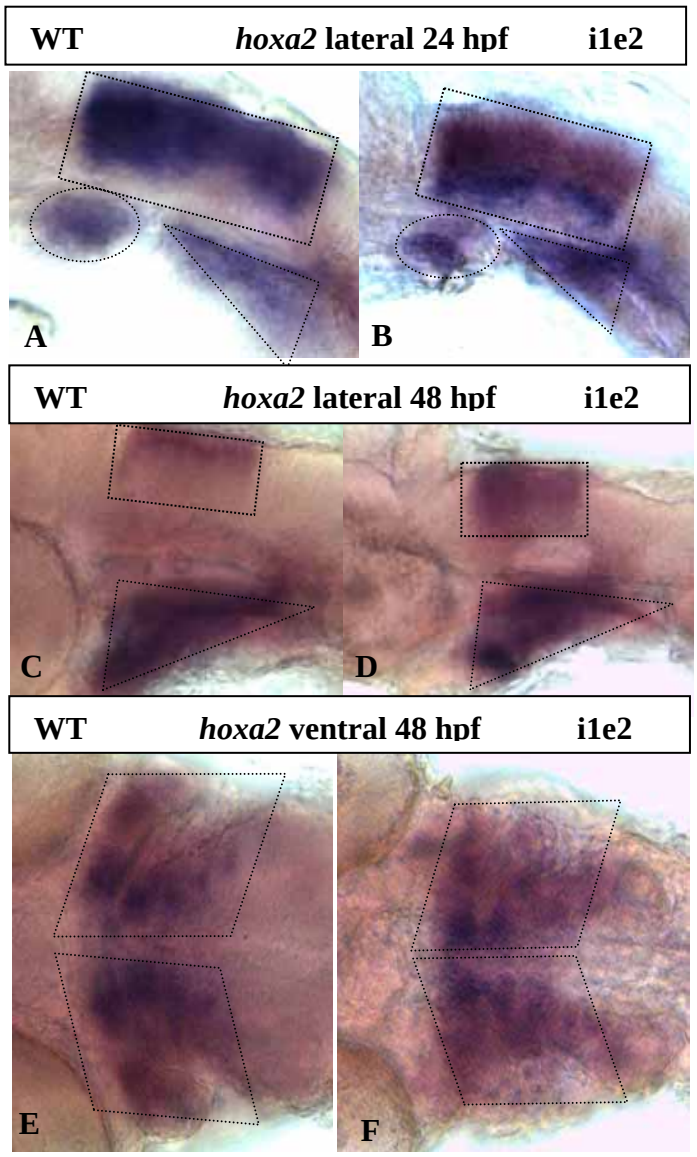

Figure 16: Knock-down of *tbx2a* does not affect the early hindbrain patterning. *hoxa2* staining labels the rhombomeres 2 to 5 and streams of NCCs in the WT early **(A-lateral)** and later on **(C-lateral).** These normal pattern is maintained in the morphants **(B-lateral-24 hpf)** and **(D-lateral-48 hpf).** The normal patterning of the neural crest streams which continue migrating into the pharyngeal arch region are shown both in WT **(E)** and morphant **(F).**

NCCs are induced during gastrulation at the neural plate border and begin to separate from the other neuronal cell types in this territory by expressing neural crest specific genes. Neural crest-derived cartilage is one of three components building up the pharyngeal arches. Since *tbx2a* morphants displayed defective cartilage in the arches, we checked several genetic markers involved in neural crest development.

foxD3 is expressed during initial stage of neural crest specification and later on, during differentiation (Odenthal and Nusslein-Volhard, 1998; Kelsh et al., 2000a, b). There were no significant difference in *foxD3* expression between control and morphant at 12 hpf and later (data not shown). With *hoxa2*, we followed neural crest migration until 2 dpf. *Hoxa2* positive NCCs in both morphant and wild type (Fig. 16E, F) migrated to the pharyngeal region.

Similarly, *dlx2a* expression was examined. By 24 hpf, NCCs migrating as streams of cells were *dlx2* positive. At 0.8 pmole MO (Fig. 17C), morphants still displayed three distinctive groups of NCCs (Fig. 17A). It was noted that the third group of cells, by this stage (24 to 26 hpf), would normally be separated into 2 subgroups by the endodermal pouch (arrow in Fig. 17A). We allowed the morphants to develop 2-4 hours further than controls to rule out developmental delay that is common to many morphants. However, in the morphants, the third group of NCCs failed to separate (arrows in Fig. 17B, C). This is consistent with defects in endodermal pouch development shown earlier. *dlx2a* staining of morphants at 48 hpf revealed the presence of post migrating NCCs in the pharyngeal region (Fig. 18A, B). The sagittal sections showed clumps of *dlx2*-positive NCCs segregated into seven groups in accordance to the seven arches. Even though there were traces of post-migratory NCCs in the morphant, they did not seem to be well segregated by undeveloped endodermal pouches (*tbx2a* transcript in red for endodermal pouches in

Fig. 18D). Overall, our data suggest that *tbx2a* is not essential for the normal patterning and migration of NCCs.

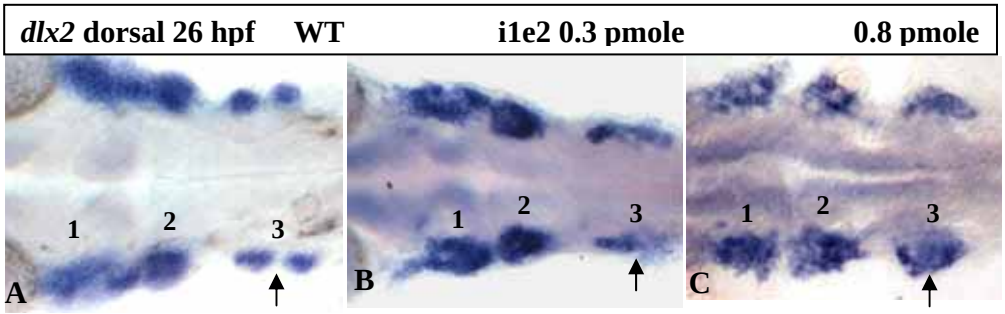

Figure 17: The early neural crest markers show normal induction of neural crest. (A) *dlx2a* labels three main streams of migratory neural crests at 26 hpf. **(B)** These streams are normally formed in the morphant (0.3 pmole) or **(C,** 0.8 pmole). The arrows point the third stream is segregated in the WT (A), but not in the morphants (B, C).

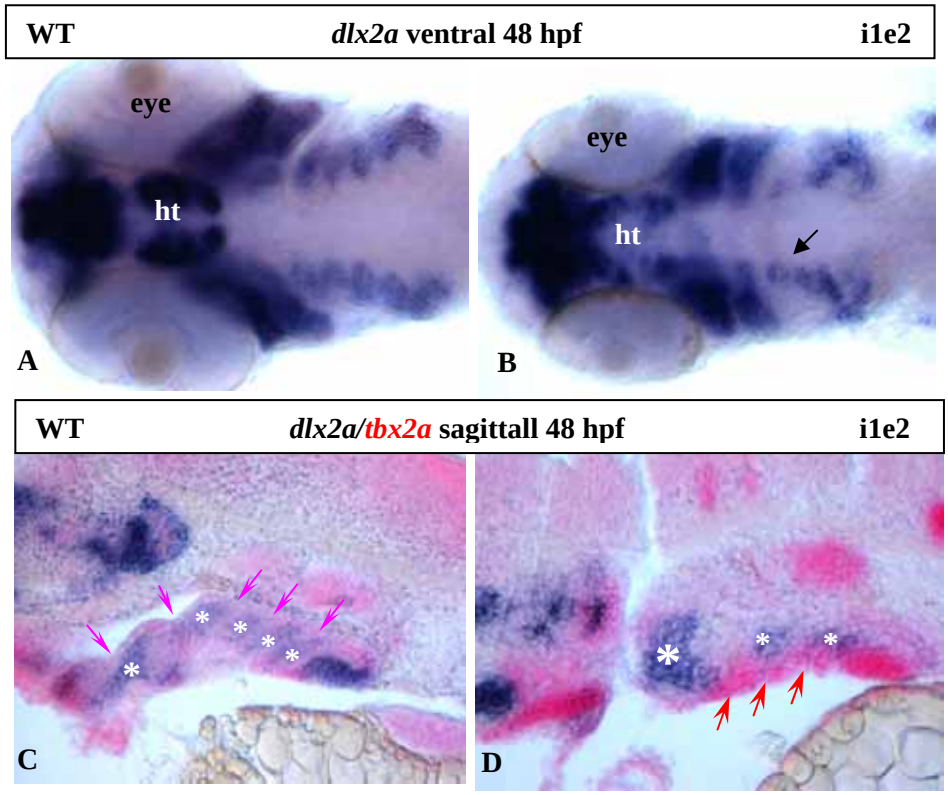

Figure 18: Post migratory neural crests in the pharyngeal region at 48hpf. **(A)** Streams of NCCs labelled with *dlx2a* riboprobe migrate into seven pharyngeal arches. **(B)** There are still traces of NCCs that arrive in the posterior arches (arrow) in the morphants. **(C)** Sagittal section show streams of NCCs (*dlx2a*-purple) separated into discrete arches by endodermal pouches (*tbx2a*-red). **(D)** In the morphant streams of NCCs still strongly express *dlx2a*, but seem to be fused (asterisk, **D**) due to the undeveloped endodermal pouches.

3.5.5 Neural crest differentiation is affected

In the previous section, we have provided lines of evidence for the notion that the induction and migration of neural crests are not affected under the absence of Tbx2a caused by the splice morpholino i1e2 MO. However, to have cartilage tissue established, the NCCs must be committed to differentiate after arriving at their destination from 54 hpf onwards (Schilling and Kimmel, 1997). So, we asked if those unaffected crests in the morphants are able to carry on with the normal process of differentiation.

pax9 is the transcription factor which appears in endodermal pouches and plays a role during chondrogenesis in mouse (Neubüser et al., 1995). In zebrafish, *pax9* appears in the mesenchymal tissue (Nornes et al., 1996; this study). *pax9* has been known as a marker for the initial step of neural crest differentiation (reviewed by Lefebvre and Smits, 2005; Rychel and Swalla, 2007). We analyzed *pax9* transcript distribution in the morphants in comparison with that of the controls. It was noticed that the expression pattern of *pax9* was strongly affected in the *tbx2a* morphants (Fig. 19B). Instead of appearing as bilateral stripes at the distal parts of the seven arches as in the control (Fig. 19A), *pax9* is positive in only one or two disorganized stripes far away from the midline (Fig. 19B). This malformation suggests that *tbx2a*-depletion interferes with the initiation of chondrogenesis, which means the transdifferentiation of the NCCs is affected in the *tbx2a* morphants.

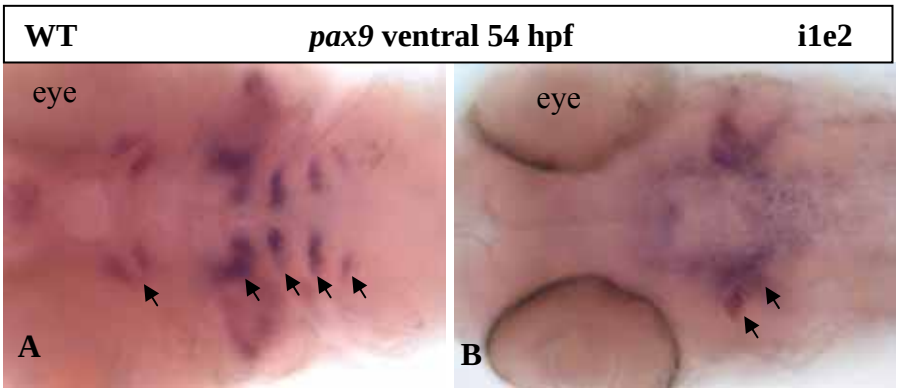

Figure 19: Cartilage differentiation is severely affected in *tbx2a* morphants. (A) *pax9* starts to express at the onset of chondrogenesis in the pharyngeal arches (54 hpf). **(B)** In the morphant, *pax9* pattern is altered and does not show discrete stripes unlike that in the WT.

3.5.6 The differentiation of epibranchial ganglia is affected upon endodermal defect caused by *tbx2a* knock-down

Epibranchial ganglia are formed in close association with endodermal pouches and the number of ganglia is matched with the number of pouches. It was shown that ganglia development is dependent on endodermal pouch morphology and molecular signals (David et al., 2002; Nechiporuk et al., 2005). In this study, we have demonstrated the role of *tbx2a* in endodermal pouch patterning. We now extend the analyses to the epibranchial ganglia. *phox2b* (Fig. 20A, B) and *phox2a* (Fig. 20C, D) (Pattyn et al., 1997) expression revealed consistent defects in epibranchial ganglia in i1e2 MO morphants (Fig. 20B, D). We observed subsets of ganglia which were diminished in size and in level of expression of specific markers phox2a/2b. We also examined neuronal markers at earlier stage when contact between the endodermal pouches and the epibranchial placodes is not fully established. Staining of *ngn1* (*neurog1*_Zebrafish Information Network; Korzh et al., 1998; Andermann et al., 2002) (Fig. 20E, F) and *sox3* (Kan *et al*., 2004; Sun et al., 2007) (Fig. 20G, H) at 24 hpf showed no obvious change in their expression patterns in the morphants compared to the controls. Therefore, the early induction of these epibranchial arches was not affected; however, the later specification could be secondary to endodermal pouch defect.

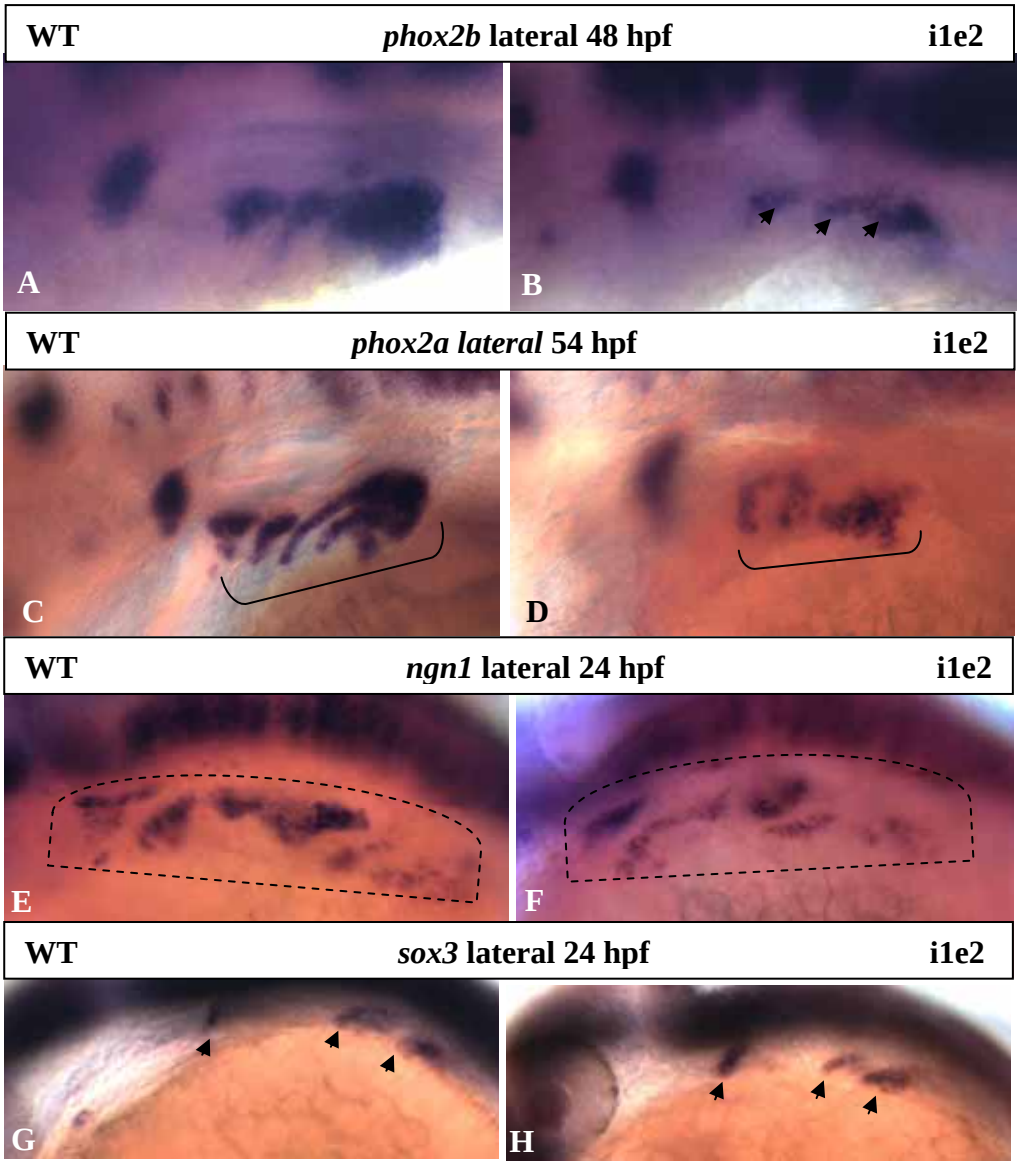

Figure 20: ***tbx2a*** **morphants exhibit defect in epibranchial ganglia differentiation.** All the images are lateral view. Epibranchial placode differentiation is affected in 2 dpf embryos. *phox2b* expressed in differentiating placodes **(A)** reveals that the distal parts of the placodes are affected **(B, arrows)**. *phox2a* labelling the epibranchial placodes **(C)** are also affected in the morphant **(D).** However, early neuronal marker *ngn1* expressed in the early eipibranchial placodes from the early stage of 24 hpf **(E)** is almost unaffected in the morphant **(F)**. Similarly, *sox3* expression pattern **(G)** is also maintained in the morphant at the early stage **(H).**

We looked into motor neuron development in the morphants in greater detail using the islet1 GFP transgenic line coupled with Zn5 immunohistochemistry staining of DM-GRASP, an adhesion molecule expressed on the surface of a subset of growing motor neurons and early endodermal cell-types (Fashena and Westerfield, 1999). Compared to controls (Fig. 21A), the morphants (Fig. 21B) displayed motor neurons that migrated laterally toward the pharyngeal arches but failed to form axons and innervate pharyngeal arches. Hence, the failure to innervate target pharyngeal aches in *tbx2a* morphants is probably a result of defective pharyngeal pouches.

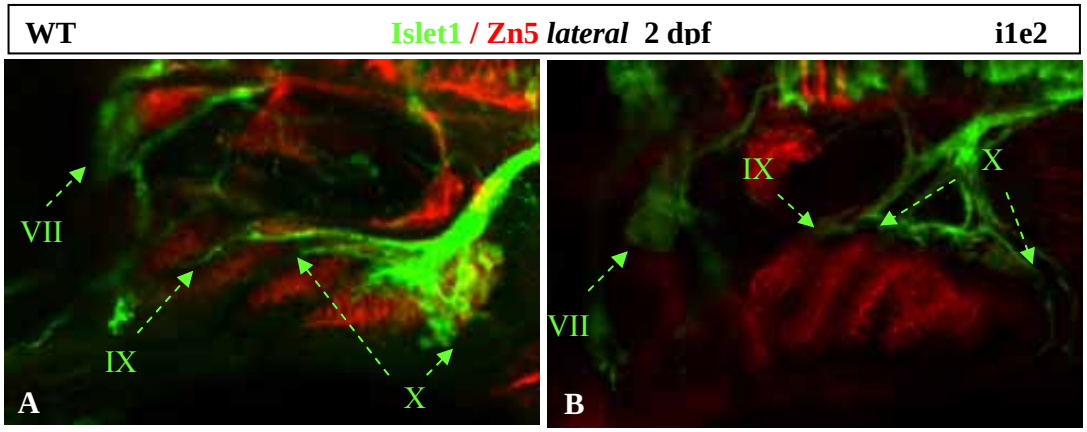

Figure 21: Tbx2a knock-down causes defect in three epibranchial placode-derived sensory ganglia (VII, XI, X) in the islet1-GFP transgenic larvae are visualized with GFP immuno-staining in green (broken arrows). Endodermal pouches are visualized by Zn5 immuno-staining in red. In the control **(A)** sensory ganglia (VII, XI, X) send processes that grew between the endodermal pouches and innervate pharyngeal arches. **(B)** In the morphant, the processes of three ganglia reach the pharyngeal arches but fail to innervate.

3.5.7 Cell Death and Cell proliferation

To determine if the defect in the pharyngeal arches of the *tbx2a* morphants was correlative with cell apoptosis, we applied TdT mediated dUTP nick-end labeling (TUNEL) assay on 2 dpf embryos and confocal imaging for a close look at the arch region. In the control specimens (Fig. 22B – WT, C – p53 MO injected), very few apoptotic cells were detected. Conversely, there was an obvious increase in apoptosis in the i1e2 morphant specimen (arrowheads in Fig. 22D). Even with the co-injection of p53 MO, the morphants still exhibited specific cell death in the pharyngeal arches (fig. 22E), which means the cell death in pharyngeal arches is a specific effect of *tbx2a* MO and independent from p53 signaling. The assay was repeated on three different sets of embryos (three each of WT and morphant embryos). In general, the data suggest that *tbx2a*-knock down caused p53-independent apoptosis and may be an indirect consequence of the pharyngeal arch defect or vice versa.

Cells rapidly divide during embryogenesis. These cells could be detected via the expression of phospho-histone 3 (pH3) - a mitotic cell marker (Wei et al., 1998). Indeed, we find that the ability to initiate cell division is not reduced in *tbx2a* morphants (Fig 23). Therefore, the data suggest that although tbx2a is not required for cell proliferation, it may be important for cell viability.

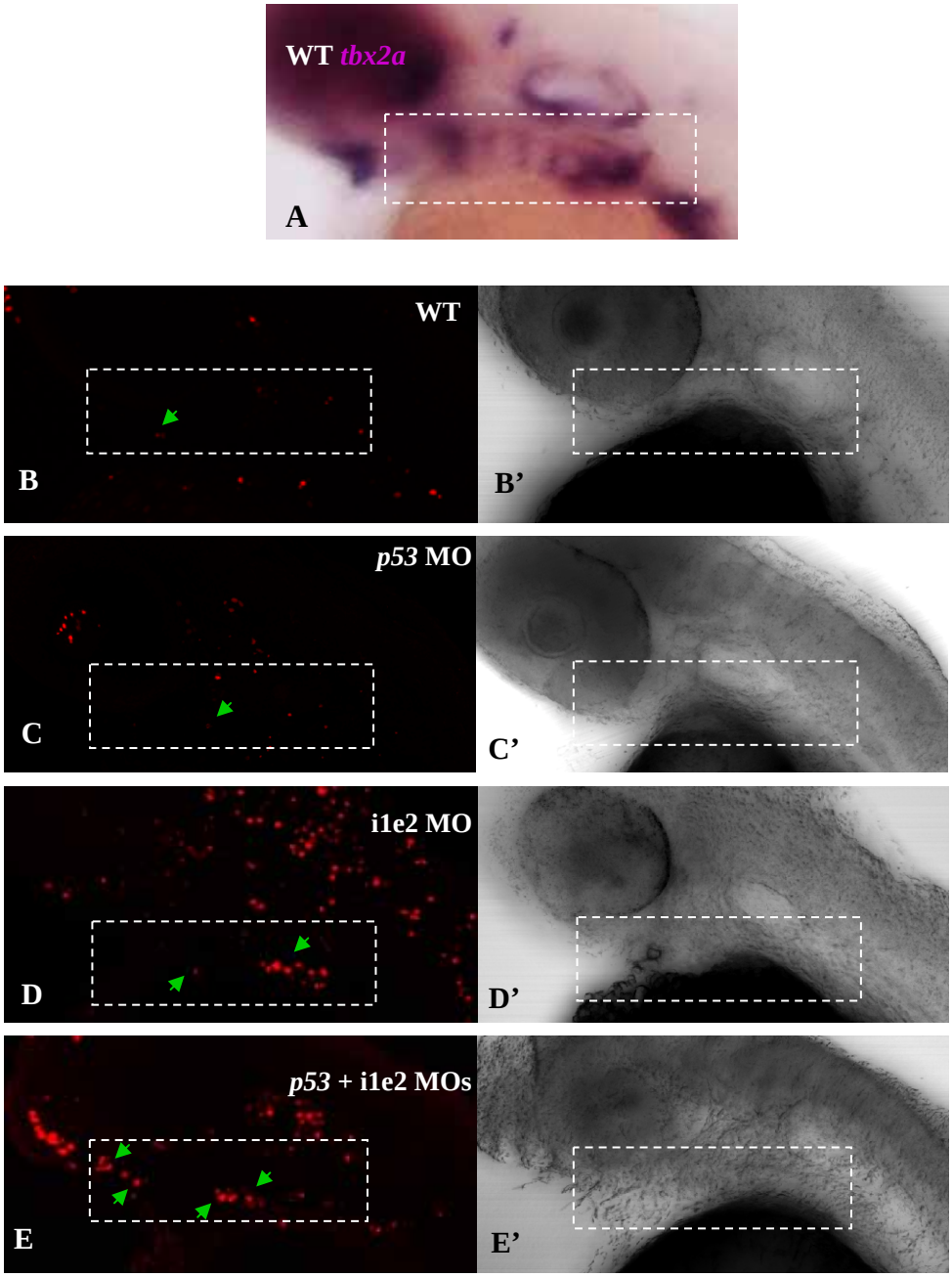

Figure 22: Cell death TUNEL in situ staining on 48 hpf embryos. Broken rectangulars indicate the pharyngeal arch region. Images on left side are dark **(A)** Lateral view of embryo stained with *tbx2a* to locate pharyngeal arch region. **(B, B')** WT embryo shows very few dead cells. **(C, C')** *p53* MO-injected embryos exhibit similar pattern as in WT. **(D, D')** i1e2 morphant exhibit cell death in CNS and pharyngeal arches, **(E, E')** co-injection of *p53* MO does not rescue pharyngeal cell death in i1e2 morphants, number of dead cells still appear obviously higher compared to the controls.

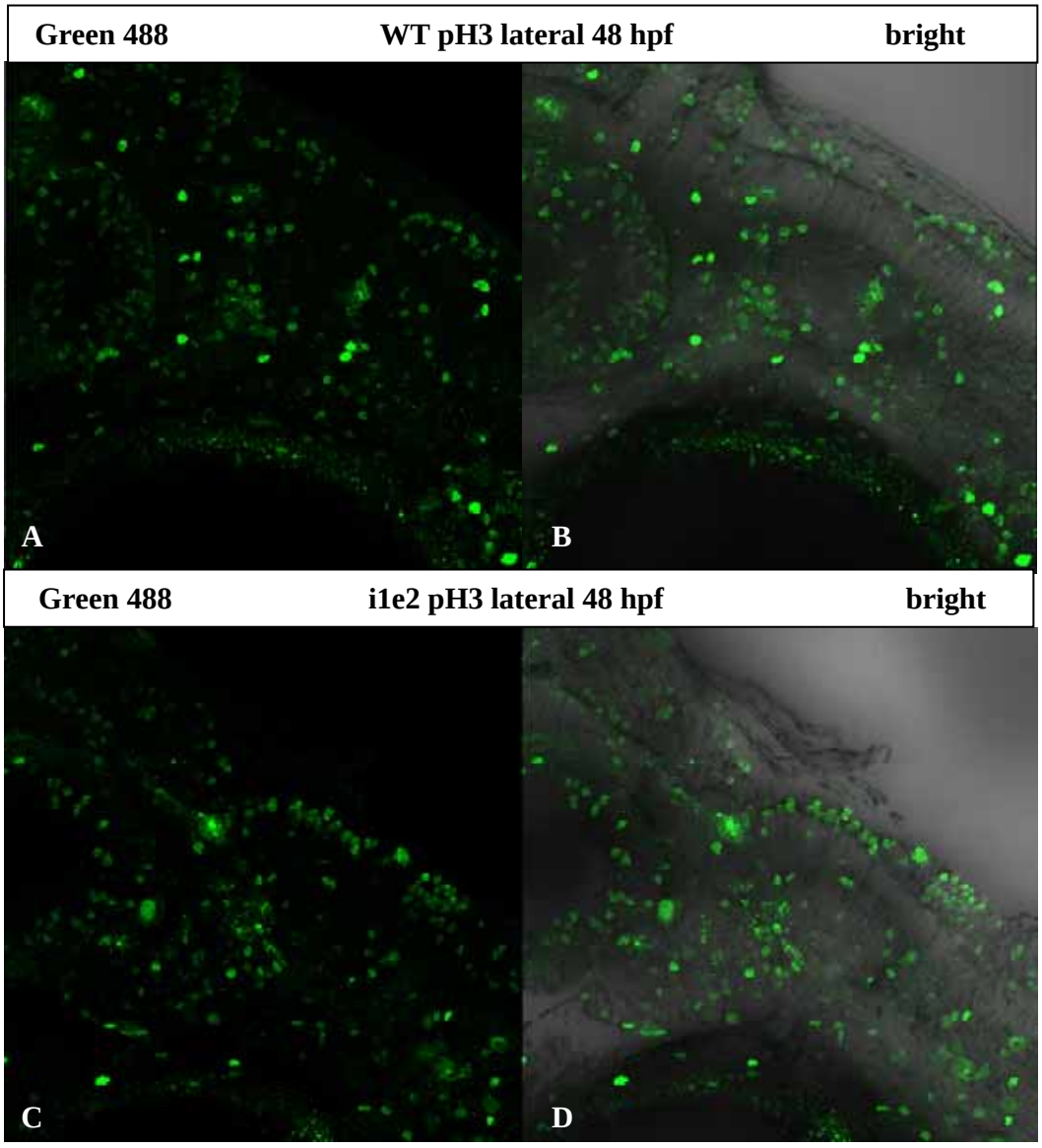

Figure 23: *Tbx2a* knock-down does not affect cell proliferation. Embryos were stained using anti-pH3 Green 488 Monoclonal antibody to detect proliferating cells. (**A, C)**: fluorescent image; **(B, D)**: composite fluorescent/bright field image. All embryos are shown in lateral view at the pharyngeal arch region. The number of pH3-positive cells in the control **(A or B)** is roughly the same with that in the morphant **(C or D)**. Estimation was done using Image-J.

3.5.8 Tissue-specific knock-down of *tbx2a* in the endoderm of pharyngeal arches

Multiple attempts to rescue the i1e2 MO morphant phenotype with *tbx2a* mRNA were unsuccessful even though a range of concentrations were tested. We co-injected the lowest dose of i1e2 MO at 0.15 pmole (the lowest dose that would produce a phenotype) with *tbx2a* mRNA at 20 pg, 35 pg and 50 pg. This negative outcome is likely due to the dose sensitive nature of Tbx2a – over-expression of Tbx2a might produce phenotypes that masked a rescue (data not shown). As such, working out the precise dosage of MO and mRNA turned out to be very challenging.

What we needed was a method to affect endodermal pouches selectively. We could then demonstrate that the phenotype observed with *tbx2a* MO is indeed specific. The zebrafish receptor kinase Taram-A is a type I subunit of the TGF-β receptor. It is expressed in presumptive endomesodermal cells during gastrulation (Renucci et al., 1996). Peyrièrat et al. (1998) have shown that constitutively active Taram-A (Taram-A*) can direct progenitors of the marginal blastomere at 16-cell stage (Fig. 24A) to develop as anterior endodermal derivatives. We employed this technique to direct *tbx2a* knocked-down cells to the endodermal pouches.

0.6 pg Taram-A* mRNA (Peyrièrat et al., 1998) was injected into one single marginal blastomere at the 16 cell stage together with 70kD fluorescine dextran. More than 50% (n = 30/55, from 3 batches) of injected embryos exhibited labeled cells in the endodermal pouches and the embryos developed normally (as shown in Peyrièrat et al., 1998, and illustrated in Fig. 24B). An advantage of this technique is that labeled pouches were found on one side of the body, leaving the other side as a control (Fig. 24B). It should be noted that there was no toxicity effect of Taram-A* mRNA at

0.6pg. We checked all 0.6pg Taram-A* injected embryos by Alcian blue staining and found none with cartilage defect (data not shown).

0.05 pmole i1e2 MO was co-injected with 0.6 pg Taram-A* mRNA and 70kD dextran into one of the marginal blastomeres at 16-cell stage (illustrated in Fig 24A). For examination, we selected approximately 50% of the total 55 injected embryos (from 3 batches) which were clearly labeled at around 30 hpf. These injected embryos were allowed to develop until 3 dpf. By staining with Alcian blue, all of these embryos exhibited cartilage defect on the injected side, where five branchial arches fail to develop (crosses in Fig. 24C). In addition, dextran-labeled cells were not found in endodermal pouches. In view of previous findings with TUNEL assay, this could be the result of cell death in the arch region.

In summary, our analysis has provided systematic and substantial evidence for the roles of *tbx2a* during specification of pharyngeal arches. We have shown that *tbx2a* is initially required to regulate morphogenesis of endodermal pouches, and subsequently affect the development of mesodermal cores and differentiation of NCCs. Interestingly, the loss of *tbx2a* in the endoderm pouches also affects differentiation of the ventral part of epibranchial placodes. Altogether, our data strongly support the central role of endodermal pouch during specification of pharyngeal arches.

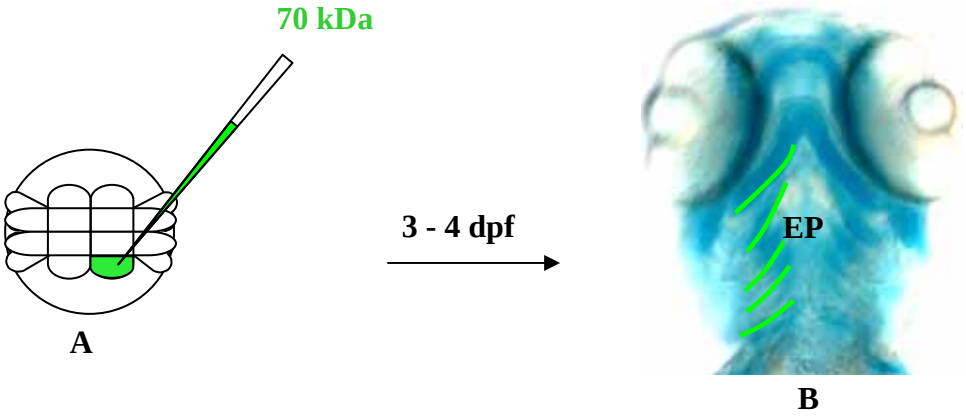

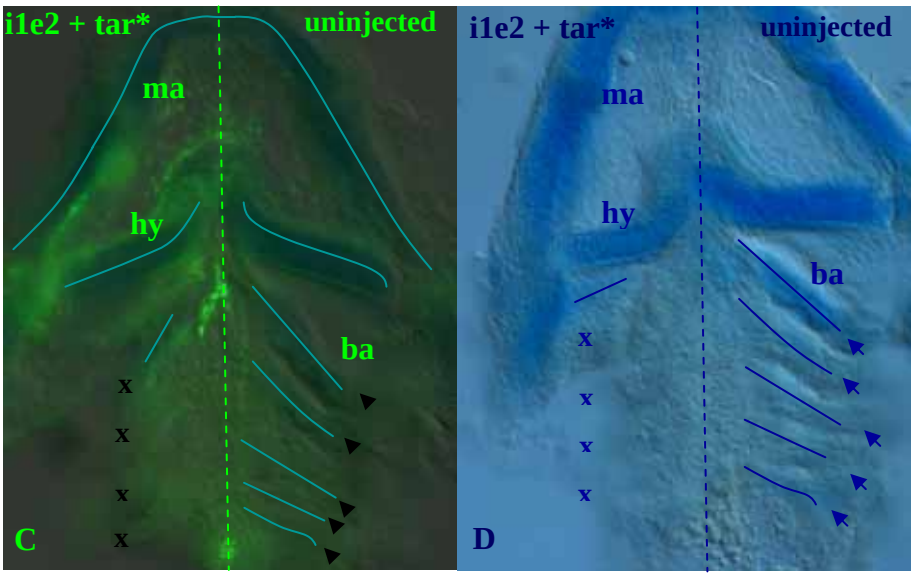

Figure 24: Knock-down of Tbx2a in branchial arches causes their anomaly. (A) The injection of a single marginal blastomere at 16-cell stage. This blastomere gave rise to the future endoderm. In presence of *tar** mRNA all descendants became endodermal, which resulted in the specifically labelled endodermal pouches **(B)** on left-hand side only_illustrated by green drawn lines. **(C)** Tissue specific knock-down of *tbx2a* in the endodermal pouches on the left-hand side caused absence of the posterior branchial arches (crosses). The Alcian bule stained pharyngeal arches are marked with blue lines. **(D)** Bright field imaging of **(C)**

Chapter 4

Discussion

4.1 Morpholinos designed specifically disrupt *tbx2a* translation

tbx2a is not maternally expressed and is only detectable after 10 hpf by both WISH and RT-PCR. It has been shown in mammalian cells that Tbx2 contains serine residues 336, 623 and 675, located within the DNA binding domain (T-box domain), which are phosphorylation targets for p38 MAPK – mitogen-activated protein kinase (Abrahams et al., 2007). These residues are conserved across vertebrate species. The T-box domain is encoded by a part of exon 1, and complete exons 2, 3 and 4 (shown in Chapter 3) and is a good target for splice-targeting MOs. In addition, Tbx2a has a C-terminal trans-activation domain that is required for protein-protein interaction and is essential for its function (Minguilon and Logan, 2003). The 5' terminus encoded by exons 5 and 6 is also a potential target for MOs. The three MOs designed (e1i1, i1e2, i5e6) all produced a single class of phenotype which is consistent with the expression pattern of *tbx2a*. Of these, MO i1e2 is the most efficient, consistently producing specific phenotype at the lowest dose (0.05-0.1 pmole/embryo). The interference of i1e2 leads to a peptide of less than 100 amino acids that lacks a functional T-box domain. An estimation of efficiency of morpholino-dependent reduction of *tbx2a* transcript by RT-PCR (Fig. 5) showed reduction of transcript. This RT-PCR result is not in conflict with the more intense WISH staining (Fig. 14D and 18D) which could be attributed to the possibility that WISH staining may also pick up signal from both normal and abnormal transcripts.

More importantly, we have confirmed the phenotype on the background of *p53* morphants, which strongly ruled out the off-target effects of MOs described by Robu et al., (2007). Also, with the considerably low concentration (0.1 pmole/embryo) employed in this study, *tbx2a* MO is not expected to produce severe off-target effects.

4.2 Tbx2a is indispensable for morphogenesis of endodermal pouches

The expression of *tbx2* in the pharyngeal arches is conserved across species (Table 3, Chapter 3). This suggests an important role for the gene in the development of this organ. We report in this study that *tbx2a* is involved in the morphogenesis of endodermal pouches. Since *tbx2a* is not expressed in the endodermal pouches at early stages, we are not surprised that the induction and segmentation of the endodemal pouches are normal in the morphants. With the endoderm-specific marker *nkx2.3*, it is clearly shown that endoderm can be segmented into distinct slits or pouches. However, these pouches either failed to expand along the dorso-ventral axis towards to the ectoderm or they are broken and disorganized in *tbx2a* morphants. This is also illustrated by the marker *pea3*, and by the GFP pattern of the transgenic line ET33-1B. While pouches are successfully induced to bud from the lateral walls of the pharynx, with endodermal cells of the pouch extending along the proximo-distal axis (seen clearly from ventral perspective as six *nkx2.3* positive discrete pouches), they failed to migrate dorso-ventrally, and are stuck on the horizontal axis instead. So, although *tbx2a* is not involved in endodermal segmentation, it is required for pouch outgrowth. Previously, Quinlan et al. (2004) have shown that an accumulation of F-actin at the apical surface of cells in the pouch is necessary to direct and constrain the movement of endodermal cells into a narrow group with a slit-like shape (reviewed by Graham et al., 2005). Because N-cadherin connects to the actin cables, it is possible that it is also involved in the regulation of pouch morphogenesis. T-box transciption factors have been shown to regulate cell adhesion molecules (e.g *cx43*) and play roles in cell migration (reviewed by Smith, 1999). Fong et al. (2005) have reported the role of the paralog *tbx2b* in cell adhesion, within the context of Wnt signaling, during the migration of cells into the neural plate. It would be interesting to determine whether

during formation of the endodermal pouches, *tbx2a* regulates expression of cell adhesion molecules. This might be a constitutive part of the *tbx2a*-dependent mechanism regulating morphogenesis of pharyngeal arch endoderm. Given the fact that earlier it was shown that depending on developmental situation Tbx2 acts downstream of Nodal signaling during notochord development (Dheen et al., 1999) and downstream of Wnt signaling during formation of the neural plate (Fong et al., 2005), it is of interest to determine within which signaling pathway Tbx2a acts during morphogenesis of the endodermal pouches of pharyngeal arches.

tbx1 is another *t-box* gene also expressed in endodermal pouches and *van gogh* (*vgo*, *tbx1*$^{-/-}$) mutant exhibits pharyngeal skeletal defects as a result of the defect in endodermal pouches (Piotrowski et al., 2003). In addition, that study observed a fusion of neural crest-derived cartilage in the posterior arches of the mutant. *tbx2a* morphants also display defect in endoderm pouch morphogenesis, however cartilage deriving from post-migratory NCCs does not form in the position of pharyngeal arches. Our observation was confirmed on the *p53* morphant background, in which the Alcian blue stained cartilage was totally lost, ruling out off-target effects of the MO (Robu et al., 2007). Therefore, *tbx2a* possibly functions as an inducer of endoderm-derived secreted signals necessary to trigger specification of NCCs towards the chondrogenic fate. Moreover, the absence of the thymic differentiation marker *rag1* (Willett et al., 1997) revealed a defect in the third pharyngeal pouch where the thymus is derived from (Gordon et al., 2001). Altogether, the data strongly support the role of *tbx2a* in the development of the endodermal pouches.

It has been hypothesized that endodermal pouches play a leading role in pharyngeal arch development (reviewed by Graham et al., 2003 and 2005). In contrast, Cerny et al. (2004) have shown that instead of the endodermal pouch, the

epidermis could direct the navigation of NCCs in axolotl. Our study on *tbx2a* function within the endodermal pouches provides molecular evidence in support of the idea that the endodermal pouches play a leading regulatory role in the development of pharyngeal arches.

4.3 Tbx2a acts upstream of endoderm-derived signals regulating cartilage development

sox9a, runx2b, tbx2b, pea3, and *ET33-1B gfp* transcripts normally present in the mesodermal cores are reduced or lost in *tbx2a* morphants. Although the GFP expression in *tbx2a* MO-injected ET33 embryos disappears from the pharyngeal region, it is nevertheless present in other cartilaginous structures like the cleithrum. Similarly, while *sox9a* expression is vastly diminished in the pharyngeal elements of the morphants, its expression is normal in the neural cranium. These observations are also indicative of the specificity of the MO used in this study. Therefore, it is highly possible that the mesodermal cores of the pharyngeal arches themselves are not developed properly or strongly diminished in *tbx2a* morphants, which may in turn contribute to the failure in cartilage formation.

In parallel, we would like to discuss the role of NCCs in cartilage formation. The normal expression of markers early on at 24 hpf, as well as later on at 48 hpf (*dlx2a, hox2a*), strongly suggests that neural crest induction and migration is not perturbed by the absence of *tbx2a*. In other words, NCCs are able to reach the future pharyngeal arches. We also checked the expression pattern of *crestin*, a specific marker for all migratory and post-migratory NCCs (Luo et al., 2001). Its expression in the morphants is similar to that in the wild type controls (data not shown). The data clearly demonstrates that *tbx2a* is not required for neural crest induction and migration. This is consistent with studies done in *vgo* mutants where in the face of

endodermal pouch defect, neural crest induction and migration is not affected. However, the NCCs in *vgo* mutants were unable to assemble into discrete arches.

Kimmel *et al.* (2001) described that in zebrafish the NCCs migrate from outside into the primordia of pharyngeal arches to wrap around the mesodermal cores. They referred to these cores as ectomesenchymal cores that will give rise to cartilage and then endochondral bones. Cerny *et al.* (2004) also demonstrated similar movement in axolotl. They further highlighted that the first sign of endodermal pouch appeared only after the first pharyngeal neural crest stream reached the endoderm at the ventral level. In our study, by 2 dpf, *dlx2a*-positive post-migratory NCCs are present as discrete patches at the first two arches and mildly decreased at the posterior arches in the morphants. Having noticed that endodermal pouches were malformed and mesodermal cores were not developed by that stage in the *tbx2a* morphants, we interpret that migration of NCCs to the pharyngeal arch area is independent from development of mesodermal cores and endodermal pouches. Altogether, our observation is compatible with that of Kimmel et al. (2001) and Cerny et al. (2004).

Although the migration of NCCs is normal, chondrogenesis from 44 hpf onward is strongly affected in *tbx2a* morphants. That was demonstrated by the strong negative effect of the i1e2 MO on expression of *sox9a* and *runx2b*, both early markers for mesoderm-derived chondrogenesis (Yan et al., 2005; Flores et al., 2006). In mammals, the Sox9 protein binds to a chondrocyte-specific enhancer within the intron of *col2a1*, and plays a role as an upstream activator (Bell et al., 1997; Ng et al., 1997). In fact, *col2a1* expression in the zebrafish s*ox9a* mutant *jellyfish* (*jef*) has been reported to be affected (Yan et al., 2002). It is also highlighted that *jef* has normal prechondrogenic cores however progression into differentiated cartilage from 54 hpf onward is affected (Schilling and Kimmel, 1997). This is different from *tbx2a*

morphants which do not possess normal prechondrogenic cores, which has been demonstrated with other markers such as *runx2b, pea3*. Therefore, it is suggested that *tbx2a* may affect the chondrogensis earlier than the chondrogenic markers shown (*sox9a, runx2b, pea3*).

Fgf signaling has been proposed to play a role of a general endodermal regulator governing neural crest migration and trans-differentiation into cartilage (Crump et al, 2004). In contrast to Fgfs, Tbx2a affects the NCCs later and this is more obvious at the trans-differentiation stage after arriving at their destined segments.

Altogether, the defects in mesodermal cores and cartilage specification can be attributed to the disruption of *tbx2a* endogenously in the endodermal pouches. Even though the post-migratory NCCs are present in the future pharyngeal arches, we found that they are not able to proceed with cartilage differentiation. This event is coupled with undeveloped mesodermal cores. Hence, this supports the idea that an interaction between these two components (NCCs and mesodermal cores) is necessary for chondrogenesis or cartilage formation to take place (Sperber et al., 2008). It also means that post-migratory neural crest differentiation is strongly dependent on environmental influence.

4.4 *tbx2a* knock-down indirectly affects pharyngeal neurogenesis

A number of cranial sensory ganglia are derived from two sources: the NCCs and the placode, the border region between the epidermis and neural plate. In this study, we report no defect found during specification and migration of NCCs in the morphants. However, *phox2a* and *phox2b* positive epibranchial ganglia are dramatically reduced. And yet, *tbx2a* is not expressed in these structures. A previous study in zebrafish has revealed that pharyngeal neurogenic differentiation in the

ectoderm commenced within a few hours of endodermal contact (Holzschuh et al., 2005), which suggests a direct interaction arising from proximity of these tissues. *phox2a*-positive ganglia consist of the proximal and distal parts. The distal part is adjacent to the pharyngeal pouch and has been hypothesized to depend on signals from the pharyngeal pouch (Holzschuh et al., 2005). The expression pattern of *phox2a* in *tbx2a* morphants is similar to that in *vgo* mutant (Holzschuh et al.a, 2005), where the distal part is affected. As shown by our analysis of the *islet1-GFP* transgenic line, three epibranchial placode-derived sensory ganglia (VII, XI, X) fail to innervate the pharyngeal arches of morphants at 48 hpf (Fig. 21B). Hence, the perturbation of epibranchial neurogenesis in the *tbx2a* morphants is likely to result from the defect in the endoderm. Thus, our data is entirely consistent with the role of endoderm signaling on epibranchial neurogenesis (Begbie et al., 1999; Holzschuh et al., 2005; Nechiporuk et al., 2005; Trokovic et al., 2005).

However, *tbx2a* is not involved in the early specification of epibranchial placodes. Indeed, *ngn1* which is present prior to *phox2a/2b* and regulates all sensory ganglia in zebrafish (Andermann et al., 2002) exhibits a normal expression pattern in the morphants. The *sox3*-positive epibranchial placodes (Sun et al., 2007) are also unaffected. Therefore, these observations strongly suggest that the early initiation of placodes is independent from *tbx2a* in the endoderm. This is expected due to the fact that the contact between epibranchial placodes and endoderm is not fully established at this early stage.

Our study has shown that *tbx2a* within the endodermal pouches of pharyngeal arches may play a key role upstream of signals involved in the neurogenic differentiation of epibranchial placodes at the later stage, but not at the early induction stage. Several signaling molecules such as Bmps and Fgfs within the pharyngeal

endoderm have been hypothesized to be involved in epibranchial neurogenesis (Holzschuh et al., 2005; Nechiporuk et al, 2005). It has been shown in chick that Bmp2-mediated upregulation of *tbx2* is involved in the development of the heart (Yamada et al., 2000) and hypothalamus (Manning et al., 2006). Thus, Tbx2a might be functioning within the context of Fgf or Bmp signaling.

4.5 *tbx2a* knock-down is correlated to apoptosis in the pharyngeal arches

Using confocal microscopy, we did not detect a difference in the number of proliferating cells (pH3+) between the controls and morphants (n=3). However, TUNEL assay clearly show an increase in apoptosis specific to the pharyngeal arch region of the *tbx2a* morphants co-injected with *p53* MO. As reported by Harrelson et al., (2004) *p53* signaling is unaffected in *tbx2* null mice. Therefore, we think that cells destined to contribute into endodermal pouches are unable to migrate properly, which in turn triggers cell death in a p53-independent manner. Although the signaling pathway involved was not characterized in this study, our data suggest that *tbx2a* is required for cell survival within the pharyngeal arch region.

4.6 Chimaeric morphants: tissue specific gene knock-down

tbx2a expression is present in both pharyngeal endoderm and anterior neuroectoderm rather early in the hindbrain rhombomere 2 (14 hpf), and subsequently at rhombomere 4 and vagal motor nuclei later on (48 hpf). We have shown that pharyngeal neural crest migration and specification are not affected in the *tbx2a* morphants. Besides, we also checked pigment cells – one of neural crest derivatives in the morphants with two specific markers: *dopachrome tautomerase_dct* (Kelsh et al, 2000b) and *crestin* (Rubinstein et al., 2000), and found no major difference between the WT and morphants (data not shown). Thus, despite the presence of *tbx2a* in the

hindbrain, neural crest derivatives were unaffected in the morphants. This is to be expected, since *tbx2a* is not expressed in the pre-migratory NCCs and/or *tbx2a* may play a redundant role in respect to *tbx2b* in the hindbrain. In contrast, we were able to demonstrate that the tissue-specific ablation of *tbx2a* within the pharyngeal endoderm after 1/16 injection resulted in cartilage deficiency. Therefore, it is conclusive that the loss of pharyngeal arches is solely attributed to the defect in the pharyngeal endoderm.

Although we have obtained some understanding about the role of *tbx2a* in regulating endodermal pouch morphology and its indirect effect on the chondrogenesis of the pharyngeal arches, downstream signals involved in this process are unknown thus far and must require further investigation.

4.7 Possible divergent functions of *tbx2a* and *tbx2b* during pharyngeal arch development

In the mouse, *Tbx2* is expressed in the pharyngeal arch region. Nevertheless, it has not been described which germ layer *Tbx2* is restricted to as well as its specific function in this organ. In chick, *tbx2* is known to express in both pharyngeal pouch epithelium and mesenchyme. However, in zebrafish the two paralogues, *tbx2a* and *tbx2b* are expressed in a complementary manner in the pharyngeal arch. For example, while *tbx2a* is restricted to the endodermal pouches, *tbx2b* is in the arch mesenchyme. It would be interesting to identify the role of *tbx2b* in the pharyngeal arches. The split in expression of two *tbx2* probably results in the separation of their functions. This developmental situation is useful for dissecting the role of the respective genes in each compartment. This may be helpful in attempts to reveal the interaction of various compartments of the arch during its development. In the case of *tbx2a*, we established that the gene is not involved in neural crest patterning but can affect the overall

development of the pharyngeal arches including chondrogenesis and epibranchial neurogenesis by affecting the morphogenesis of the endodermal pouches.

4.8 Conclusion

Our study revealed a role for *tbx2a* during development of the endodermal components of pharyngeal arches. Detailed description of its expression pattern revealed a number of domains where the expression was conserved between different species while highlighting domains that are species-specific. This provided the foundation for subsequent functional analysis.

From the functional analysis, we have shown for the first time these important findings:

1. *tbx2a* is indispensable for morphogenesis, but not induction, of the pharyngeal endodermal pouches.
2. The defect in endodermal pouches in turn affects the process of development of the mesodermal cores.
3. Neural crest induction and migration are independent from *tbx2a* in the endoderm and mesodermal core. However, the later event of differentiation of mesenchymal cells (NCCs and mesodermal cells) into cartilage was severely affected in the absence of *tbx2a*.
4. It highlights a role for *tbx2a* in the endodermal pouches for the patterning of epibranchial placodes.
5. Importantly, our data suggest that cell death in the absence Tbx2a correlates to the phenotype observed in *tbx2a* gene knock-down.

Thus far, there has been no knowledge of how *tbx2* is involved in development of the pharyngeal arches in mammals. Our study suggests a local impact of *tbx2a* within the endoderm. It is important to analyze the function of other *t-box* genes during pharyngeal arch development and hopefully shed more light on the roles of

endodermal pouches in comparison with that of mesodermal cores and NCCs (illustrated in scheme 4).

Moreover, the fact that *tbx2a* is also found in other endodermal derivatives such as liver, swim bladder and anterior gut (shown in this study) has triggered a critical question of whether *tbx2a* acts via a common mechanism to regulate the development of endoderm-budding organs.

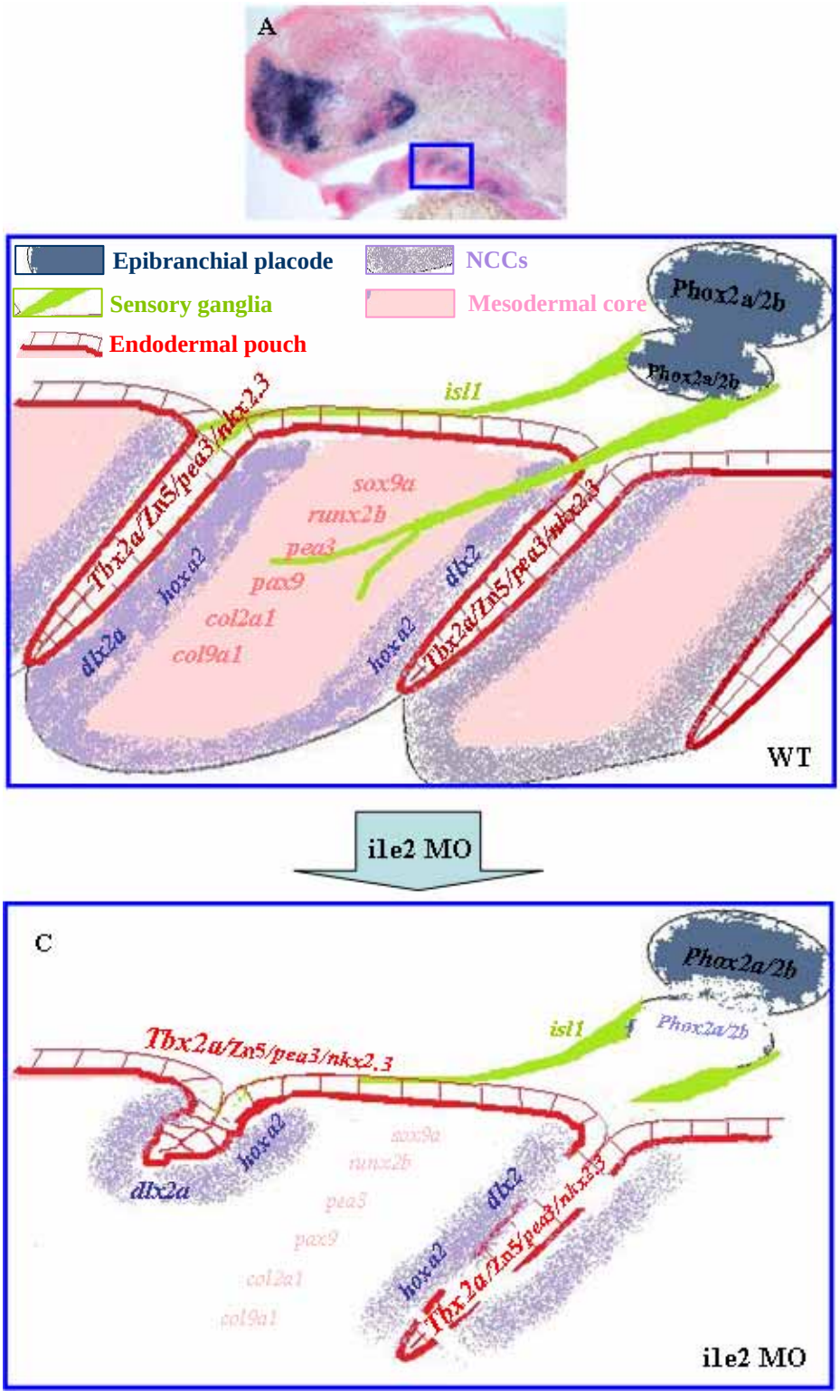

Scheme 4: Summary of function of tbx2a in the pharyngeal arches. *tbx2a* knockdown causes dysmorphic endodermal pouches autonomously. Subsequently, neural crest and mesodermal core differentiation are undeveloped as the secondary defect. Pharyngeal neurogenesis is also affected. Altogether, they contribute to the total loss of pharyngeal arches.

References

Abrahams, A., Mowla, S., Parker, M., Goding, C. and Prince, S. (2008). UV-mediated regulation of the anti-senescence factor Tbx2. *J Biol Chem* **283**, 2223-30.

Akimenko, M., Ekker, M., Wegner, J., Lin, W. and Westerfield, M. (1994). Combinatorial expression of three zebrafish genes related to distal-less: part of a homeobox gene code for the head. *J Neurosci* **14**, 3475-86.

Akiyama, H., Chaboissier, M., Martin, J., Schedl, A. and de Crombrugghe, B. (2002). The transcription factor Sox9 has essential roles in successive steps of the chondrocyte differentiation pathway and is required for expression of Sox5 and Sox6. *Genes Dev* **16**, 2813-28.

Alexander, J., Rothenberg, M., Henry, G. and Stainier, D. (1999). casanova plays an early and essential role in endoderm formation in zebrafish. *Dev Biol* **215**, 343-57.

Alexander, J. and Stainier, D. (1999). A molecular pathway leading to endoderm formation in zebrafish. *Curr Biol* **9**, 1147-57.

Andermann, P., Ungos, J. and Raible, D. (2002). Neurogenin1 defines zebrafish cranial sensory ganglia precursors. *Dev Biol* **251**, 45-58.

Alt, B., Reibe, S., Feitosa, N., Elsalini, O., Wendl, T. and Rohr, K. (2006). Analysis of origin and growth of the thyroid gland in zebrafish. *Dev Dyn* **235**, 1872-83.

Ayer-Le Lievre, C. S. and Le Douarin, N. M. (1982). The early development of cranial sensory ganglia and the potentialities of their component cellsstudied in quail-chick chimeras. *Dev. Biol.* **94**, 291-310.

Bamshad, M., Lin, R., Law, D., Watkins, W., Krakowiak, P., Moore, M., Franceschini, P., Lala, R., Holmes, L., Gebuhr, T. et al. (1997). Mutations in human TBX3 alter limb, apocrine and genital development in ulnar-mammary syndrome. *Nat Genet* **16**, 311-5.

Basson, C., Bachinsky, D., Lin, R., Levi, T., Elkins, J., Soults, J., Grayzel, D., Kroumpouzou, E., Traill, T., Leblanc-Straceski, J. et al. (1997). Mutations in human TBX5 [corrected] cause limb and cardiac malformation in Holt-Oram syndrome. *Nat Genet* **15**, 30-5.

Begbie, J., Brunet, J., Rubenstein, J. and Graham, A. (1999). Induction of the

epibranchial placodes. *Development* **126**, 895-902.

Begemann, G., Schilling, T., Rauch, G., Geisler, R. and Ingham, P. (2001). The zebrafish neckless mutation reveals a requirement for raldh2 in mesodermal signals that pattern the hindbrain. *Development* **128**, 3081-94.

Bell, D., Leung, K., Wheatley, S., Ng, L., Zhou, S., Ling, K., Sham, M., Koopman, P., Tam, P. and Cheah, K. (1997). SOX9 directly regulates the type-II collagen gene. *Nat Genet* **16**, 174-8.

Bilican, B. and Goding, C. (2006). Cell cycle regulation of the T-box transcription factor tbx2. *Exp Cell Res* **312**, 2358-66.

Bishwanath Chatterjee, Alvin J. Chin, Gunnar Valdimarsson, Carla Finis, Jennifer M. Sonntag, Bo Yon Choi, Liang Tao, Krithika Balasubramanian, Carolyn Bell, Alison Krufka, David J. Kozlowski, Ross G. Johnson, and Cecilia W. Lo. (2005). Developmental Regulation and Expression of the Zebrafish Connexin43 Gene. Dev Dyn. **233**, 890–906.

Bollag, R. J., Siegfried, Z., Cebra-Thomas, J. A., Garvey, N., Davison, E. M. and Silver, L. M. (1994). An ancient family of embryonically expressed mouse genes sharing a conserved protein motif with the *T* locus. *Nat. Genet.* **7**, 383-389.

Borke, J., Yu, J., Isales, C., Wagle, N., Do, N., Chen, J. and Bollag, R. (2003). Tension-induced reduction in connexin 43 expression in cranial sutures is linked to transcriptional regulation by TBX2. *Ann Plast Surg* **51**, 499-504.

Carreira, S., Dexter, T., Yavuzer, U., Easty, D. and Goding, C. (1998). Brachyury-related transcription factor Tbx2 and repression of the melanocyte-specific TRP-1 promoter. *Mol Cell Biol* **18**, 5099-108.

Cerny, R., Meulemans, D., Berger, J., Wilsch-Bräuninger, M., Kurth, T., Bronner-Fraser, M. and Epperlein, H. (2004). Combined intrinsic and extrinsic influences pattern cranial neural crest migration and pharyngeal arch morphogenesis in axolotl. *Dev Biol* **266**, 252-69.

Chapman, D., Garvey, N., Hancock, S., Alexiou, M., Agulnik, S., Gibson-Brown, J., Cebra-Thomas, J., Bollag, R., Silver, L. and Papaioannou, V. (1996). Expression of the T-box family genes, Tbx1-Tbx5, during early mouse development. *Dev Dyn* **206**, 379-90.

Chen, J., Chatterjee, B., Meyer, R., Yu, J., Borke, J., Isales, C., Kirby, M., Lo, C.

and Bollag, R. (2004). Tbx2 represses expression of Connexin43 in osteoblastic-like cells. *Calcif Tissue Int* **74**, 561-73.

Chiang, C., Litingtung, Y., Lee, E., Young, K., Corden, J., Westphal, H. and Beachy, P. (1996). Cyclopia and defective axial patterning in mice lacking Sonic hedgehog gene function. *Nature* **383**, 407-13.

Christoffels, V., Hoogaars, W., Tessari, A., Clout, D., Moorman, A. and Campione, M. (2004). T-box transcription factor Tbx2 represses differentiation and formation of the cardiac chambers. *Dev Dyn* **229**, 763-70.

Chuang, J. C., Mathers, P. H. and Raymond, P. A. (1999). Expression of three Rx homeobox genes in embryonic and adult zebrafish. *Mech. Dev.* **84**, 195-198.

Cordier, A. and Haumont, S. (1980). Development of thymus, parathyroids, and ultimo-branchial bodies in NMRI and nude mice. *Am J Anat* **157**, 227-63.

Couly, G., Coltey, P. and Le Douarin, N. (1993). The triple origin of skull in higher vertebrates: a study in quail-chick chimeras. *Development* **117**, 409-29.

Couly, G., Creuzet, S., Bennaceur, S., Vincent, C. and Le Douarin, N. (2002). Interactions between Hox-negative cephalic neural crest cells and the foregut endoderm in patterning the facial skeleton in the vertebrate head. *Development* **129**, 1061-73.

Couly, G. and Le Douarin, N. (1990). Head morphogenesis in embryonic avian chimeras: evidence for a segmental pattern in the ectoderm corresponding to the neuromeres. *Development* **108**, 543-58.

Crump, J., Maves, L., Lawson, N., Weinstein, B. and Kimmel, C. (2004). An essential role for Fgfs in endodermal pouch formation influences later craniofacial skeletal patterning. *Development* **131**, 5703-16.

D'Amico-Martel, A. and Noden, D.M. (1983). Contributions of placodal and neural crest cells to avian cranial peripheral ganglia. *Am. J. Anat.***166**, 445-468.

David, N., Saint-Etienne, L., Tsang, M., Schilling, T. and Rosa, F. (2002). Requirement for endoderm and FGF3 in ventral head skeleton formation. *Development* **129**, 4457-68.

Deschet, K., Bourrat, F., Ristoratore, F., Chourrout, D. and Joly, J. (1999). Expression of the medaka (Oryzias latipes) Ol-Rx3 paired-like gene in two

diencephalic derivatives, the eye and the hypothalamus. *Mech Dev* **83**, 179-82.

Dheen, S., Rajkumar, K. and Murphy, L. (1997). Islet cell proliferation and apoptosis in insulin-like growth factor binding protein-1 in transgenic mice. *J Endocrinol* **155**, 551-8.

Dickmeis, T., Mourrain, P., Saint-Etienne, L., Fischer, N., Aanstad, P., Clark, M., Strähle, U. and Rosa, F. (2001). A crucial component of the endoderm formation pathway, CASANOVA, is encoded by a novel sox-related gene. *Genes Dev* **15**, 1487-92.

Drummond, I., Majumdar, A., Hentschel, H., Elger, M., Solnica-Krezel, L., Schier, A., Neuhauss, S., Stemple, D., Zwartkruis, F., Rangini, Z. et al. (1998). Early development of the zebrafish pronephros and analysis of mutations affecting pronephric function. *Development* **125**, 4655-67.

Driever, W., Stemple, D., Schier, A. and Solnicka-Krezel, L. (1994). Zebrafish: genetic tools for studying vertebrate development. *Trends Genet.* **10, No. 5.**

Fashena, D. and Westerfield, M. (1999a). Secondary motoneuron axons localize DM-GRASP on their fasciculated segments. *J Comp Neurol* **406**, 415-24.

Fashena, D. and Westerfield, M. (1999b). Secondary motoneuron axons localize DM-GRASP on their fasciculated segments. *J Comp Neurol* **406**, 415-24.

Flores, M., Lam, E., Crosier, P. and Crosier, K. (2006). A hierarchy of Runx transcription factors modulate the onset of chondrogenesis in craniofacial endochondral bones in zebrafish. *Dev Dyn* **235**, 3166-76.

Flores, M., Tsang, V., Hu, W., Kalev-Zylinska, M., Postlethwait, J., Crosier, P., Crosier, K. and Fisher, S. (2004). Duplicate zebrafish runx2 orthologues are expressed in developing skeletal elements. *Gene Expr Patterns* **4**, 573-81.

Fong, S., Emelyanov, A., Teh, C. and Korzh, V. (2005). Wnt signalling mediated by Tbx2b regulates cell migration during formation of the neural plate. *Development* **132**, 3587-96.

Garg, V., Yamagishi, C., Hu, T., Kathiriya, I., Yamagishi, H. and Srivastava, D. (2001). Tbx1, a DiGeorge syndrome candidate gene, is regulated by sonic hedgehog during pharyngeal arch development. *Dev Biol* **235**, 62-73.

Gibson-Brown, J., I Agulnik S, Silver, L. and Papaioannou, V. (1998a).

Expression of T-box genes Tbx2-Tbx5 during chick organogenesis. *Mech Dev* **74**, 165-9.

Glasgow, E., Karavanov, A. and Dawid, I. (1997). Neuronal and neuroendocrine expression of lim3, a LIM class homeobox gene, is altered in mutant zebrafish with axial signaling defects. *Dev Biol* **192**, 405-19.

Gordon J**.,** Bennett, A.R**.,** Blackburn, C.C**.,** Manley, N.R. (2001). Gcm2 and Foxn1 mark early parathyroid- and thymus-specific domains in the developing third pharyngeal pouch. *Mech Dev* **103**, 141-3.

Graham, A. (2001). The development and evolution of the pharyngeal arches. *J Anat* **199**, 133-41.

Graham, A., Okabe, M. and Quinlan, R. (2005). The role of the endoderm in the development and evolution of the pharyngeal arches. *J Anat* **207**, 479-87.

Graham, A. and Smith, A. (2001). Patterning the pharyngeal arches. *Bioessays* **23**, 54-61.

Griffiths-Jones S. (2004) The microRNA Registry. *Nucleic Acids Res.* 32 (DATABASE ISSUE), D109-D111 **Griffiths-Jones, S.** (2004). The microRNA Registry. *Nucleic Acids Res* **32**, D109-11.

Griffiths-Jones, S. (2004). The microRNA Registry. *Nucleic Acids Res* **32**, D109-11.

Griffiths-Jones S, Grocock RJ, van Dongen S, Bateman A and Enright AJ. (2006). miRBase: microRNA sequences, targets and gene nomenclature. *Nucleic Acids Res.* 34 (DATABASE ISSUE), D140-D144.

Griffiths-Jones, S. (2006). miRBase: the microRNA sequence database. *Methods Mol Biol* **342**, 129-38. **Griffiths-Jones, S.** (2004). The microRNA Registry. *Nucleic Acids Res* **32**, D109-11.

Gross, J. and Dowling, J. (2005). Tbx2b is essential for neuronal differentiation along the dorsal/ventral axis of the zebrafish retina. *Proc Natl Acad Sci U S A* **102**, 4371-6.

Guo, S., Brush, J., Teraoka, H., Goddard, A., Wilson, S., Mullins, M. and Rosenthal, A. (1999). Development of noradrenergic neurons in the zebrafish hindbrain requires BMP, FGF8, and the homeodomain protein soulless/Phox2a. *Neuron* **24**, 555-66.

Hall, C., Flores, M., Murison, G., Crosier, K. and Crosier, P. (2006). An essential role for zebrafish Fgfrl1 during gill cartilage development. *Mech Dev* **123**, 925-40.

Harrelson, Z., Kelly, R., Goldin, S., Gibson-Brown, J., Bollag, R., Silver, L. and Papaioannou, V. (2004). Tbx2 is essential for patterning the atrioventricular canal and for morphogenesis of the outflow tract during heart development. *Development* **131**, 5041-52.

Hayata, T., Kuroda, H., Eisaki, A. and Asashima, M. (1999). Expression of Xenopus T-box transcription factor, tbx2 in Xenopus embryo. *Dev Genes Evol* **209**, 625-8.

Herzog, W., Sonntag, C., von der Hardt, S., Roehl, H., Varga, Z. and Hammerschmidt, M. (2004). Fgf3 signaling from the ventral diencephalon is required for early specification and subsequent survival of the zebrafish adenohypophysis. *Development* **131**, 3681-92.

Higashijima, S., Hotta, Y. and Okamoto, H. (2000). Visualization of cranial motor neurons in live transgenic zebrafish expressing green fluorescent protein under the control of the islet-1 promoter/enhancer. *J Neurosci* **20**, 206-18.

Holzschuh, J., Wada, N., Wada, C., Schaffer, A., Javidan, Y., Tallafuss, A., Bally-Cuif, L. and Schilling, T. (2005). Requirements for endoderm and BMP signaling in sensory neurogenesis in zebrafish. *Development* **132**, 3731-42.

Jerome, L. and Papaioannou, V. (2001). DiGeorge syndrome phenotype in mice mutant for the T-box gene, Tbx1. *Nat Genet* **27**, 286-91.

Jerome-Majewska, L., Jenkins, G., Ernstoff, E., Zindy, F., Sherr, C. and Papaioannou, V. (2005). Tbx3, the ulnar-mammary syndrome gene, and Tbx2 interact in mammary gland development through a p19Arf/p53-independent pathway. *Dev Dyn* **234**, 922-33.

Kan, L., Israsena, N., Zhang, Z., Hu, M., Zhao, L., Jalali, A., Sahni, V. and Kessler, J. (2004). Sox1 acts through multiple independent pathways to promote neurogenesis. *Dev Biol* **269**, 580-94.

Kelsh, R., Dutton, K., Medlin, J. and Eisen, J. (2000). Expression of zebrafish fkd6 in neural crest-derived glia. *Mech Dev* **93**, 161-4.

Kelsh, R.N., Schmid, B., Eisen, J.S. (2000b). Genetic analysis of melanophore development in zebrafish embryos. *Dev Biol* **225**, 277– 293.

Kerney, R., Gross, J. and Hanken, J. (2007). Runx2 is essential for larval hyobranchial cartilage formation in Xenopus laevis. *Dev Dyn* **236**, 1650-62.

Kikuchi, Y., Agathon, A., Alexander, J., Thisse, C., Waldron, S., Yelon, D., Thisse, B. and Stainier, D. (2001). casanova encodes a novel Sox-related protein necessary and sufficient for early endoderm formation in zebrafish. *Genes Dev* **15**, 1493-505.

Kikuchi, Y., Trinh, L., Reiter, J., Alexander, J., Yelon, D. and Stainier, D. (2000). The zebrafish bonnie and clyde gene encodes a Mix family homeodomain protein that regulates the generation of endodermal precursors. *Genes Dev* **14**, 1279-89.

Kimmel, C., Miller, C. and Keynes, R. (2001). Neural crest patterning and the evolution of the jaw. *J Anat* **199**, 105-20.

King, M., Arnold, J., Shanske, A. and Morrow, B. (2006). T-genes and limb bud development. *Am J Med Genet A* **140**, 1407-13.

Kispert, A. & Herrmann, B. G. (1993). The Brachyury gene encodes a novel DNA binding protein. *EMBO J* **12**, 3211–3220.

Knight, R. and Schilling, T. (2006). Cranial neural crest and development of the head skeleton. *Adv Exp Med Biol* **589**, 120-33.

Krauss, S., Johansen, T., Korzh, V. and Fjose, A. (1991). Expression of the zebrafish paired box gene pax[zf-b] during early neurogenesis. *Development* **113**, 1193-206.

Köntges, G. and Lumsden, A. (1996). Rhombencephalic neural crest segmentation is preserved throughout craniofacial ontogeny. *Development* **122**, 3229-42.

Korzh, V., Sleptsova, I., Liao, J., He, J.Y., and Gong, Z. (1998). Expression of zebrafish bHLH genes ngn1 and nrd defines distinct stages of neural differentiation. Dev Dyn **213**, 92-104.

Le Douarin, N.M., Kalcheim, C. (1999). The Neural Crest, Second ed. Cambridge Univ. Press, New York.

Lee, J., Wu, S., Goering, L. and Dorsky, R. (2006). Canonical Wnt signaling through Lef1 is required for hypothalamic neurogenesis. *Development* **133**, 4451-61.

Lee, K., Xu, Q. and Breitbart, R. (1996). A new tinman-related gene, nkx2.7, anticipates the expression of nkx2.5 and nkx2.3 in zebrafish heart and pharyngeal

endoderm. *Dev Biol* **180**, 722-31.

Lefebvre, V. and Smits, P. (2005). Transcriptional control of chondrocyte fate and differentiation. *Birth Defects Res C Embryo Today* **75**, 200-12.

Li, Q., Newbury-Ecob, R., Terrett, J., Wilson, D., Curtis, A., Yi, C., Gebuhr, T., Bullen, P., Robson, S., Strachan, T. et al. (1997). Holt-Oram syndrome is caused by mutations in TBX5, a member of the Brachyury (T) gene family. *Nat Genet* **15**, 21-9.

Lieschke, G. and Currie, P. (2007). Animal models of human disease: zebrafish swim into view. *Nat Rev Genet* **8**, 353-67.

Lowe, T. and Eddy, S. (1997). tRNAscan-SE: a program for improved detection of transfer RNA genes in genomic sequence. *Nucleic Acids Res* **25**, 955-64.

Lumsden, A., Sprawson, N. and Graham, A. (1991). Segmental origin and migration of neural crest cells in the hindbrain region of the chick embryo. *Development* **113**, 1281-91.

Luo, R., An, M., Arduini, B. and Henion, P. (2001). Specific pan-neural crest expression of zebrafish Crestin throughout embryonic development. *Dev Dyn* **220**, 169-74.

Mathieu, J., Barth, A., Rosa, F., Wilson, S. and Peyriéras, N. (2002). Distinct and cooperative roles for Nodal and Hedgehog signals during hypothalamic development. *Development* **129**, 3055-65.

Minguillon, C. and Logan, M. (2003). The comparative genomics of T-box genes. Brief Funct Genomic Proteomic **2**, 224–233

Miyahara, K., Suzuki, N., Ishihara, T., Tsuchiya, E. and Katsura, I. (2004). TBX2/TBX3 transcriptional factor homologue controls olfactory adaptation in Caenorhabditis elegans. *J Neurobiol* **58**, 392-402.

Morita, T., Nitta, H., Kiyama, Y., Mori, H. and Mishina, M. (1995). Differential expression of two zebrafish emx homeoprotein mRNAs in the developing brain. *Neurosci Lett* **198**, 131-4.

Noden, D. M. (1983). The role of the neural crest in patterning of avian cranial skeletal, connective, and muscle tissues. *Dev. Biol.* **96:** 141–165.

Nechiporuk, A., Linbo, T. and Raible, D. (2005). Endoderm-derived Fgf3 is necessary and sufficient for inducing neurogenesis in the epibranchial placodes in

zebrafish. *Development* **132**, 3717-30.

Neubüser, A., Koseki, H. and Balling, R. (1995). Characterization and developmental expression of Pax9, a paired-box-containing gene related to Pax1. *Dev Biol* **170**, 701-16.

Ng, L., Wheatley, S., Muscat, G., Conway-Campbell, J., Bowles, J., Wright, E., Bell, D., Tam, P., Cheah, K. and Koopman, P. (1997). SOX9 binds DNA, activates transcription, and coexpresses with type II collagen during chondrogenesis in the mouse. *Dev Biol* **183**, 108-21.

Niederreither, K., Remboutsika, E., Gansmuller, A., Losson, R. and Dollé, P. (1999). Expression of the transcriptional intermediary factor TIF1alpha during mouse development and in the reproductive organs. *Mech Dev* **88**, 111-7.

Nissen, R., Amsterdam, A. and Hopkins, N. (2006). A zebrafish screen for craniofacial mutants identifies wdr68 as a highly conserved gene required for endothelin-1 expression. *BMC Dev Biol* **6**, 28.

Noden, D. (1983). The role of the neural crest in patterning of avian cranial skeletal, connective, and muscle tissues. *Dev Biol* **96**, 144-65.

Nornes, S., Mikkola, I., Krauss, S., Delghandi, M., Perander, M. and Johansen, T. (1996). Zebrafish Pax9 encodes two proteins with distinct C-terminal transactivating domains of different potency negatively regulated by adjacent N-terminal sequences. *J Biol Chem* **271**, 26914-23.

Odenthal, J. and Nüsslein-Volhard, C. (1998). fork head domain genes in zebrafish. *Dev Genes Evol* **208**, 245-58.

Oxtoby, E. and Jowett, T. (1993). Cloning of the zebrafish krox-20 gene (krx-20) and its expression during hindbrain development. *Nucleic Acids Res* **21**, 1087-95.

Packham, E. A. and Brook, J. D. (2003). T-box genes in human disorders Human *Mol Gen* **12**, Review Issue 1, R37-R44

Parinov, S., Kondrichin, I., Korzh, V. and Emelyanov, A. (2004). Tol2 transposon-mediated enhancer trap to identify developmentally regulated zebrafish genes in vivo. *Dev Dyn* **231**, 449-59.

Pattyn, A., Morin, X., Cremer, H., Goridis, C. and Brunet, J. (1997). Expression and interactions of the two closely related homeobox genes Phox2a and Phox2b

during neurogenesis. *Development* **124**, 4065-75.

Peyriéras, N., Strähle, U. and Rosa, F. (1998). Conversion of zebrafish blastomeres to an endodermal fate by TGF-beta-related signaling. *Curr Biol* **8**, 783-6.

Piotrowski, T., Ahn, D., Schilling, T., Nair, S., Ruvinsky, I., Geisler, R., Rauch, G., Haffter, P., Zon, L., Zhou, Y. et al. (2003). The zebrafish van gogh mutation disrupts tbx1, which is involved in the DiGeorge deletion syndrome in humans. *Development* **130**, 5043-52.

Piotrowski, T. and Nüsslein-Volhard, C. (2000). The endoderm plays an important role in patterning the segmented pharyngeal region in zebrafish (Danio rerio). *Dev Biol* **225**, 339-56.

Plageman, T. J. and Yutzey, K. (2005). T-box genes and heart development: putting the "T" in heart. *Dev Dyn* **232**, 11-20.

Prince, S., Carreira, S., Vance, K., Abrahams, A. and Goding, C. (2004). Tbx2 directly represses the expression of the p21(WAF1) cyclin-dependent kinase inhibitor. *Cancer Res* **64**, 1669-74.

Püschel, A., Westerfield, M. and Dressler, G. (1992). Comparative analysis of Pax-2 protein distributions during neurulation in mice and zebrafish. *Mech Dev* **38**, 197-208.

Quinlan, R., Gale, E., Maden, M. and Graham, A. (2002). Deficits in the posterior pharyngeal endoderm in the absence of retinoids. *Dev Dyn* **225**, 54-60.

Quinlan, R., Martin, P. and Graham, A. (2004). The role of actin cables in directing the morphogenesis of the pharyngeal pouches. *Development* **131**, 593-9.

Renucci, A., Lemarchandel, V. and Rosa, F. (1996). An activated form of type I serine/threonine kinase receptor TARAM-A reveals a specific signalling pathway involved in fish head organiser formation. *Development* **122**, 3735-43.

Ribeiro, I., Kawakami, Y., Büscher, D., Raya, A., Rodríguez-León, J., Morita, M., Rodríguez Esteban, C. and Izpisúa Belmonte, J. (2007). Tbx2 and Tbx3 regulate the dynamics of cell proliferation during heart remodeling. *PLoS ONE* **2**, e398.

Robu, M., Larson, J., Nasevicius, A., Beiraghi, S., Brenner, C., Farber, S. and Ekker, S. (2007). p53 activation by knockdown technologies. *PLoS Genet* **3**, e78.

Roehl, H. and Nüsslein-Volhard, C. (2001). Zebrafish pea3 and erm are general targets of FGF8 signaling. *Curr Biol* **11**, 503-7.

Rowley, M., Grothey, E. and Couch, F. (2004). The role of Tbx2 and Tbx3 in mammary development and tumorigenesis. *J Mammary Gland Biol Neoplasia* **9**, 109-18.

Rubinstein, A.L., Lee, D., Luo, R., Henion, P.D., Halpern, M.E. (2000). Genes dependent on zebrafish cyclops function identified by AFLP differential gene expression screen. *Genesis* **26**, 86–97.

Ruvinsky, I., Oates, A., Silver, L. and Ho, R. (2000). The evolution of paired appendages in vertebrates: T-box genes in the zebrafish. *Dev Genes Evol* **210**, 82-91.

Rychel, A. and Swalla, B. (2007). Development and evolution of chordate cartilage. *J Exp Zoolog B Mol Dev Evol* **308**, 325-35.

Sbrogna, J., Barresi, M. and Karlstrom, R. (2003). Multiple roles for Hedgehog signaling in zebrafish pituitary development. *Dev Biol* **254**, 19-35.

Schaeffer, B. (1987). Deuterostome monophyly and phylogeny. *Evol Bio.* **21**, 179-235.

Schier, A., Joyner, A., Lehmann, R. and Talbot, W. (1996). From screens to genes: prospects for insertional mutagenesis in zebrafish. *Genes Dev* **10**, 3077-80.

Schilling, T. and Kimmel, C. (1994). Segment and cell type lineage restrictions during pharyngeal arch development in the zebrafish embryo. *Development* **120**, 483-94.

Schilling, T. and Kimmel, C. (1997). Musculoskeletal patterning in the pharyngeal segments of the zebrafish embryo. *Development* **124**, 2945-60.

Schilling, T., Piotrowski, T., Grandel, H., Brand, M., Heisenberg, C., Jiang, Y., Beuchle, D., Hammerschmidt, M., Kane, D., Mullins, M. et al. (1996a). Jaw and branchial arch mutants in zebrafish I: branchial arches. *Development* **123**, 329-44.

Schilling, T., Prince, V. and Ingham, P. (2001). Plasticity in zebrafish hox expression in the hindbrain and cranial neural crest. *Dev Biol* **231**, 201-16.

Schilling, T., Walker, C. and Kimmel, C. (1996b). The chinless mutation and neural crest cell interactions in zebrafish jaw development. *Development* **122**, 1417-26.

Schoenwolf G.C. **, Francis-West** P.H. **, Brauer** P.R. **, Bleyl** S.B. (2009). Larsen's

human embryology, Forth ed. Elsevier Health Sciences, Philadelphia.

Seufert, D. and Hall, B. (1990). Tissue interactions involving cranial neural crest in cartilage formation in Xenopus laevis (Daudin). *Cell Differ Dev* **32**, 153-65.

Showell, C., Christine, K., Mandel, E. and Conlon, F. (2006). Developmental expression patterns of Tbx1, Tbx2, Tbx5, and Tbx20 in Xenopus tropicalis. *Dev Dyn* **235**, 1623-30.

Sinclair, C., Rowley, M., Naderi, A. and Couch, F. (2003). The 17q23 amplicon and breast cancer. *Breast Cancer Res Treat* **78**, 313-22.

Sleptsova-Friedrich, I., Li, Y., Emelyanov, A., Ekker, M., Korzh, V. and Ge, R. (2001). fgfr3 and regionalization of anterior neural tube in zebrafish. *Mech Dev* **102**, 213-7.

Smith, J. (1999). T-box genes: what they do and how they do it. *Trends Genet* **15**, 154-8.

Solnica-Krezel, L., Stemple, D., Mountcastle-Shah, E., Rangini, Z., Neuhauss, S., Malicki, J., Schier, A., Stainier, D., Zwartkruis, F., Abdelilah, S. et al. (1996). Mutations affecting cell fates and cellular rearrangements during gastrulation in zebrafish. *Development* **123**, 67-80.

Sperber, S., Saxena, V., Hatch, G. and Ekker, M. (2008). Zebrafish dlx2a contributes to hindbrain neural crest survival, is necessary for differentiation of sensory ganglia and functions with dlx1a in maturation of the arch cartilage elements. *Dev Biol* **314**, 59-70.

Stewart, R., Arduini, B., Berghmans, S., George, R., Kanki, J., Henion, P. and Look, A. (2006). Zebrafish foxd3 is selectively required for neural crest specification, migration and survival. *Dev Biol* **292**, 174-88.

Teng, H., Davis, E., Abrahams, A., Mowla, S., Parker, M. and Prince, S. (2007). A role for Tbx2 in the regulation of the alpha2(1) collagen gene in human fibroblasts. *J Cell Biochem* **102**, 618-25.

Thisse, B., Thisse, C. (2004) Fast Release Clones: A High Throughput Expression Analysis. ZFIN Direct Data Submission (http://zfin.org).

Trainor, P. and Krumlauf, R. (2000a). Patterning the cranial neural crest: hindbrain segmentation and Hox gene plasticity. *Nat Rev Neurosci* **1**, 116-24.

Trainor, P. and Krumlauf, R. (2000b). Plasticity in mouse neural crest cells reveals a new patterning role for cranial mesoderm. *Nat Cell Biol* **2**, 96-102.

Trainor, P. and Krumlauf, R. (2002). Development. Riding the crest of the Wnt signaling wave. *Science* **297**, 781-3.

Trokovic, N., Trokovic, R. and Partanen, J. (2005). Fibroblast growth factor signalling and regional specification of the pharyngeal ectoderm. *Int J Dev Biol* **49**, 797-805.

van der Meulen, T., Kranenbarg, S., Schipper, H., Samallo, J., van Leeuwen, J. and Franssen, H. (2005). Identification and characterisation of two runx2 homologues in zebrafish with different expression patterns. *Biochim Biophys Acta* **1729**, 105-17

Vance, K., Carreira, S., Brosch, G. and Goding, C. (2005). Tbx2 is overexpressed and plays an important role in maintaining proliferation and suppression of senescence in melanomas. *Cancer Res* **65**, 2260-8.

Varga, Z., Amores, A., Lewis, K., Yan, Y., Postlethwait, J., Eisen, J. and Westerfield, M. (2001). Zebrafish smoothened functions in ventral neural tube specification and axon tract formation. *Development* **128**, 3497-509.

Varga, Z., Wegner, J. and Westerfield, M. (1999). Anterior movement of ventral diencephalic precursors separates the primordial eye field in the neural plate and requires cyclops. *Development* **126**, 5533-46.

Veitch, E., Begbie, J., Schilling, T., Smith, M. and Graham, A. Pharyngeal arch patterning in the absence of neural crest. *Curr Biol* **9**, 1481-4.

Webb, J. F. and Noden, D. M. (1993). Ectodermal placodes: Contributions to the development of the vertebrate head. *Amer. Zool.* **33**, 434-447.

Wei, Y., Mizzen, C., Cook, R., Gorovsky, M. and Allis, C. (1998). Phosphorylation of histone H3 at serine 10 is correlated with chromosome condensation during mitosis and meiosis in Tetrahymena. *Proc Natl Acad Sci U S A* **95**, 7480-4.

Wendling, O., Dennefeld, C., Chambon, P. and Mark, M. (2000). Retinoid signaling is essential for patterning the endoderm of the third and fourth pharyngeal arches. *Development* **127**, 1553-62.

Westerfield, M. (2000). *The Zebrafish Book. A Guide for the Laboratory use of*

Zebrafish (Danio rerio). Eugene: University of Oregon Press.

Willett, C., Zapata, A., Hopkins, N. and Steiner, L. (1997). Expression of zebrafish rag genes during early development identifies the thymus. *Dev Biol* **182**, 331-41.

Wilson, S. and Houart, C. (2004). Early steps in the development of the forebrain. *Dev Cell* **6,** 167-81**.**

Wilson, V. and Conlon, F. (2002). The T-box family. *Genome Bio* **3(6)**:reviews3008.1–3008.7

Woo, K. and Fraser, S. (1995). Order and coherence in the fate map of the zebrafish nervous system. *Development* **121**, 2595-609.

Wright, E., Hargrave, M., Christiansen, J., Cooper, L., Kun, J., Evans, T., Gangadharan, U., Greenfield, A. and Koopman, P. (1995). The Sry-related gene Sox9 is expressed during chondrogenesis in mouse embryos. *Nat Genet* **9**, 15-20.

Yamada, M., Revelli, J., Eichele, G., Barron, M. and Schwartz, R. (2000). Expression of chick Tbx-2, Tbx-3, and Tbx-5 genes during early heart development: evidence for BMP2 induction of Tbx2. *Dev Biol* **228**, 95-105.

Yan, Y., Miller, C., Nissen, R., Singer, A., Liu, D., Kirn, A., Draper, B., Willoughby, J., Morcos, P., Amsterdam, A. et al. (2002). A zebrafish sox9 gene required for cartilage morphogenesis. *Development* **129**, 5065-79.

Yan, Y., Willoughby, J., Liu, D., Crump, J., Wilson, C., Miller, C., Singer, A., Kimmel, C., Westerfield, M. and Postlethwait, J. (2005). A pair of Sox: distinct and overlapping functions of zebrafish sox9 co-orthologs in craniofacial and pectoral fin development. *Development* **132**, 1069-83.

Yagi, H., Furutani, Y., Hamada, H., Sasaki, T., Asakawa, S., Minoshima, S., Ichida, F., Joo, K., Kimura, M., Imamura, S. et al. (2003). Role of *TBX1* in human del22q11.2 syndrome. *Lancet* **362**, 1366-1373.

Yelick, P. and Schilling, T. (2002). Molecular dissection of craniofacial development using zebrafish. *Crit Rev Oral Biol Med* **13**, 308-22.

Zhang, J., Talbot, W. and Schier, A. (1998). Positional cloning identifies zebrafish one-eyed pinhead as a permissive EGF-related ligand required during gastrulation. *Cell* **92**, 241-51.

Zhang, Z., Cerrato, F., Xu, H., Vitelli, F., Morishima, M., Vincentz, J., Furuta,

Y., Ma, L., Martin, J., Baldini, A. et al. (2005). Tbx1 expression in pharyngeal epithelia is necessary for pharyngeal arch artery development. *Development* **132**, 5307-15.

Zhao, Q., Eberspaecher, H., Lefebvre, V. and De Crombrugghe, B. (1997). Parallel expression of Sox9 and Col2a1 in cells undergoing chondrogenesis. *Dev Dyn* **209**, 377-86.

Appendix

“Tbx2a plays a role in hypothalamus patterning and neurogenesis”

The hypothalamus is derived from the most ventral region of the anterior diencephalon. Although the initial step of hypothalamic identity induction and the migration of hypothalamic precursors in zebrafish has been extensively characterized (Woo and Fraser, 1995; Varga et al., 1999), the molecular mechanisms that underline later induction and patterning as well as differentiation processes are rather limited. So far, there have been separate lines of evidence suggesting involvement of Hedgehog (Hh), Nodal and Wnt signalling pathways in hypothalamus development. Hh is required for induction the anterior hypothalamus; whereas Nodal is required for the posterior hypothalamus (Chiang et al., 1996; Mathieu et al., 2002). In 2006 Lee et al. shown that the transcription factor of Canonical Wnt signaling - Lef1, specifically regulates posterior hypothalamus neurogenesis. In our study, we identified a conserved expression of *tbx2a* in the posterior ventral hypothalamus, and we sought to investigate whether *tbx2a* is involved in hypothalamus patterning and neurogenesis. We also examined if *tbx2a* acts through known signalling pathways in the hypothalamus.

App.1 Specific *tbx2a* expression pattern suggests a role in hypothalamus development

tbx2a transcript appeared in the anterior ventral diencephalon and the eyes at around 11 hpf (App. Fig. 1A). By 24 hpf, it remained in that region which was excluded from the adenohypophyseal anlage, as demonstrated by double staining with adenohypophysis specific marker_*lim3* (Glasgow et al., 1997; App. Fig. 1C, D). This restriction is sufficient to cover the neurohypophysis domain. From 30 hpf, as the developing forebrain folded, *tbx2a* positive domain developed into the posterior ventral hypothalamus (App. Fig. 1E). At 48 hpf, cross sections through the most posterior hypothalamus revealed expression in the mitotic cells restricted to the

medial region, and in post-mitotic cells spreading to the lateral region (App. Fig. 1G). In the more anterior section, we found *tbx2a* expression in the mitotic cells and at the most ventral part that constituted the neurohypophysis (App. Fig. 1F). Outside the hypothalamus, *tbx2a* was also present in rhombomeres 2, and 6, and the vagal nerve nucleus (App. Fig. 1H, I). However, we focused on the hypothalamic expression of *tbx2a* which was conserved during early development and therefore suggests an important role in this region.

To approach the functional study, we utilized the morpholino (MO) oligonucleotides which had already been characterized previously, i1e2 MO.

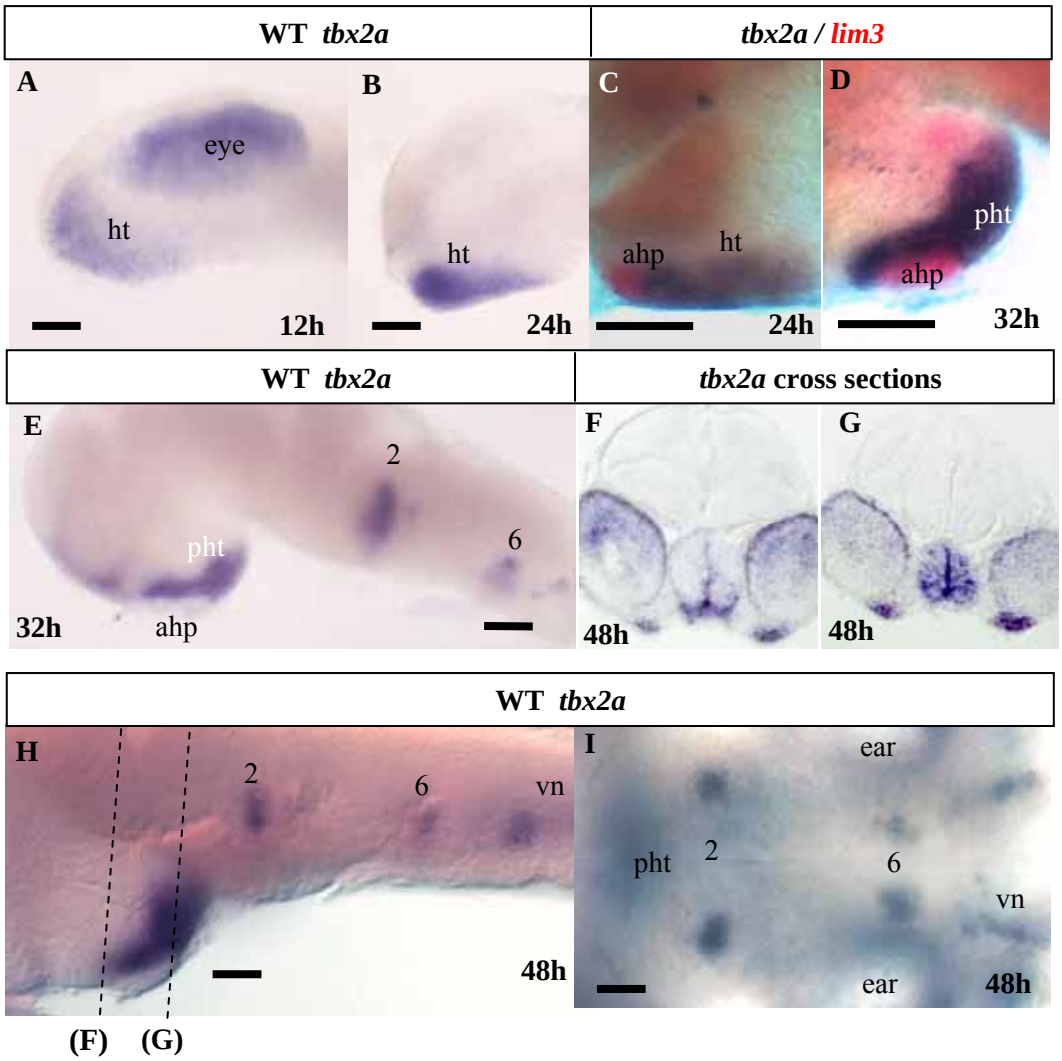

Appendical Figure 1: The expression pattern of *tbx2a*.
During development *tbx2a* is expressed in the ventral posterior hypothalamus. A, B, C, D, E - lateral views; D - ventral view; I - dorsal view. A, B, E, H, I - single color WISH with anti-*tbx2a* probe. C, D-magenta - *tbx2a*, red - *lim3*; G, F-cross-section at the positions marked in H.
Abbreviations: h - hours post fertilization; ahp - adenohypophysis; ht - hypothalamus; pht - posterior hypothalamus; vn - vagus nerve nucleus. Numbers define rhombomeres.
Scale bar, 50 μm.

App. 2 *Tbx2a* is involved in anterior-posterior patterning of the hypothalamus

tbx2a is first expressed during the early stage of the ventral diencephalon formation (11 hpf). Therefore, it is critical to determine whether *tbx2a* is involved in induction of the hypothalamus. For that, one of the earliest specific markers of hypothalamic induction, *nk2.1a* (Rohr et al., 2001) has been employed. We did not find any change in *nk2.1a* expression in the morphants (App. Fig. 2B) in comparison with that of control embryos (App. Fig.2A). So, the hypothalamus is normally induced in *tbx2a* morphants.

Following induction, the hypothalamus is patterned into sub-domains. In the hypothalamus, at 24 hpf *shh* expression is restricted to the anterior dorsal domain (reviewed in Wilson and Houart, 2004) whereas we found *tbx2a* restricted to the ventral domain. Therefore, it is suggested that *shh* and *tbx2a* expression are non-overlapping but complementary with each other. Varga el al., (2001) and Mathieu et al., (2002) have shown that interference with Hh pathway in the anterior hypothalamus led to an elimination of molecular markers in the anterior dorsal hypothalamus and an expansion of the posterior ventral hypothalamus. The role of Hh expression in the anterior domain could be interpreted to simultaneously promote an anterior fate, and inhibit expansion of the posterior domain. We postulated that *tbx2a* is expressed in a complementary manner with *shh* expression domain, subsequently we asked if *tbx2a* plays a role in the patterning of the hypothalamus. Since there was an ectopic expansion of *shh* toward the posterior domain in *tbx2a* morphants (App. Fig. 3B), we expected this to result in an up-regulation of anterior hypothalamic markers and down-regulation of posterior ones. *rx3* (Chuang et al., 1999) is a specific marker for the anterior hypothalamus, whereas *emx2* (Morita et al., 1995) is a marker for the posterior part. In morphants, the two markers showed opposite changes.

Compared to controls (App. Fig. 2C), *rx3*-positive domain in the morphants (App. Fig. 2D) was broader and extended to the posterior territory. In contrast, *emx2* expression domain was significantly reduced in the morphants (App. Fig. 2F). These data could be improved upon with double in situ hybridization of these two markers. That would allow us to evaluate relative changes in sizes between the complementary anterior and posterior domains. Nevertheless, these preliminary data strongly hint at a function of *tbx2a* as an upstream repressor of *shh* signaling for the specification of anterior and posterior hypothalamic fate (App. Scheme 1). In addition, our finding highly supports the study in mouse by Jeong and Epstein (2003). They have shown that T-box binding site residing in the intron 2 of *Shh* is required for the repression of *Shh* in regions of the brain where its transcript is not normally present.

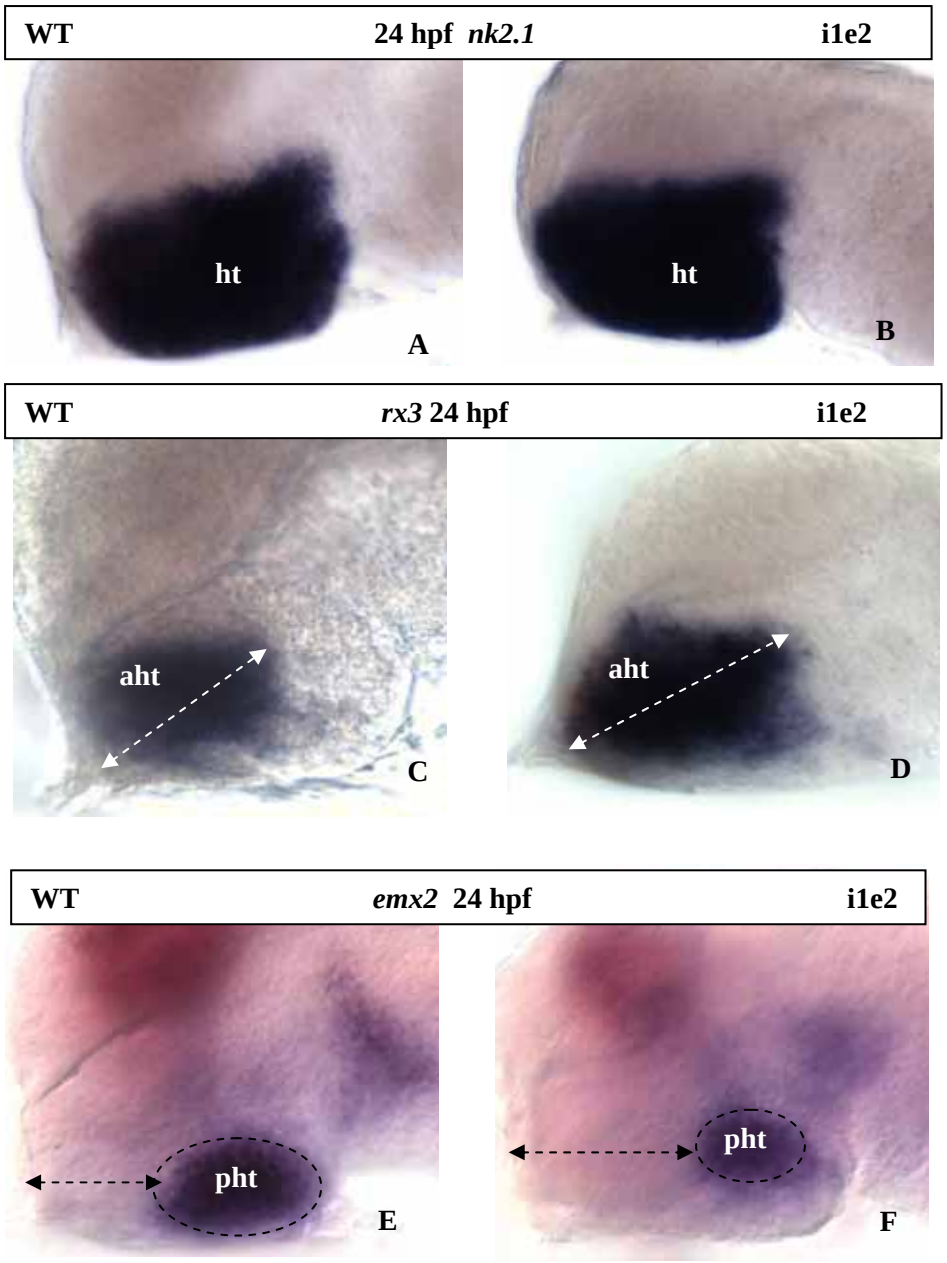

<u>Appendical Figure 2:</u> *tbx2a* has effect on hypothalamus patterning but not on induction.

A, C, E - controls; B, D, F - morphants. All specimen are in lateral view.

(A, B) *nk2.1* expression is unchanged in the morphant

(C, D) The morphant (D) exhibits extended anterior sub-domain labelled by *rx3*.

(E, F) *emx2* reveals a contrast pattern of *rx3* expression. In the morphant (F) the posterior domain positive for *emx2* is diminished or even lost in the most ventral part.

Abbreviations: ht - hypothalamus; mhb - midbrain-hindbrain boundary; apt – anterior hypothalamus; pht - posterior hypothalamus; t - telencephalon.

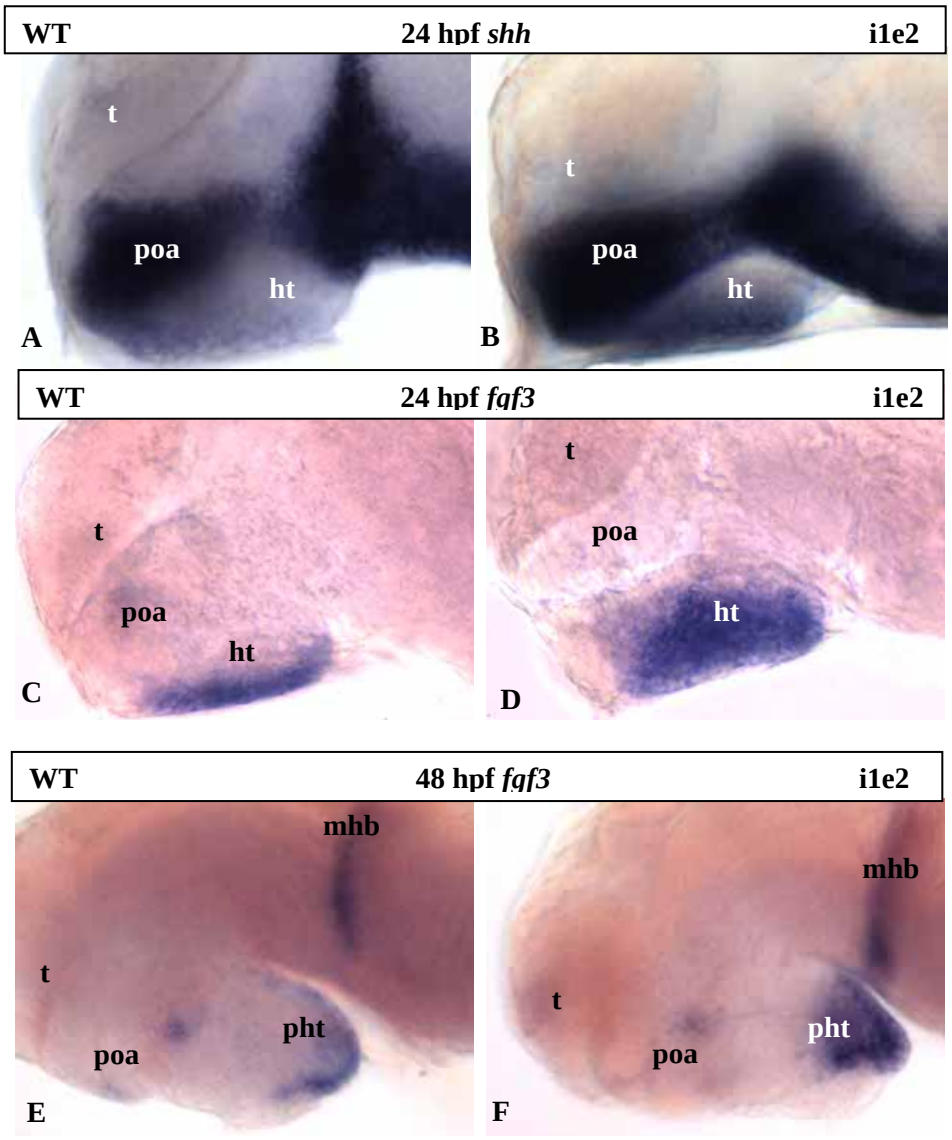

<u>Appendical Figure 3:</u> Morpholino-mediated knockdown of *tbx2a* caused an increase in expression of markers *shh* and *fgf3* in the hypothalamus. A, C, E - controls; **B, D, F** - morphants. All specimens are in lateral view.

Abbreviations: ht - hypothalamus; mhb - midbrain-hindbrain boundary; poa - preoptic area; pht - posterior hypothalamus; t - telencephalon.

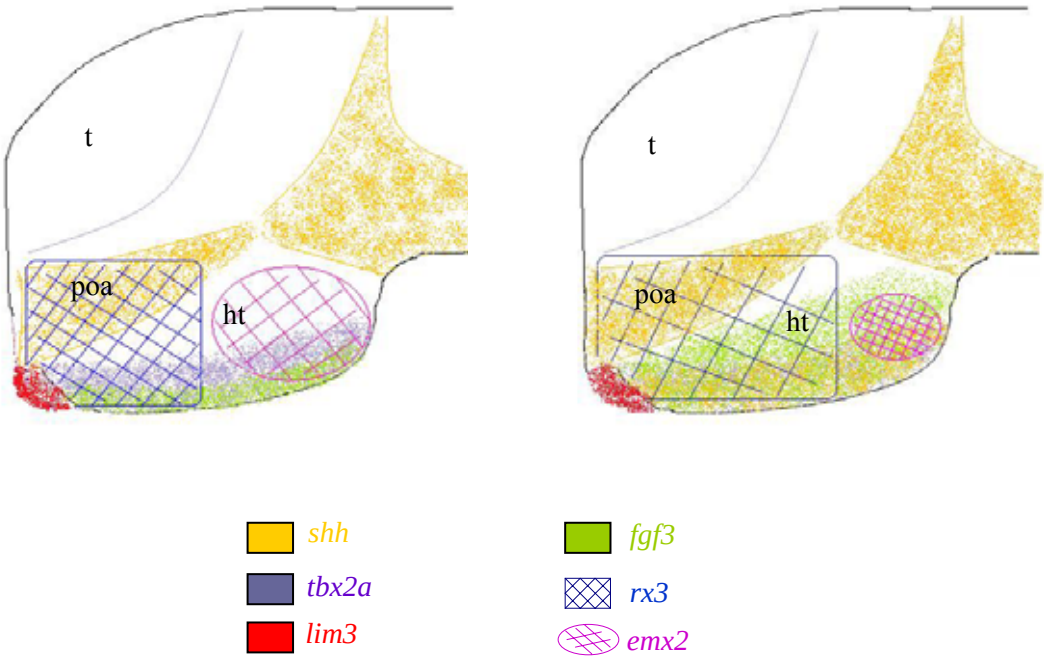

Appendical Scheme 1: Expression domain of genes in the hypothalamus. (A) *tbx2a* expression domain is in the ventral diencephanlon, broader than *fgf3* and non-overlapping with *lim3* or *shh* domains. **(B)** *tbx2a* knock-down causes an ectopic expression of *shh* in the ventral diencephalon, expansion of *fgf3* from the most ventral up to the dorsal, expansion of anterior marker *rx3* and elimination of posterior marker *emx2*.
ht - hypothalamus; mhb - midbrain-hindbrain boundary; poa - preoptic area; pht - posterior hypothalamus; t - telencephalon.

App. 3Tbx2a may act through Shh and Fgf3 to regulate adenohypophysis development

Another function of *shh* signaling has been shown in adenohypophyseal induction and patterning (Sbrogna et al., 2003). We examined whether *tbx2a* is also important for development of this organ. Adenohypophysis is also known as the posterior pituitary gland and originated from non-neural ectoderm; whereas neurohypophysis (anterior pituitary gland) is from the infundibulum, a ventral structure of the diencephalon. It has been shown that over-expression of *shh* resulted in an expansion of adenohypophyseal markers (Sbrogna et al., 2003). As above, we showed that *shh* is upregulated in *tbx2a* morphants. *lim3* is an anterior pituitary specific marker (Glasgow et al., 1997). A majority of *tbx2a* morphant embryos (n = 8/15) displayed extended *lim3* expression domain even though the morphants were generally shorter than controls (App. Fig. 4A, B). To countercheck the phenotype, we over-expressed *tbx2a* with 50 pg/embryo of *tbx2a* mRNA. 6 out of 15 embryos examined had reduced *lim3* expression domain (App. Fig. 4C, D). This observation supports the notion that *tbx2a* may act through *shh* signaling to regulate adenohypophysis development.

In addition to *shh*, *fgf3* has been reported to be involved in pituitary development (Herzog et al., 2004). Thus, we checked *fgf3* expression in the *tbx2a* morphants. In controls, *fgf3* was expressed in the most ventral cell layers in the diencephalons (App. Fig. 3C). However, its expression expanded to the whole hypothalamus in the morphants (App. Fig. 3F). This suggests that *tbx2a* may act as a negative regulator of *fgf3*. It has been shown that transcriptional activation of pituitary genes was affected in *lia* mutant (*fgf3*$^{-/-}$), suggesting that *lim3* is required for early steps of adenohypophyseal specification (Herzog et al., 2004). However, there was no

report for the reverse whereby an increase in *fgf3* signaling resulted in the up-regulation of pituitary markers and enlarged pituitary anlage. Thece data shown in this study revealed that the enlargement of adenohypophyseal anlage in *tbx2a* morphants could be a result of the up-regulation of *shh* and/or *fgf3* expression in the hypothalamus. If our hypothesis is correct, then ectopic over-expression of *tbx2a* should lead to eliminated expression domains of *shh* and *fgf3*, and support the idea that *shh* and *fgf3* function downstream of *tbx2a* in regulating the development of the pituitary. However, whether *shh* and *fgf3* act dependently or independently in this scenario is unclear.

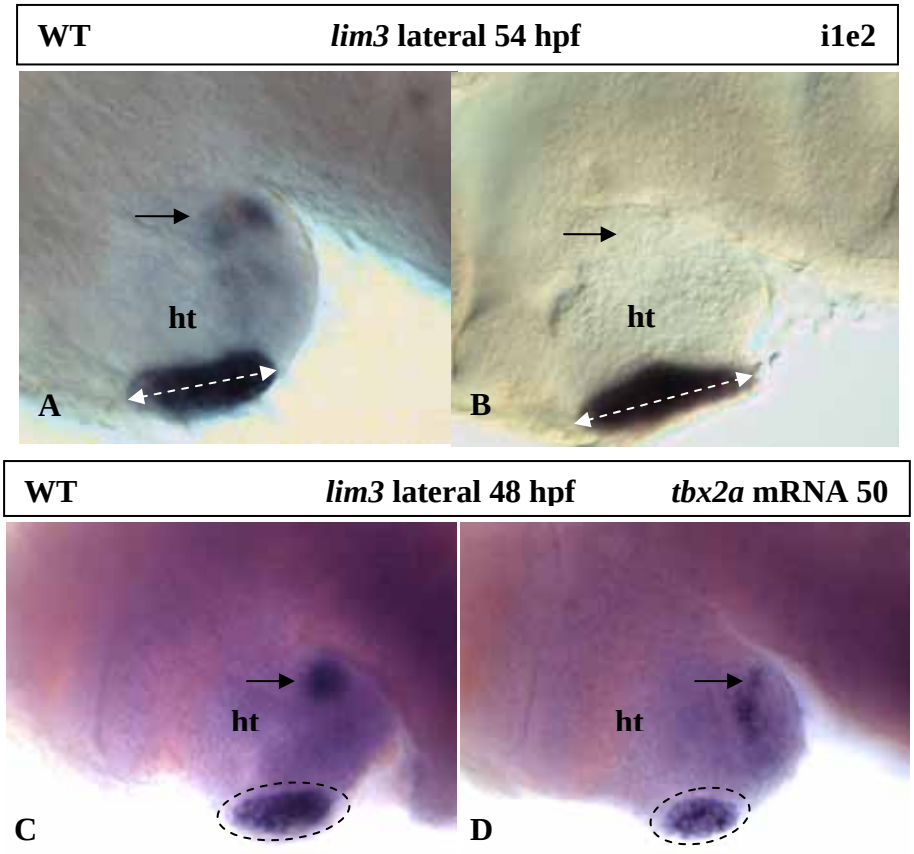

<u>Appendical Figure 4:</u> *tbx2a* plays a role in the development of the adenohypophysis
A, C - controls; B, D - morphants. All specimens are in lateral view, stained with adenohypophyseal marker *lim3*.

(A, B) *tbx2a* knock-down caused an expansion in adenohypophyseal anlage

(C, D) *tbx2a* mRNA over-expression caused a reverse effect.

App. 4 *Tbx2a* may regulate local neurogenesis of the posterior hypothalamus through *shh* signaling

The patterning step is followed by neurogenesis that generates populations of neurons in specific domains. Therefore an alteration of patterning might have effects on neurogenesis. Given the action of *tbx2a* knock-down on AP hypothalamus patterning, we next assessed the effect of *tbx2a* on neurogenesis. *sox3* is a proneural gene expressed during the earliest step of neurogenesis (Kan *et al*., 2004). At 24 hpf, its expression in the morphants is moderately weaker compared to controls (App. Fig. 5A, B). However, its expression recovered by 48hpf (App. Fig. 5C, D). The expression of a later neural marker, *dlx2a* (Akimenko et al., 1994), was specifically reduced in the posterior ventral hypothalamus at 24 hpf where *tbx2a* is normally expressed (App. Fig. 6B). This loss of *dlx2* expression remained until a later stage (App. Fig. 6C, D). Similar result was obtained with *islet1* at 48 hpf (App. Fig. 7E, F). Altogether, although manipulation of *tbx2a* mildly affects the expression of *sox3*, it does have a significant effect later on in neural differentiation in the posterior ventral hypothalamus.

In conclusion, these preliminary data support the hypothesis that *tbx2a* plays a role during hypothalamus patterning and neurogenesis via *fgf3* and/or *shh* signaling. It remains to be seen if the inhibition of *shh* and/or *fgf3* signaling will rescue the phenotype caused by *tbx2a* knock-down. This would provide further support for our hypothesis.

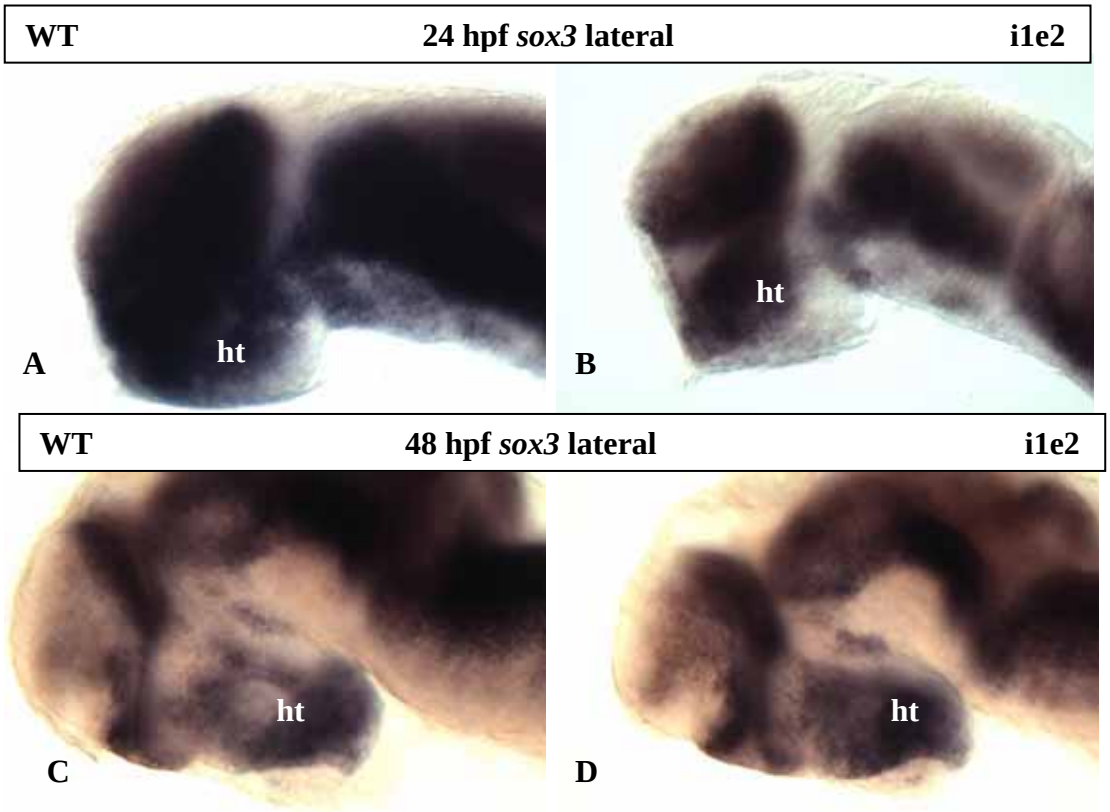

Appendical Figure 5: ***tbx2a*** **overexpression does not affect expression of the early neural marker** ***sox3.*** A, C - controls; B, D - morphants. All specimens are in lateral view, stained with *sox3*

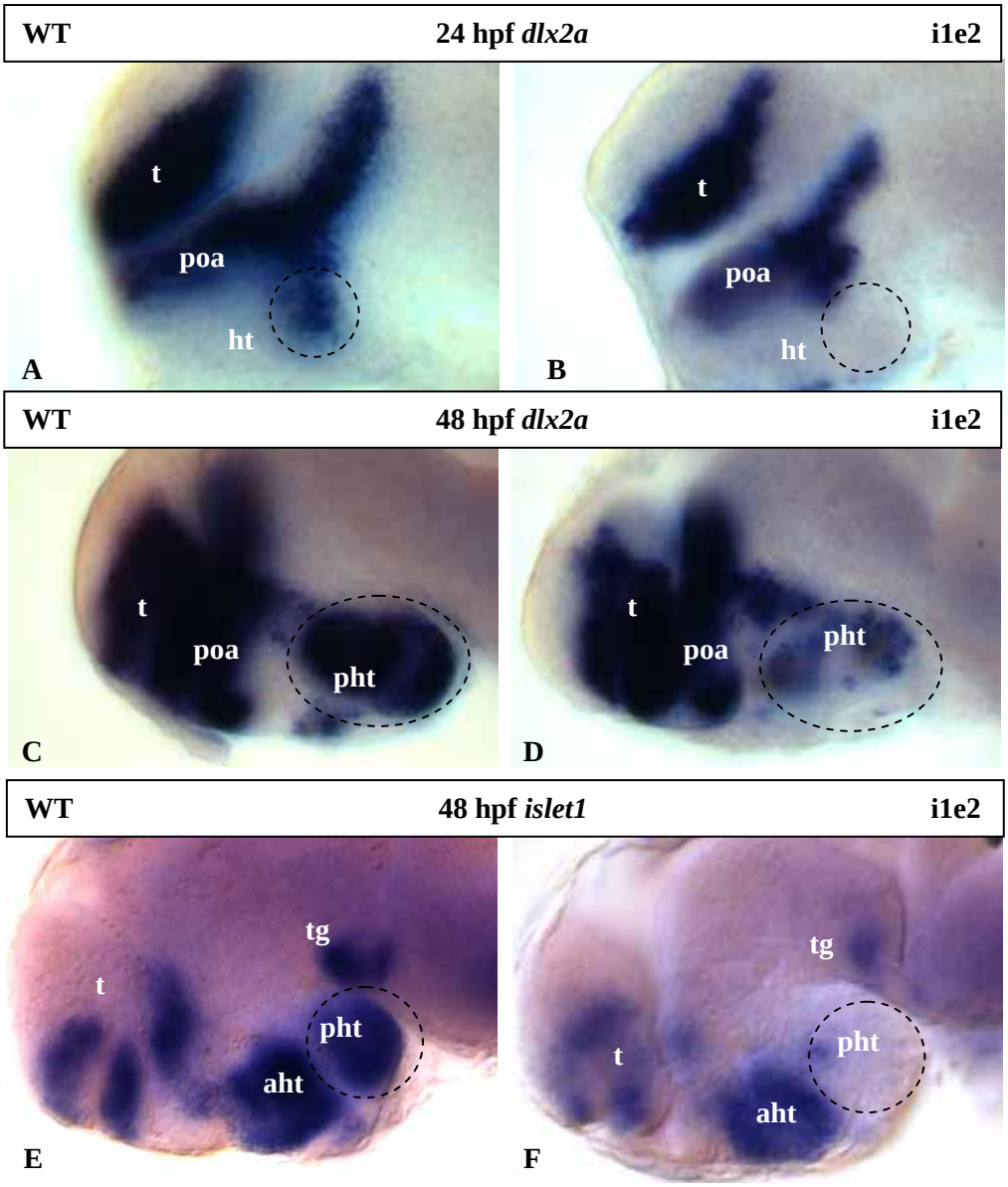

Appendical Figure 6: ***tbx2a*** **knock-down affects neural differentiation markers in the posterior hypothalamus.** A, C, E- controls; B, D, F - morphants. All the specimens are in lateral view

(A, B) *dlx2a* expression exhibits a specific loss in the hypothalamus of the morphants.

(C, D) This pattern is retained up to later stage 48 hpf.

(E, F) *islet1* expression is affected and almost disappeared in the posterior hypothalamus of the morphants